



**FINITE VOLUME ANALYSIS AND
OPTIMISATION OF A HIGH
PRESSURE HOMOGENISER**

Student: Andrew Patrick Clarke

2009

**School of
Mechanical and Manufacturing
Engineering**



FINITE VOLUME ANALYSIS AND OPTIMISATION OF A HIGH PRESSURE HOMOGENISER

by

A.P. CLARKE

B.Eng

A thesis submitted for the degree of
Master of Science (MSc)

School of Mechanical and Manufacturing Engineering
Faculty of Engineering and Computing
Dublin City University

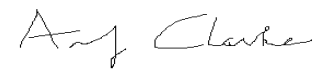
July 2009

Supervisors

DR. ABDUL GHANI OLABI, DR. TIM PRESCOTT

Declaration

I hereby certify that this material, which I now submit for assessment on the programme of study leading to the award of Master of Science is entirely my own work, that I have exercised reasonable care to ensure that the work is original, and does not to the best of my knowledge breach any law of copyright, and has not been taken from the work of others saved and to the extent that such work has been cited and acknowledged within the text of my work.



ANDREW PATRICK CLARKE

Student ID Number: 53461149

Date: July 2009

Publications

This work has been disseminated through the following publications.

Journal Papers:

Andrew Clarke, Tim Prescott, Aazir Khan, Abdul Olabi, “Causes of breakage and disruption in a homogeniser”, *Journal of Power Sources*, 2009 (in review)

Andrew Clarke, Tim Prescott, Aazir Khan, Abdul Olabi, “Optimisation of homogeniser valve design to maximise cell breakage by shear forces”, *Journal of Power Sources*, 2009 (in review)

Conferences:

Andrew Clarke, Abdul Olabi, Tim Prescott, Aran Rafferty & Khaled Benyounis, “Development of Computational Fluid Dynamics (CFD) for Complicated Flow”, *Symposium for Mechanical Engineering Research and Practice (SMERP)*, 2008, Dublin City University, Ireland.

Andrew Clarke, Abdul Olabi, Tim Prescott, Aran Rafferty & Khaled Benyounis, “Finite Element Analysis of Homogeniser”, *Ansys/Enginsoft Conference on Simulation Based Engineering and Science*, Venice, Italy, 16-17 October, 2008

Andrew Clarke, Abdul Olabi, Tim Prescott, Aazir Khan, “Homogeniser Optimisation”, *Symposium for Mechanical Engineering Research and Practice (SMERP)*, 2009, Dublin City University, Ireland.

Acknowledgments

Firstly, I would like to thank Dr. Abdul Ghani Olabi for all of his support and inspiration throughout the course of my work. I would also like to thank him on giving me the opportunity to work on this particular work of Computational Fluid Dynamics. I would also like to thank Dr. Aran Rafferty and Dr. Tim Prescott for taking time from their work to help provide purpose and direction in my thesis contributions. Their help and my respect for them will always be remembered long after I part from this university. Many thanks to the staff in the School of Mechanical and Manufacturing Engineering who have provided many resources at both undergraduate and postgraduate level over the five and a half years here.

I would like to offer my deepest gratitude for my girlfriend Claire for her encouragement and splendid company. These acknowledgements cannot be written without the mentoring and abundant advice (including opinions) of Dr. Aazir Khan during his one year in DCU. I would also like to offer thanks to my work colleague and friend Habibullah Chowdhury for the plentiful exchange of ideas and discussion on many aspects of my category of study. Thanks go out for Mustafa Sajjia for great company and the printing of the draft thesis. Other work colleagues I must mention that were influential are Otgon Dashnyam, Dr. Khaled Benyounis, Dr. Harun Rasheed, Albert Vilaprinyo and James Carton.

I would finally like to thank in person the various work colleagues I have encountered throughout the abundant varieties of offices I have worked in throughout my masters. I must not forget to offer sincere blessings for my family.

Abstract

The homogeniser is a machine that is mostly used to change the appearance and rheological properties of a fluid by means of a high pressure radial gap. It can be implemented to kill off harmful bacteria and organisms as well as reduce the size of individual components or particles to increase the shelf life of many products. The homogeniser can be used to release useful organic materials from within cells or microbes. The homogeniser can be found in small scale production and large scale production. The small scale production homogeniser allows smaller gap sizes but is restricted to lower flow rates in relation to the larger scale homogeniser.

The primary aim of this thesis is to determine optimum geometries for the small-scale high-pressure homogeniser in the disruption of anaerobic microbes from waste water sludge to release organic material to produce methane with maize crop. It is believed that breaking apart microbial walls of microbes in the sludge can release organic material that can further increase methane production and also reduce digester volume. In this case, the waste water sludge with microbes was implemented with a mixture of dry maize silage to produce methane by means of anaerobic conditions. The homogeniser is used to break up tough microbes in secondary waste water sludge to reduce digester volume and anaerobic methane production waiting times.

Geometries of the homogeniser and prototypes were generated using **Gambit 2.3**. Pressure, velocity and flow fields were estimated and analysed using **Fluent 6.3**. The model was estimated by means of a stationary microbe model. Shear forces on microbes were analysed for various positions along the streamline of flow and compared. The homogeniser setup with the highest peak shear forces was used as an optimum homogeniser setup. The initial homogeniser model was replicated from the original experimental homogeniser in the lab. Model simulations were validated from empirical formulae from other works. The optimised design made use of a 27.8° inlet chamfer with the valve gap chamfer diverging at 2.5° each side (valve seat and valve head) downstream of the valve beginning. The finalised optimised design is presented using **Pro-Engineer** in Appendix C.

List of Tables

Table 3.1: Overview of previous CFD works carried out on homogeniser	35
Table 4.1: Water flow rates in homogeniser	44
Table 4.2: Boundary conditions for single phase water model used for preliminary validation	45
Table 4.3: Microbe Positions	51
Table 4.4: Boundary conditions for microbe model	55
Table 4.5: Trailing shear forces for the 5 μm diameter	56
Table 4.6: Lead shear forces for the 5 μm diameter	56
Table 4.7: Trailing shear forces for the 10 μm diameter	59
Table 4.8: Trailing shear forces for the 10 μm diameter	59
Table 5.1: Chamfer angles used for concept 1-7	79
Table 5.2: Shear forces for concept 1-7	79
Table 5.3: Chamfer angles used for concept 8-17	82
Table 5.4: Shear forces for concept 8-17 in comparison to concept 3	83

List of Figures

Figure 1.1: (a) Homogeniser machine with (b) pro-engineer 3-d model cross section of the valve parts in yellow, (c) front view x-section of valve gap region and (d) parts of valve gap region	2
Figure 1.2: Use of anaerobic digestion processes according to industry in the United Kingdom (Asia Biogas 2008)	3
Figure 1.3: Simplified process flow schematic of the Microsludge process (R. L. Stevenson 2007)	5
Figure 1.4: How the homogeniser is related to the overall Biowell project process for increased methane production from anaerobic digestion.....	5
Figure 1.5: Summary of the research process in thesis.....	7
Figure 2.1: (a) Plan View and (b) front view of homogeniser studied	10
Figure 2.2: XY section of homogeniser valve region.....	12
Figure 2.3: Fluid flow properties of (a) movement, (b) interference and (c) eddies	14
Figure 2.4: Flow around internal obstacle at Reynold's number 13.5 and 39.0 (Taneda 1956).	14
Figure 2.5: Vortex shedding (NASA 2000).....	15
Figure 2.6: Summary of the research process in chapter two.	16
Figure 3.1: Kleinig's results (Kleinig A.R. 1996) of (a) normalised pressure across the centre plane of the valve gap for the rounded valve seat inlet and (b) for the square-edged valve seat at the inlet.....	18
Figure 3.2: Pressure gradient of liquid passing through the homogeniser valve based on CFD results	19
Figure 3.3: How the pressure gradient is found.....	21
Figure 3.4: Particle size distribution data (Siddiqi 1996) for packed baker's yeast cells obtained for (a) Constant pressure 500 bar with number of passes variable and (b) 5 th pass at various pressures.....	34
Figure 3.5: Critical gap ratio (G_w/D)	38
Figure 3.6: Summary of the research process in chapter three	40

Figure 4.1: Valve seat geometries.....	43
Figure 4.2: Axi-symmetric model created in Gambit 2.1 for the homogeniser valve with 20 μm gap.	43
Figure 4.3: Pressure drop versus gap for computational model and empirical formulae	46
Figure 4.4: Mesh convergence of single phase water model for original dimensions (Meshes 18-24 and 27-28 were excluded for purposes of clarity)	47
Figure 4.5: Maximum velocity and velocity at start of gap in terms of gap size.....	48
Figure 4.6: Velocity contours of (a) homogeniser gap and exit region, (b) exit region and (c) velocity vectors at impact ring with small velocity values.	49
Figure 4.7: The axi-symmetric view of the six locations of microbes along the expected streamline of flow	51
Figure 4.8: Clockwise force (F_{CW}) and anticlockwise force (F_{CW}) examples	52
Figure 4.9: Shear force categories and null categories where flow approaches microbe surface near right angle	54
Figure 4.10: Trailing shear force profile for microbes at position 1 to 6 for the microbe of 5 μm diameter	57
Figure 4.11: Lead shear force profile for microbes at position 1 to 6 for the microbe of 5 μm diameter.....	57
Figure 4.12: Water velocity past microbe at positions (a) 1 (b) 2 (c) 3 and (d) 4	58
Figure 4.13: Lead shear force profile for microbes at position 1 to 6 for the microbe of 10 μm diameter.....	60
Figure 4.14: Lead shear force profile for microbes at position 1 to 6 for the microbe of 10 μm diameter.....	60
Figure 4.15: Summary of Chapter	62
Figure 5.1: Change of original design towards optimising for cell disruption	64
Figure 5.2: Sequence of chamfer size optimisation for concepts 1-17	65
Figure 5.3: Vena contracta.....	65
Figure 5.4: Creating coordinates to create angle	66
Figure 5.5 : Meshes of (a) concept 0 and (b) concept 1.....	67
Figure 5.6: Water velocity around microbes for position (a) 1, (b) 2, (c) 3 and (d) 4	68
Figure 5.7: Position 2 - Sudden change in microbe pattern at position 2 for concept 1	69
Figure 5.8: Comparison of lead shear for concept 1 and original.....	69
Figure 5.9 : Meshes of (a) concept 1 and (b) concept 2.....	71
Figure 5.10: Water velocity around microbes for position (a) 1, (b) 2, (c) 3 and (d) 4	72

Figure 5.11: Comparison of concept 2 to previous concepts.....	72
Figure 5.12 : Meshes of (a) concept 2 and (b) concept 3.....	73
Figure 5.13: Water velocity around microbes for position (a) 1, (b) 2, (c) 3 and (d) 4.....	74
Figure 5.14: Circulation downstream of microbe at position 2.	75
Figure 5.15: Comparison of concept 3 to previous concepts.....	75
Figure 5.16 : Meshes of (a) concept 3 and (b) concept 4.....	76
Figure 5.17: Water velocity around microbes for position (a) 1, (b) 2.....	77
Figure 5.18: Comparison of concept 4 to previous concepts.....	77
Figure 5.19: Comparisons of concept 3 with subsequent concepts in terms of shear force profiles from microbe position 1-4	78
Figure 5.20: Left chamfer angle and right chamfer angle	79
Figure 5.21: Comparison of shear force profile from microbe position 1-4 for concept 1-7 ..	80
Figure 5.22: Evolution of vena contracta with left and right chamfer change for (a) concept 10 (30°), (b) concept 11 (40°), (c) concept 12 (50°), (d) concept 13 (60°), (d) concept 14 (70°), (d) concept 15 (80°) for the microbe at position 1	81
Figure 5.23: Evolution of vena contracta with left and right chamfer change for (a) concept 10 (30°), (b) concept 11 (40°), (c) concept 12 (50°), (d) concept 13 (60°), (d) concept 14 (70°), (d) concept 15 (80°) for the microbe at position 2	81
Figure 5.24: Shear forces for concept 8 – 17 and for concept 3	82
Figure 5.25: Chamfer angle for concept 8 – 17 and for concept 3 (not to scale)	83
Figure 5.26: Comparison of pressure drop of original concept against optimised concept.....	84
Figure 5.27: Summary of the research process in chapter five.....	86
Figure 6.1: Instructions of material removal with dotted lines and rounding at red circles	90
Figure A.1: The homogeniser (a) full assembly, (b) X-section of valve and turnwheel, (c) axi-symmetric view of valve region and (d) 2-d view of valve region	A-1
Figure B.1: Valve geometry of (a) Nakayama straight and round edge nozzle (Nakayama 1964), (b) Kawaguichi parallel disc setup (Kawaguichi 1971) and (c) Phipps cross section of plane faced valve (Phipps, "The fragmentation of oil drops in emulsions by a high-pressure homogeniser" 1975).	B-1
Figure B.2: Homogeniser Geometry.....	B-2
Figure B.3: Total pressure loss versus gap size calculated based on homogenizer setup used in laboratory.....	B-7
Figure B.4: Modelling setup	B-8
Figure B.5: Solver setup	B-9

Figure B.6: Example of face defined as a 1 st quadrant face as (a) part of a microbe and (b) defined as 1 st quadrant	B-10
Figure B.7: Step 1	B-10
Figure B.8: Step 2	B-11
Figure B.9: Step 3	B-11
Figure B.10: Angle measurement system in (a) general engineering mathematics and (b) Microsoft Excel	B-11
Figure B.11: Step 4 - Angle of face projection (“theta vector”) calculated from face angle (“theta face”) for a 1 st quadrant face	B-12
Figure B.12: Step 5 – Projection of coordinates of face by 1 micron.....	B-12
Step B.13: Step 6 - Exporting of projected coordinates from MS-Excel to Fluent	B-13
Figure B.14: Step 7 – Importing of velocity data and calculation of velocity gradient.....	B-14
Figure B.15: Step 8 – Shear stress calculation.....	B-14
Figure B.16: Step 9 – Calculation of shear forces	B-15
Figure D.1: Simple setup of anaerobic digestion.....	D-1
Figure D.2: LVDT being used to measure the gap size of the homogeniser	D-2

Contents

Chapter 1 - Introduction	1
1.1 Introduction	1
1.2 Motivation and Purpose of Study	2
1.3 Biowell Project	4
1.4 Outline of Thesis	6
1.5 Chapter Summary	7
Chapter 2 – Materials, Equipment and Software	8
2.1 Materials	8
2.1.1 Choice of Fuel	8
2.1.2 Choice of Material for Methane Production	8
2.1.3 Ethics	10
2.2 Equipment and software	10
2.2.2 The Homogeniser – Historical and Types	10
2.2.3 High Pressure Homogeniser	11
2.2.4 Advantages and Disadvantages	12
2.2.5 Computational Fluid Dynamics (CFD)	14
2.3 Chapter 2 Summary	16
Chapter 3 – Literature Review	18
3.1. Introduction	18
3.2. Disruption and breakage theories	18
3.2.1 High Pressure Gradients/Rapid Decompression	18
3.2.2 Turbulence	21
3.3.3 Cavitation	23
3.3.4 Wall Impact and Impingement	25
3.3.5 Shear Stress	28
3.3.6 Others (Number of passes, Separation)	34
3.3.8 Measuring Breakage	35
3.4 Finite Volume Analysis of homogeniser	35
3.5 Suggestions from Other Works	37
3.6 Chapter 3 Summary	40
Chapter 4 – Validation and Simulations	41
4.1 Introduction	41
4.2 Validation	42

4.2.1	Introduction to validation	42
4.2.2	Pressure drop validation	42
4.2.3	Convergence methods for residuals and mesh	47
4.2.4	Preferences for further work carried out	47
4.3	Microbe breakage model	50
4.3.1	Introduction	50
4.3.2	Effective model used.....	50
4.4.	Breakage results	56
4.5.	Optimal setup required.....	60
4.6.	Chapter 4 summary.....	62
Chapter 5 – Optimisation and results		63
5.1	Introduction	63
5.2	Optimisation parameters.....	64
5.2.1	Concepts.....	65
5.2.2	Optimised setup.....	83
5.2.3	Optimised setup versus original design in terms of pressure drop	84
5.3	Chapter 5 summary.....	86
Chapter 6 - Conclusion and recommendations		87
6.1	Conclusions	87
6.2	Recommendations	88
Appendix A – Equipment Specifications.....		A-1
A.1.	Main Features of the Homogeniser	A-1
A.2.	Recommendations for Installing the Gaulin High-Pressure Homogeniser	A-2
A.3.	Starting Up Procedure	A-3
A.4.	Shut Down Procedure.....	A-3
A.5.	Specifications	A-3
Appendix B – Calculations and procedures		B-1
B.1	Empirical validation.....	B-1
B.1.1.	General Expression of Formulae to be Used:	B-1
B.1.2.	Model Descriptions:.....	B-1
B.1.3.	Inlet Region Losses.....	B-2
B.1.4.	Gap Region Losses	B-3
B.1.5.	Exit Region Losses	B-6
B.1.6.	Total Pressure Drop:	B-6

B.2 Pressure drop validation	B-8
B.2.1 Introduction	B-8
B.2.2 Steps Involved in Pressure Drop Validation	B-8
B.3 Microbe Breakage Model ("10D_POS1_m20")	B-9
B.3.1 Introduction	B-9
B.3.2 Shear force calculation steps	B-10
Appendix C - Drawings	C-1
C.1 M20 Model (Original Design)	C-1
C.2 C3 Model (Optimised design)	C-4
Appendix D - Further work	D-1
D.1 Further Work on the Biowell Project	D-1
D.2 Cellrupt project	D-2
References	R-1

Chapter 1 - Introduction

1.1 Introduction

As world oil and fossil fuel supplies are rapidly dwindling, alternative energy sources are becoming of greater need. Other means of energy that were considered overpriced are often no longer the case for today. Even oil regions that were considered not worth the effort are now being considered such as Greenland and Rockall. Finite resources, increased population, environmental aspects, possible carbon trading laws, market and registration limits are all motivations for alternatives. In recent years, many have started to look above the ground for energy reserves. One such energy resource that will be covered in some detail is the maize crop, particularly the stem which is the inedible part. If the dry maize silage is combined with waste water sludge and placed under anaerobic conditions, then methane may be produced. However, the advances of these processes are still in its infancy as yields need to be drastically improved in order to meet the levels for commercial or industrial viability.

One of the most effective means of biogas production found so far has been by means of anaerobic digestion as mentioned. The bacteria in the waste water sludge feeds on the maize silage as well as other suspended solids present in the sludge. If oxygen is present in the environment for the bacteria, the bacteria will produce carbon dioxide. However, if the bacteria are subjected to anaerobic (i.e. oxygen free) conditions, then methane will be produced. As it is near-impossible to have oxygen free conditions for experiments, some carbon dioxide may be produced. In a conventional anaerobic digester, without pre-treatment, primary sludge can be broken down by 60% over 15-20 days, but only 15-20% further breakdown occurs over the same period (Shaw 2009). The slow breakdown of the secondary sludge is believed to be due to the limited metabolic activity of microbial cells with pathogens in a conventional anaerobic digester (Shaw 2009). Similar limitations have been observed with the addition of maize crop. (However this problem is surface area related and forms other work for other members of the research group and hence will not be covered in the thesis.) In terms of sludge pre-treatment, much modification to the homogeniser geometry is necessary to optimise the process of breaking the bacterial cells on small scale but especially with large scale production. This homogenising process will be optimised for microbe breakage as the original valve parts used were based on droplet and fat globule break up. The homogeniser is a machine used for emulsions and suspensions to mix, disperse, and

reduce the sizes of the droplets or particles of the disperse phase. The size of the droplets or particles are reduced after passing through the constricted gap between the valve head and the valve seat. The homogeniser that will be specifically covered for this study is the APV-Gaulin HPH (High Pressure Homogeniser). Figure 1.1 displays the homogeniser with basic flow paths and a 3d section view.

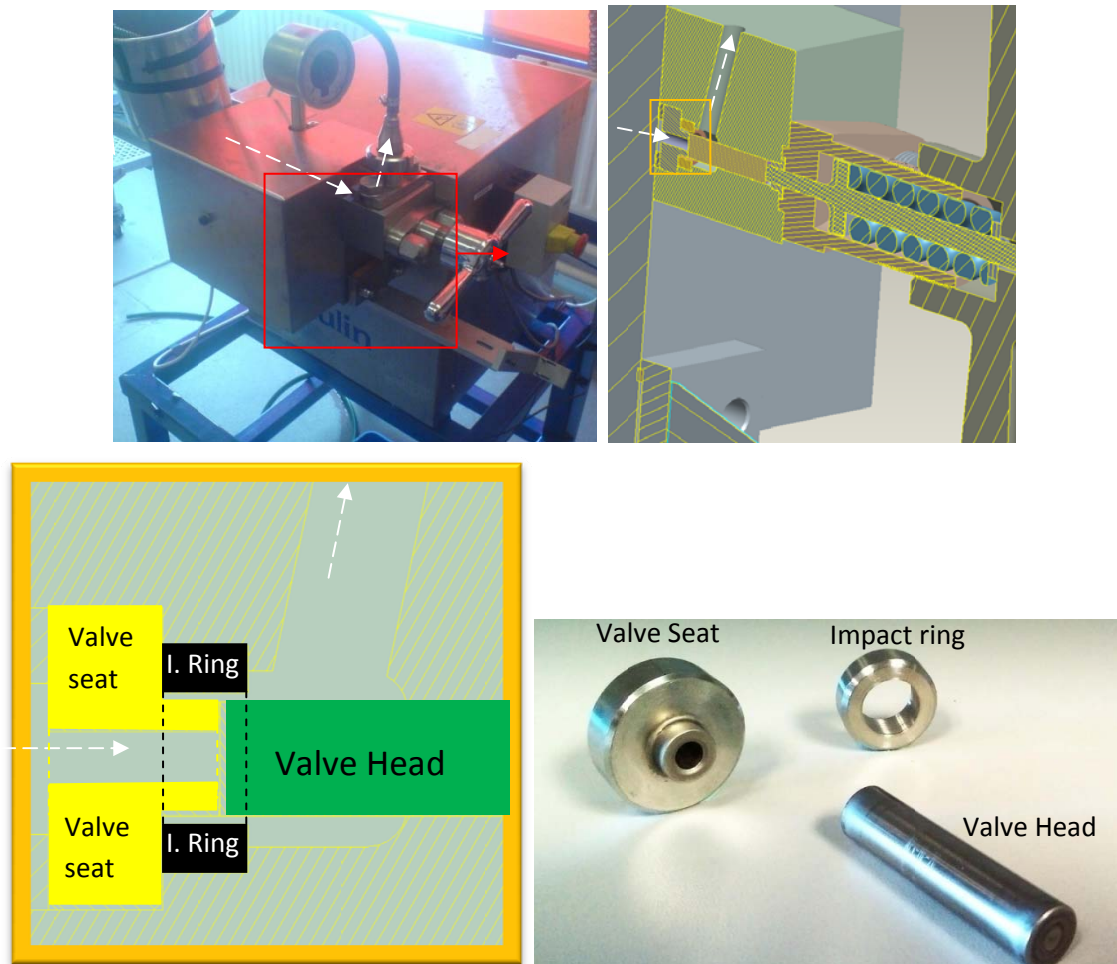


Figure 1.1: (a) Homogeniser machine with (b) pro-engineer 3-d model cross section of the valve parts in yellow, (c) front view x-section of valve gap region and (d) parts of valve gap region

1.2 Motivation and Purpose of Study

Production of methane by means of anaerobic digestion coupled with the homogeniser for waste water sludge and a mechanical pre-treatment for the maize could have potential for a viable alternative energy supply. The methane produced could be easily adapted for electricity production, transport and industry. The maize used can absorb CO₂ in its growing

stage. However, high amounts of land for the crop are required. Also, yields of crop can vary with environmental conditions (high yields in summer and low yields in winter). Current yields are not satisfactory for large scale production. Therefore, methods must be implemented to maximise the use of the land by increasing the efficiency of the process. Another problem is that large digester volumes are required for large scale production. This problem is caused by excess sludge growth and the production of solids not useful for biogas production. Sludge growth can be controlled by keeping the population of bacteria and highly propagating pathogens at a lower level and thus a reduction in digester size can be achieved. The homogeniser can breakdown tough microbes and pathogens in secondary sludge that do not greatly aid the yield of biogas and thus aid yield rates of anaerobic digestion. Simultaneous treatment of harmful pathogens could be carried out reducing the problem of excess sludge growth which would be ecologically undesirable after anaerobic digestion.

It is also worth noting that the methodologies outlined in this thesis are applicable to many industries such as the brewing, food, chemical and biopharmaceutical industries as the principles for microbe breakage are also applicable to cell breakage. The following pie chart depicts the percentage breakdown, by use, of anaerobic digestion related processes in the United Kingdom (Asia Biogas 2008).

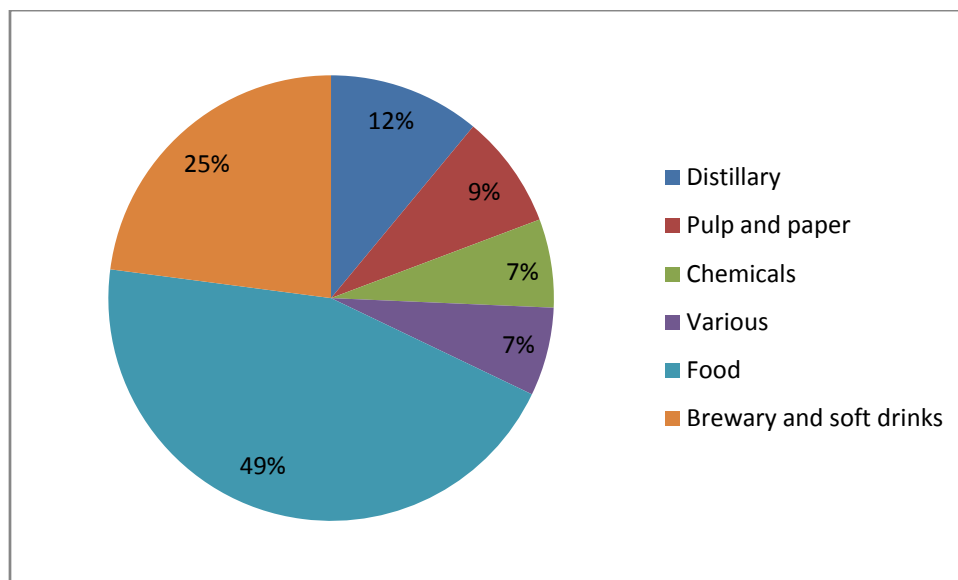


Figure 1.2: Use of anaerobic digestion processes according to industry in the United Kingdom (Asia Biogas 2008)

The role of the homogeniser could be a vital key in increasing overall yield efficiency. By breaking apart bacterial cells or microbes that store valuable organic material using homogenisation, increased efficiency in terms of sludge treatment and methane output per volume could be achieved without substantial processing costs. The purpose of this study is notified below:

- To create a CFD model of the current homogeniser design used in industry using **Gambit 2.3** and accurately determine pressure drops and flow fields using **Fluent 6.3** validated from experimental results and empirical formulae initially for water. Fluent 6.3.26 is chosen over Ansys CFX because details about boundary layers can be captured more accurately according to a comparative study carried out (O'Reilly 2007).
- To extend the finite volume model of the homogeniser to include microbes and determine criteria for measuring breakage. The microbe geometries used will be constant with the diameter based on the geometry of yeast cells.
- Based on the criteria for microbe breakage, a strategy must be developed that can be used for comparison when the microbe is at a different location or in a different homogeniser.
- Obtain the optimal geometries for breakage of microbes. Present the optimal conditions in **Pro-Engineer**.

1.3 Biowell Project

The Biowell project originated as a means study to obtain increased methane yields from biomass using anaerobic digestion. The nature of the biomass that was to be studied was not specified at first but was determined to be either maize or waste water sludge. Increasing the reactant surface area would increase methane production rate and overall production. The homogeniser was suggested as a means of breaking up the biomass, but when the biomass was specified as maize, problems were encountered in using the homogenizer with this material. Another mechanical pre-treatment process was subsequently used to break the maize silage. That work will not be included in the thesis. The study on homogenisers was continued with attempts being made to measure the gap size. This explained why they homogenizer is unsuitable for maize unless a further pre-treatment stage was included in the

process. It was found that homogenizers are more more suitable as a pre-treatment step for waste water sludges similar to the patented *Microsludge[™]* process (US *Patent* No. 6013183) as in figure 1.3 with the exceptions of no chemical additives and the implementation of maize and maize pre-treatment as in figure 1.4.

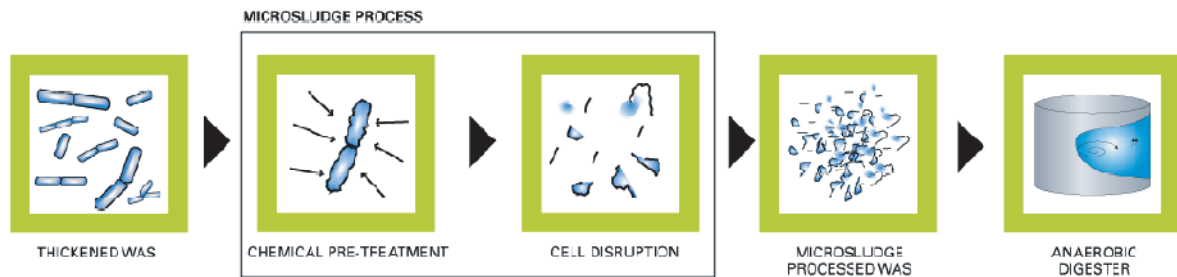


Figure 1.3: Simplified process flow schematic of the Microsludge process (R. L. Stevenson 2007)

Thus, this thesis covers the optimisation of a homogeniser to break up and disrupt microbes. A diagram is provided to show how the optimised homogeniser process is related to the Biowell project in figure 1.4.

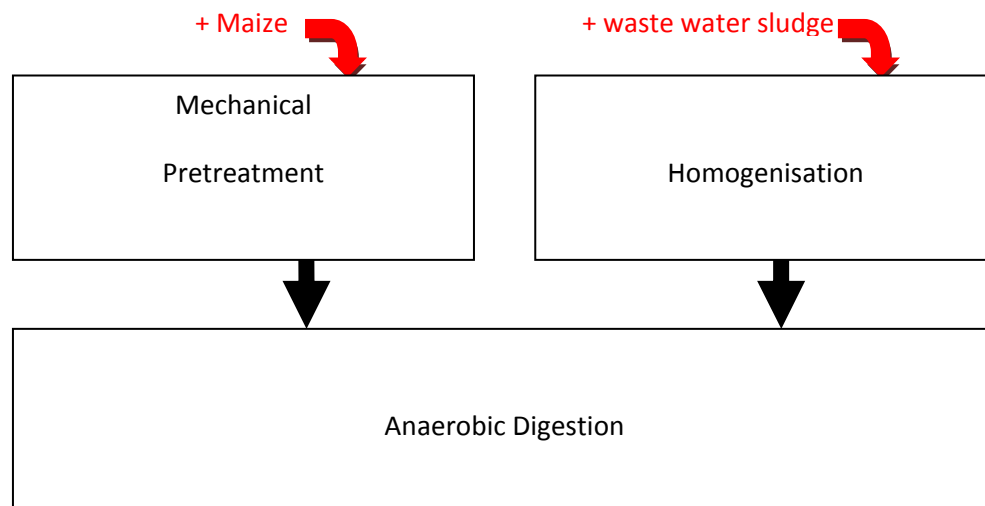


Figure 1.4: How the homogeniser is related to the overall Biowell project process for increased methane production from anaerobic digestion

1.4 Outline of Thesis

The work produced in the thesis is split up into six chapters. A brief summary of each chapter is presented in Figure 1.1. At the end of each chapter, this summary is presented with the contents of the current chapter expanded in greater detail. The following chapters in the thesis are laid out as below:

- Chapter Two: Literature review of why methane was chosen as a gas to produce. The homogeniser is also explained in terms of operation and function.
- Chapter Three: Previous studies of homogeniser flow relevant to this thesis are included in this chapter. Theories on different causes of microbe and cell breakage are discussed. The preparation of the Finite Element CFD model of the homogeniser is also provided in this chapter.
- Chapter Four: Results of effects of changing gap size for water are displayed. Comparison of CFD results with theory and experiments are included as well as information on convergence of meshes and residuals. Explanation of phenomena as well as changes in flow patterns are explained and compared. The method used for calculating microbe shear force are provided as well as results from the original configuration for microbe shear measurement are disclosed.
- Chapter Five: Justification of optimisation strategies and optimal dimensions of homogeniser valve for bacterial cell breakage
- Chapter Six: Conclusion and Recommendations

1.5 Chapter Summary

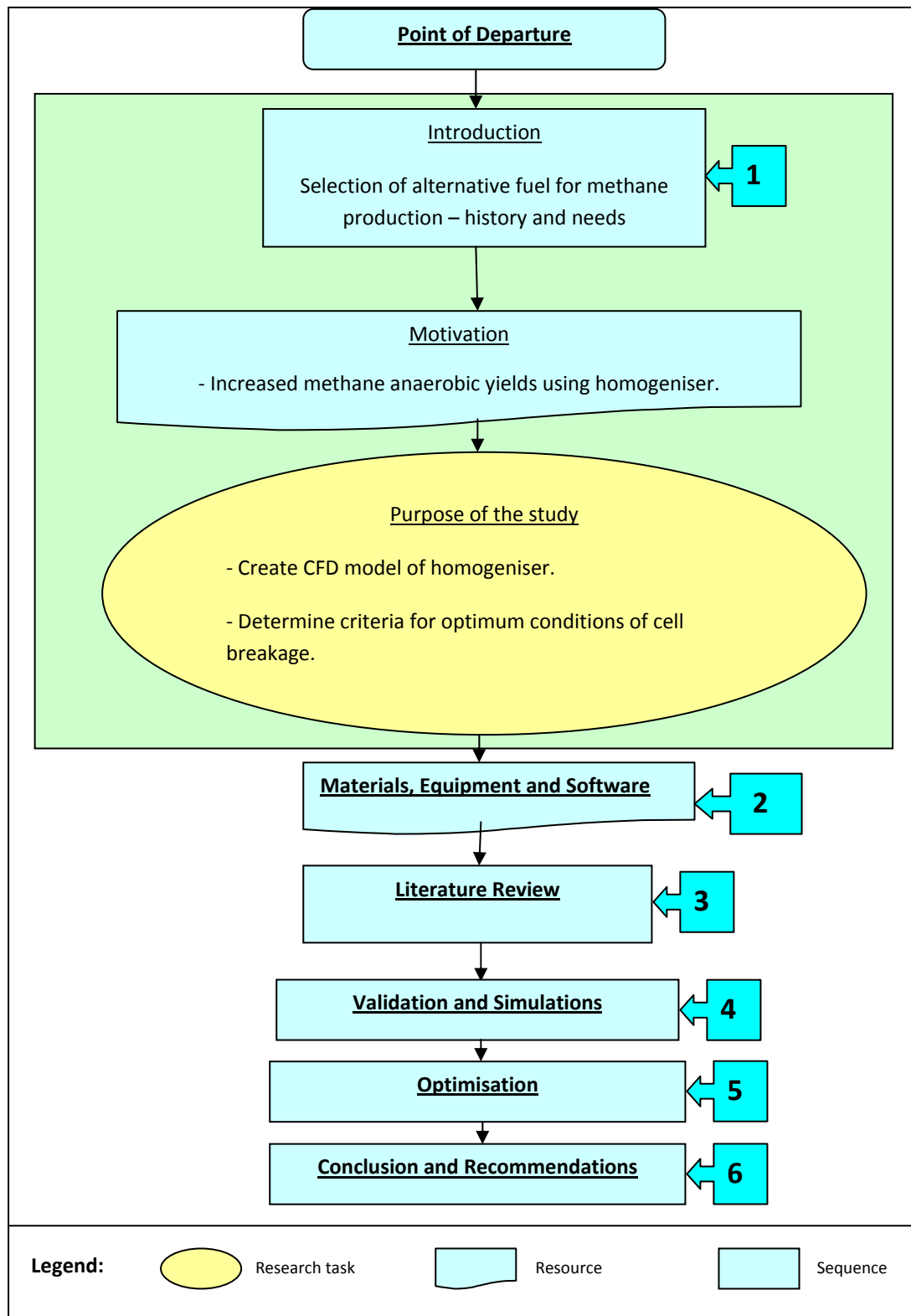


Figure 1.5: Summary of the research process in thesis.

Chapter 2 – Materials, Equipment and Software

2.1 Materials

2.1.1 Choice of Fuel

Methane was the choice of fuel to be used in this study as high yields can be obtained from anaerobic digestion. Methane is a green house gas but much of the carbon dioxide that is produced is offset by the growing of the maize crop. Minimal carbon dioxide is produced in the methane producing process as outlined in section 1.3 (as an ideal vacuum of no oxygen cannot be obtained). This is much different to petroleum and gas processes where carbon dioxide is produced during processing as well as consumption. More details on alternative fuels such as hydrogen, alcohols, electricity, coal, petrol and diesel can be obtained from Slessor and Lewis (Slessor 1979)

2.1.2 Choice of Material for Methane Production

Waste water sludge was the primary material of choice for methane production as it is one of the most common inputs for methane production behind direct gas sources. As outlined in section 1.2, there are many instances and industries where waste water sludge is a by-product. Maize is selected also for aiding the methane anaerobic process as this crop is commonly used in the biofuel industry. Maize can also be easily grown in many different climates. Maize gives off a more pleasant smell than other alternatives thus making it suitable in laboratory rooms for research. The parts of the maize crop that are not edible by humans are the best parts for methane production such as the kernal and stems as experienced from experiments carried out for the Biowell Project. This may help combat much of the issues of the ethical debate of fuel versus food. However, if lignin is to be kept at a minimum (lignin inhibits anaerobic methane production yield rates), the crops must be picked earlier than the edible part can develop. However, much negative publicity has been developed with the sharp increases in maize costs at the same time of biofuel from maize development. More

details on alternative materials such as potato, cassava, sugar beet, wood and yams is available from Slessor and Lewis (Slessor 1979).

2.1.3 Ethics

As mentioned in section 2.1.2, the food versus fuel debate dominates the scope of ethics for this project. It is worth noting that waste water sludge does not affect food supplies and decreases levels of wastage. Carbon dioxide is absorbed by the growing of the maize crop such that the overall carbon footprint of methane consumption would be less than usual. Other considerations include pollution involved in transporting as well as free information between states and academic bodies for the advancement of the technology.

2.2 Equipment and software

2.2.2 The Homogeniser – Historical and Types

The homogeniser is a machine that is commonly used in the dairy industry to break up milk fat and thus increase the shelf life. The homogeniser was invented in 1900 and was later presented at the world fair in Paris (French patent no. 295.296 n.d.).

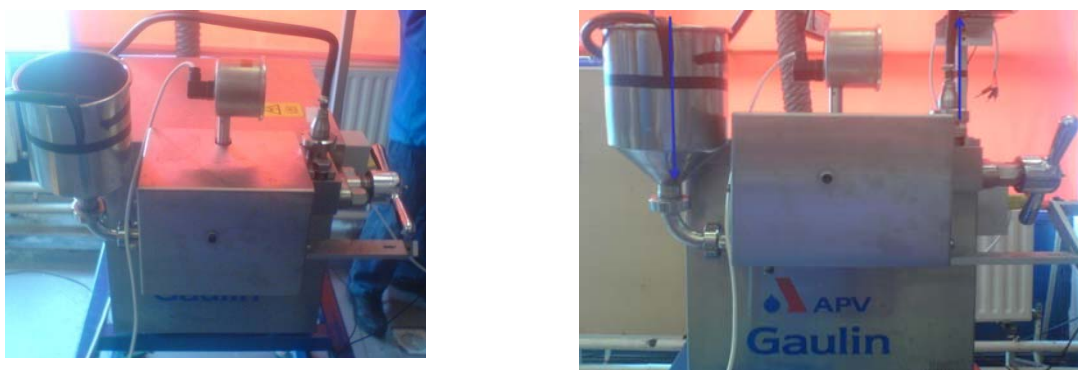


Figure 2.1: (a) Plan View and (b) front view of homogeniser studied

There are many types of equipment used for homogenisation of mixtures and suspensions. These include high shear homogenisers, ultrasound homogenisers and stirred ball mill.

2.2.3 High Pressure Homogeniser

The homogeniser is also used in the biotechnology industry to improve yield consistency. The homogeniser that will be specifically covered for this study is the APV-Gaulin HPH (High Pressure Homogeniser). Other homogenisers include the Stansted HSH (High Speed Homogeniser) and Avestin MicrofluidTM.

There is much disagreement of the use of the term high pressure homogeniser. For the earlier versions of homogenisers, high pressure could be termed for pressures of around 30 MPa but today it is common to see operating pressures of above 150. Some homogenisers are capable of homogenising pressures of above 300 MPa (Diels 2006). This means that phenomena of turbulent flow is becoming more and more pronounced particularly in the exit region of the homogeniser (see appendix A) making experimental measurements of flow in this equipment more difficult. However, with advancements in CFD, many turbulent flow phenomena such as eddies, swirl and vortices can be numerically described with sufficient accuracy.

The three regions that will be mentioned frequently in this study are the inlet region, gap region and exit region. The inlet region is from the inlet to the start of the gap in the computational domain. The gap region is the region covering the gap between the valve head and valve seat. The exit region is the region between the inner surface of the impact ring and the horizontal outer surfaces of the valve head and valve seat just after the gap region exit. The exact locations of the valve regions in the homogeniser are displayed in Fig. 2.2.

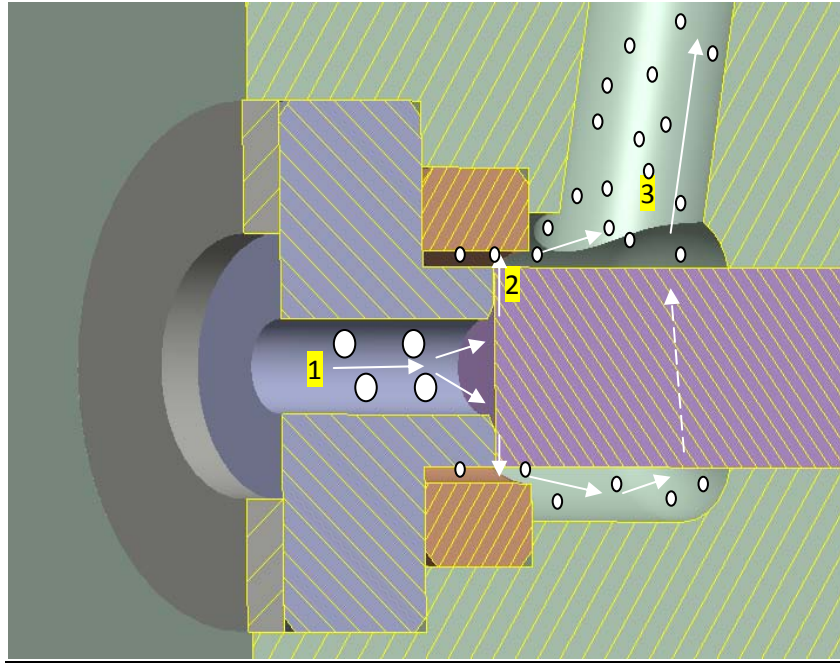


Figure 2.2: XY section of homogeniser valve region

The homogeniser (Fig. 2.2) works by.

1. The fluid is introduced and passes through the valve seat in the axial direction (inlet region).
2. The fluid passes through the gap formed between the face of the fixed valve seat and the adjustable valve head face (gap region).
3. The fluid exits the gap region and travels towards the outlet (exit region).

2.2.4 Advantages and Disadvantages

The advantages of using the high pressure homogeniser include high gap velocities and flexibility to be used with many different fluids. In addition, the valve parts are inexpensive to change and replace. Multiple cylinders allow almost constant flow rate. There are very few issues of reactivity of stainless steel with many products in the homogeniser which makes it suitable for many applications in the food and pharmaceutical industry. If there is possibilities of reaction of stainless steel with the fluid or mixture passing, zirconium could be used for the valve parts. There is mass supply of homogenisers making homogenisers inexpensive

machinery when considering the specifications that are supplied. Kopp et al (Kopp 1997) compared the effectiveness of the high-pressure homogeniser with the stirred ball mill, shear gap homogeniser and non-treatment. It was found by experimental methods that the high-pressure homogeniser was the most effective pre-treatment method in terms of degree of degradation, gas production and waste sludge produced. The reduced costs in reduced wastage as well as reduced digester volume required may make this technology practically useable for industry. Mechanical disruption can be effective within a few passes of the homogeniser while chemically, this can take days or even weeks.

A disadvantage of the homogeniser is that the measurement of the gap size between the valve seat and the valve head has been found to be very difficult from experience as the valve gap changes radically as the machine operates. This was particularly observed as the gap was reduced below 15 μm . It is the author's personal opinion that one such cause may be due to the presence of a safety spring between the turning wheel and the valve head as the gap is reduced while increased force could be applied to this spring. There are also vibrations due to the motor operating which is found also from observation to affect gap size measurement when using an LVDT at the end of the turning wheel. However, replacing plastic parts with metal parts and changing the LVDT bracket geometries to reduce vibrations appeared to have solved this problem. There is much inefficiency in the exit region due to high levels of turbulence found. There are heat losses in the gap region, especially as the gap size between the valve head and the valve seat is reduced. This was found in Table 4.1 in section 4.2.2 as the temperature of the water increased to 33°C during operation. Due to cells being broken completely by mechanical disruption, separation of products of interest is extremely difficult due to mixture of cell parts and debris production (Naglak 1990). Also there is risk that some desired released product may be denatured due to the levels of heat present (W. M. Kelly 2004).

2.2.5 Computational Fluid Dynamics (CFD)

Computational fluid dynamics is the study and analysis of fluid flow phenomena with the aid of computer algorithms and equations. Some of these phenomena include eddies, stagnation and interference as shown in figure 2.3.

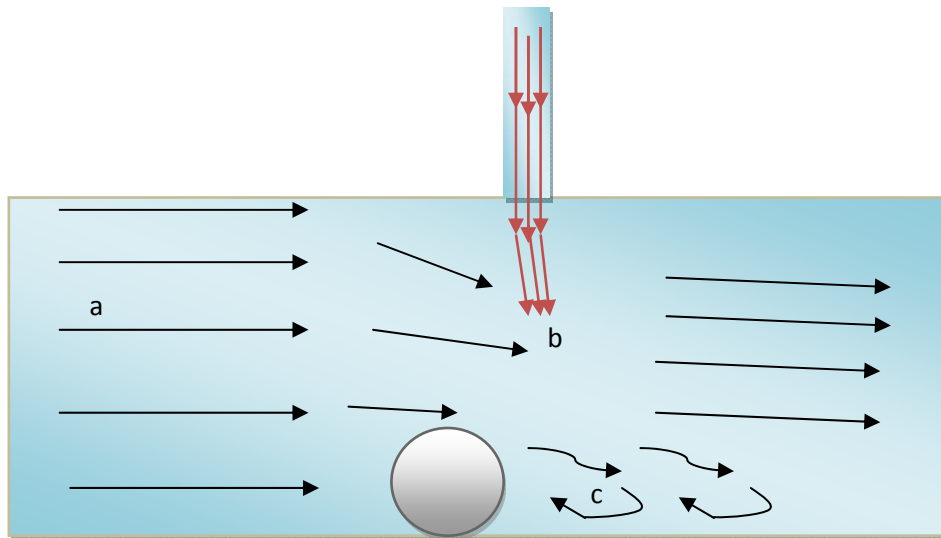


Figure 2.3: Fluid flow properties of (a) movement, (b) interference and (c) eddies

Some of the phenomena mentioned can be investigated with rapid photography but this is limited in terms of quantifying fluid movement properties such as pressure, velocity and shear forces. But rapid photography can still give a good insight into what vortex shedding looks like as seen in figure 2.4.

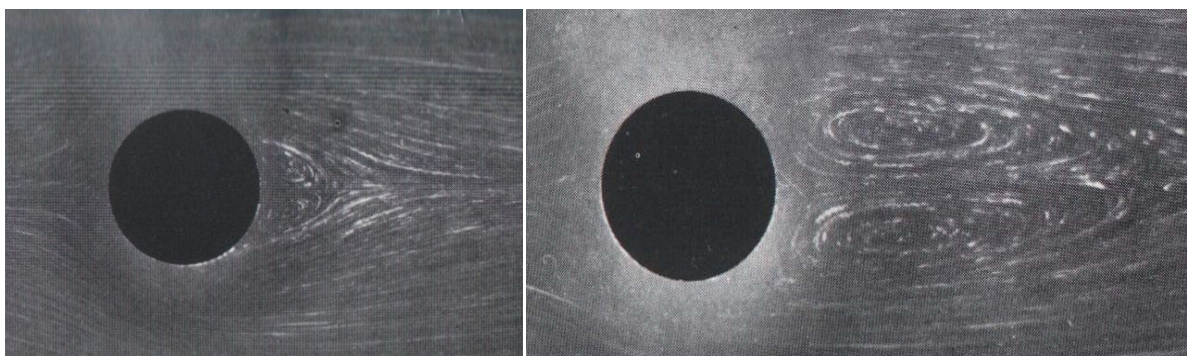


Figure 2.4: Flow around internal obstacle at Reynold's number 13.5 and 39.0 (Taneda 1956).

Unfortunately, as turbulence increases, the ability of computational fluid dynamics software to accurately capture the phenomena of vortex shedding (figure 2.5) is quite difficult due to limitations in computer performance and the number of different solvers available. Therefore, there is much room for improvement of CFD technology so that commercial desktops can be powerful enough to accurately estimate turbulent phenomena through more affordable high performance hardware and more efficient solver methods.

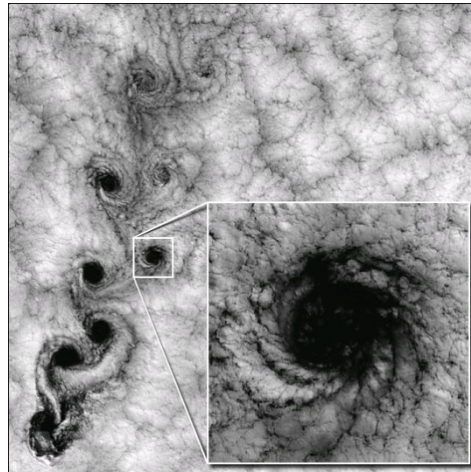


Figure 2.5: Vortex shedding (NASA 2000).

Fluent today uses the finite volume code and covers many different types of flow such as compressible, incompressible, multi-phase, multi-species, discrete phase, and transport model flow. More information on the mathematics involved as well as other models used can be found in the fluent user manual (Fluent Inc 2007).

2.3 Chapter 2 Summary

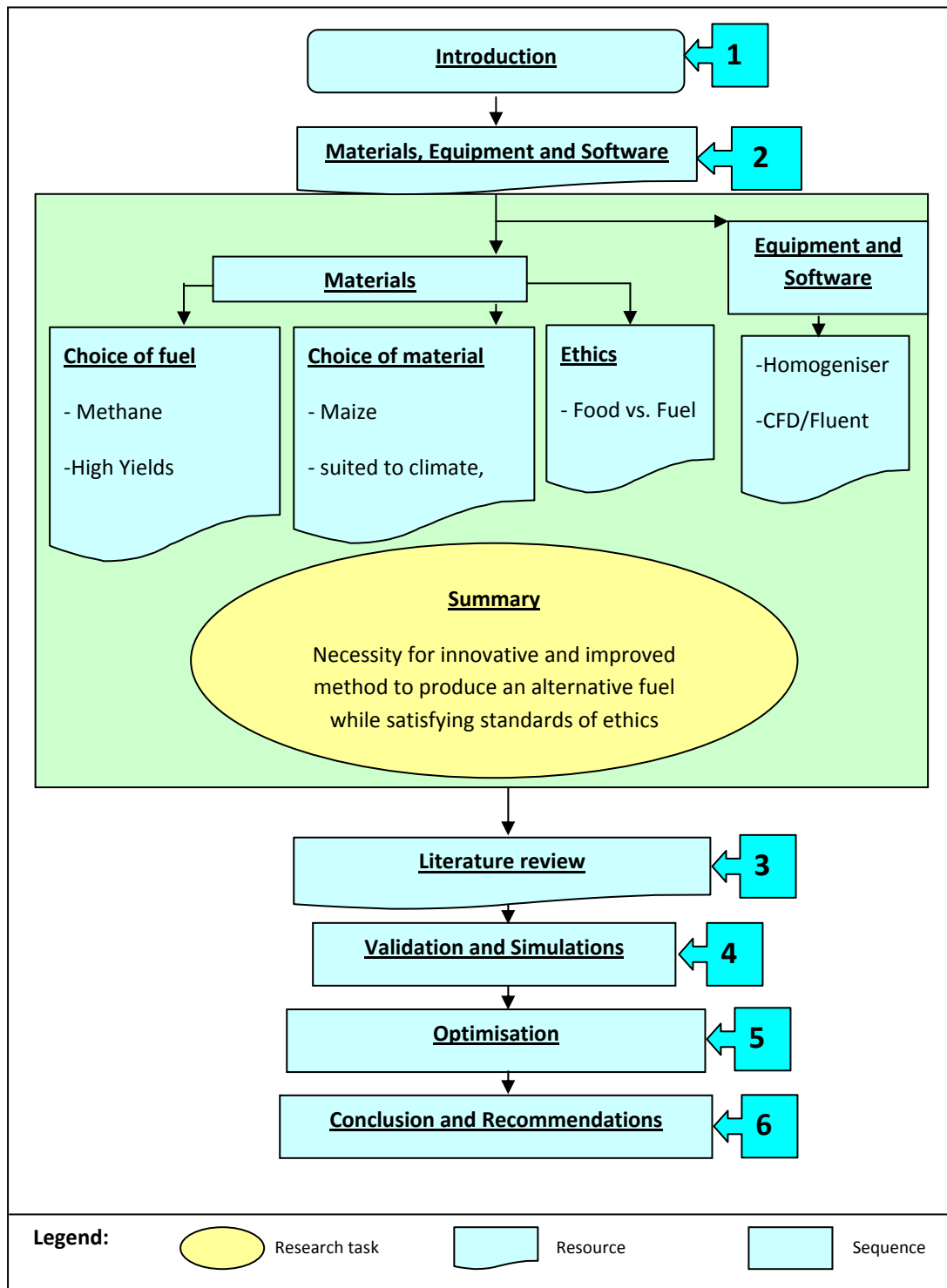


Figure 2.6: Summary of the research process in chapter two.

Chapter 3 – Literature Review

3.1. Introduction

Many works have been carried out on the homogeniser in order to understand the exact mechanisms and causes of breakage. The mechanism of disruption and breakage of microbes has been investigated in detail by many researchers. Much literature has been created in the past regarding the exact causes of breakage and disruption but there has been much disagreement.

3.2. Disruption and breakage theories

3.2.1 High Pressure Gradients/Rapid Decompression

A hypothesis was disclosed by Brookman (J. Brookman 1974) in order to explain cell rupture by rapid pressure release when microbes are passed through the high-pressure homogeniser. These variable pressure gradients can be comparably seen with Kleinig and Middelberg (Kleinig A.R. 1996) in figures 3.1(a) and 3.1(b). Results seen in Figure 3.1 shows that the rate of decompression slows down as the operating pressure reduces to atmospheric pressure.

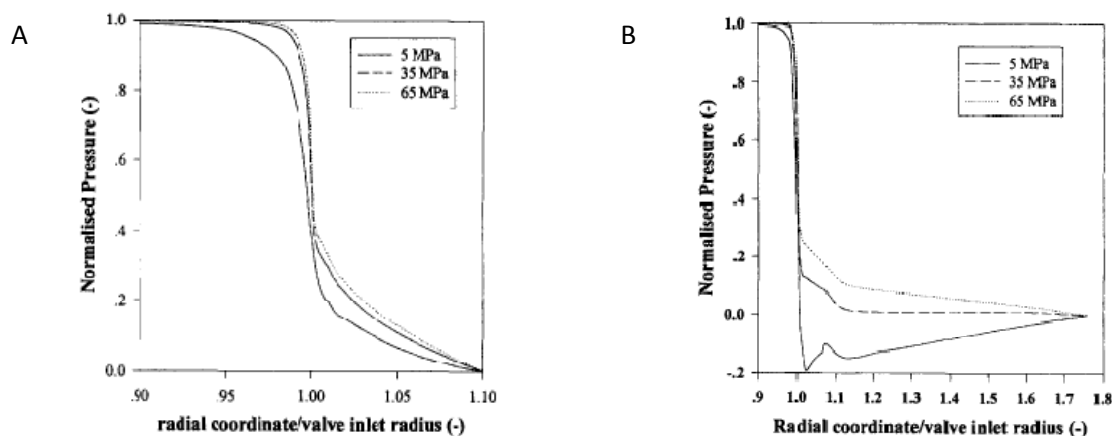


Figure 3.1: Kleinig's results (Kleinig A.R. 1996) of (a) normalised pressure across the centre plane of the valve gap for the rounded valve seat inlet and (b) for the square-edged valve seat at the inlet.

Computational fluid dynamics was used to indicate static pressure estimation for a selected flow streamline as validation for results in figure 3.2 as experimental validation and measurement within the valve was not feasible. These calculated CFD results for pressure drop were based on the homogeniser dimensions and flow rate used in the DCU laboratory as displayed in Figure 3.2. Results found from CFD work was found to closely correlate behaviour expressed by Kleinig (Kleinig A.R. 1996) as in fig. 3.1. It is worth noting that the zero pressure at the end of the streamline is artificially created by the pressure outlet boundary condition in the CFD model.

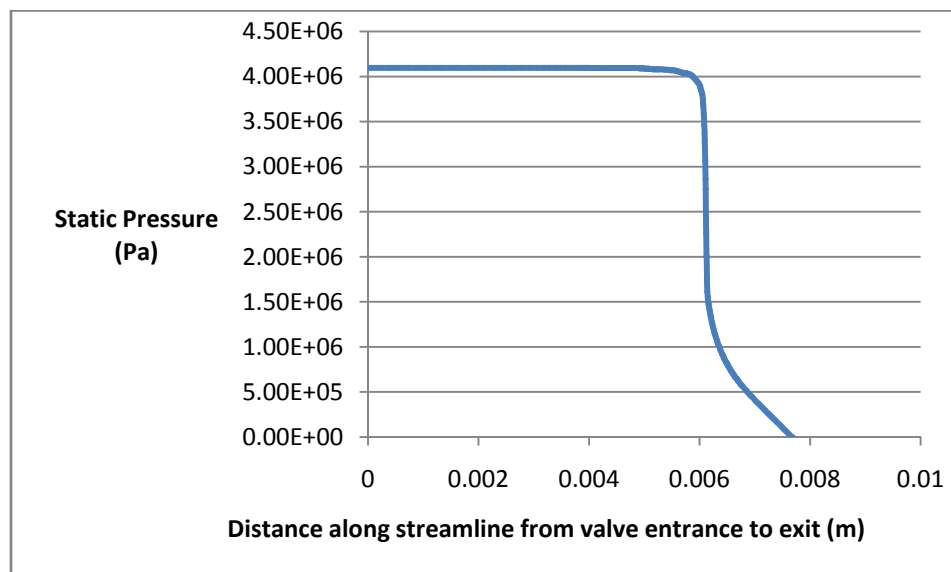


Figure 3.2: Pressure gradient of liquid passing through the homogeniser valve based on CFD results

On inspection of Brookmans work (J. Brookman 1975), it may have been assumed that the microbes reduce in size and deform under this intense pressure gradient with microbial expansion with the pressure release. If the decompression rate is sufficient, the subsequent momentum of expansion could be such that wall tensile strengths could be exceeded, thus leading to cell rupture. The slope of the graph can be used to estimate the rate of pressure drop per unit distance which was found to be 22,400 $([3.8\text{e}6-1.61\text{e}6]/[0.06-0.0061])$. However the speed of decompression is more appropriately understood as the rate of pressure change per unit time. Therefore calculations of multiplying the slope of the graph by the velocity of fluid at the gap entrance was calculated as 1657600 Pa/s (equals 1.6 MPa/s) based on a 20 micron valve gap size with 74 m/s fluid velocity. Results as displayed in figure 3.1 and 3.2 show that the rate of decompression slows down as the pressure reaches atmospheric.

Therefore there is little chance of a momentum building up causing an overshoot effect so that the cell could be placed in tension.

After these ideas were introduced by Brookman, various conclusions about these ideas can now be drawn based on expertise from the research group and further experimentation. Firstly, the contents of cells are presently known to have compressibility properties equivalent to water. Thus deformation by intense pressure gradients is nearly negligible.

Secondly, if dissolved gases are present, the damaging effects of decompression can be shown to be much greater. Today, the damage to cell walls is interpreted as most likely to be due to the forming of gas bubbles inside cell walls. These gas bubbles eventually cause rupture by tensile stresses along the wall. A suggestion of obtaining this equivalent effect on the small scale processes is to pump soluble gases at high pressure into the fluid to allow large quantities of gases to be dissolved. When the high pressure is released, solubility of the fluid is reduced and gas bubbles are released with some forming in cell walls. It has been reported that cell rupture by this effect can be maximised when the suspension is maintained at a high pressure for over an hour by allowing migration of gas by diffusion throughout the suspension and inside cells (Debs-Louka 1999). This effect is unlikely to occur in homogenisers as the liquid is compressed, not the gas and homogeniser high pressure cycles typically last under a few seconds.

It has been noticed that high pressures have a sterilising effect, probably by damaging the various microbes spores (Lenihan 2004). However, this appears to depend on the pressure magnitude and not on the rate of decompression and only at high temperatures, even though the temperatures are less than those thought to cause sterilisation at atmospheric pressures. It is therefore unlikely that the hypothesis by Brookman (J. Brookman 1975) that cell rupture caused by rapid decompression is occurring in the high pressure homogeniser. It has been previously rejected by Doulah et al (Doulah 1975) and Engler (Engler 1981).

By empirical evidences, the hypothesis seems to have been adopted by the approaches by Kleinig and Middelberg (Kleinig A.R. 1996) and Kelly et al (W. e. Kelly 2002). The logic for this is based on a better correlation between the extent of cell rupture (measured by protein released) and the maximum pressure gradient (figure 3.3) than there is between cell rupture and operational pressure. However this perceived improvement in correlation cannot be chained to pressure gradients above all other parameters. The same improvement in

correlation may be observed by the relation of cell rupture with the reciprocal of the gap size cubed, or cell rupture with the gap fluid velocity cubed.

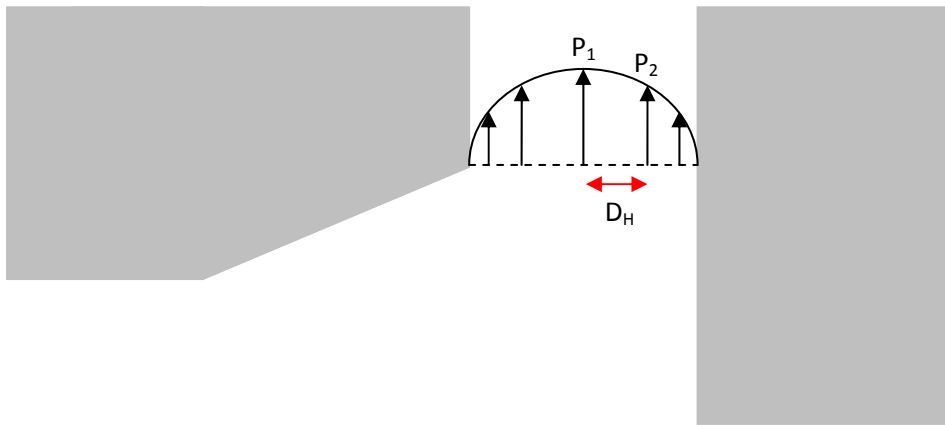


Figure 3.3: How the pressure gradient is found

A further limiting assumption has been inserted by Kelly et al (W. e. Kelly 2002) by basing results of cell breakage against pressure gradient with only short impact distances and high viscosities. Also the linear relationship of cell rupture and pressure gradient is based on only four experimental points with large impact distances and low viscosities.

3.2.2 Turbulence

Turbulence was hypothesised by Doulah et al (Doulah 1975) as being the greatest influence on homogeniser cell disruption. Success was obtained from this hypothesis, by obtaining a mathematical expression predicting the protein release which closely matched experimental results. The turbulence effects produced in a homogeniser consists totally random with no dominating frequency of oscillation. The equipment therefore must operate in a different way from other disruptors such as ones which use ultrasonic energy at a specific frequency and other equipment which relies on vibration tuned to cause intense resonance at a highly specific frequency. These designs can cause cell breakage of a highly specific size range.

According to Doulah, if the energy of turbulence exceeds the minimum energy required to break the cell wall, disruption could occur. At the time, Doulah stated that both the homogeniser turbulence characteristics and physical properties such as the cell wall breaking

stress were not known. In the hypothesis, the cells were assumed to be the same as liquid droplets and the cell wall was thought to be equivalent to a high surface tension. More recently, these experimental factors have been measured. The turbulence characteristics was estimated with cell wall breaking stress from bond breaking forces of the order 6×10^{-5} dynes which is equivalent to 6×10^{-10} N based on cellulose fibres (Prescott 2008). The hypothesis by Doulah was rejected by Engler and Robinson (Engler 1981) using experimental results with yeast. It was concluded that turbulent eddies did not have sufficient energy for cell disruption.

In the case of liquid droplets, fragmentation will occur when the energy associated with an eddy of the right size exceeding the droplet surface energy. With a microbial cell, the situation is increased with complexity. Even if a single occurrence of a violent eddy causes the bond between various molecular chains in the cell wall to be broken (the bonds being hydrogen bonding and Van der Waals forces), that would not by itself cause complete fragmentation of the whole cell wall. There would also have to follow a process of pulling and twisting to allow one molecular chain to be gradually pulled away from its neighbours, and then similar activity with many other molecular chains until the cell wall could be said to be disintegrated. There is evidence that glucan molecules in the yeast cell wall are arranged in triple helices. (Prescott 2008) While experimental evidence indicates that there is not sufficient energy to cause the initial bond to be broken between these molecules, it is probable that turbulence plays an important role in supplying the energy for the subsequent, gradual pulling apart of a molecular chain from its neighbours, once the initial bond has been broken.

The same argument of insufficient energy intensity could also be applied to the principle of using ultrasonic energy inputs within the homogeniser. Tuned vibration would also be ineffective as one frequency can only break microbes of a highly specific size range. As microbes and cells passing have very different diameters, this method would also be ineffective. According to Walstra and Smolders (Walstra 1998) turbulent flow is more likely if there is a large flow rate as found in a large scale homogenisation operation.

3.3.3 Cavitation

An explanation of cavitation was provided by Brennen (Brennen 1995). When the pressure in a pure liquid decreases below the vapour pressure of the liquid, at a given temperature, there is a tendency for vapour bubbles to form on favourable nucleation sites such as irregularities on a surface. As will be later described, when the pressure is increased again, the bubbles will collapse. According to Balasundaram (S. H. B. Balasundaram 2006), it is during this bubble collapsing phenomenon that conditions are generated which would allow cell wall breakage to occur, and therefore cavitation could be a mechanism for cell wall rupture. Gas cavities collapse when the downstream pressure of the gap recovers. The collapse of such bubbles can be studied more easily if it is assumed that the bubble has become detached from the surface irregularity (as is regularly the case) and is flowing freely in the liquid before the external pressure is increased. The bubble will often be found to be spherical.

The size of the bubble is governed by the balance of forces. The force of the vapour pressure tending to make the bubble larger is the pressure inside the bubble is higher than the pressure in the surrounding fluid. The force opposing this vapour pressure force is the surface tension of the liquid. When the external pressure in the surrounding liquid is increased, there is a change in the balance of forces, and the internal bubble pressure is no longer so much greater than the pressure in the surrounding liquid. Thus, the force tending to make the bubble larger is reduced and bubble gets smaller. It would appear to be a reasonable assumption that a new equilibrium position could be reached for a static bubble size. In practice, this does not happen (Prescott 2008). If a gas was trapped inside the bubble, the reduction in its size would cause an increase in the pressure of the gas and so a higher pressure would be created to oppose the surface tension force that is reducing its size. But this cannot happen inside a bubble containing only the liquid vapour. Its pressure is fixed at the vapour pressure which can only change if the temperature changes. The result therefore is that the bubble continues to reduce in size and the surface tension force becomes stronger in comparison to the difference in pressure between the inside and the outside of the bubble. Therefore the rate of reduction in size becomes greater as the bubble reduces in size, and so the bubble collapses and then catastrophically collapses.

The violent collapse of bubbles explains why unusual results can be found from cavitation. Although the volume of the collapsing bubble is very small, the forces causing the collapse escalate to such high values that the produced energy density is very large. It is estimated that temperatures of 40000 times ambient pressure can be reached (Brennen 1995). This is sufficient to form free chemical radicals, and explains why the iodide ion is converted first into an iodine radical and then forms molecular iodine (Kondo 1988).

It is quite difficult to produce a liquid which has no dissolved gases in it, and it is much more typical for a certain amount of gas to be present also. It is stated by Henry's law that the solubility of a gas is proportional to the pressure in the liquid. Therefore as the external pressure in a liquid is decreased, the solubility of the gas decreases also, and so gas bubbles often can be found in liquids under reduced pressure. When the external pressure is increased again, the bubbles reduce in size, but in this case there will be a gas trapped inside the bubble, so that the pressure inside the bubble will increase as it collapses and this will tend to slow down the total collapse of the cell or microbe. Therefore when dissolved gases are present, a phenomenon similar to cavitation takes place, but the violence of the bubble collapse is reduced, and if there are large quantities of dissolved gases present, the cavitation-like phenomenon produces much more gentle and gradual reduction in bubble size (Prescott 2008). When very small amounts of dissolved gases are present, serious damage can be done by cavitation-like phenomena to equipment such as ship propellers, pumps and turbo machinery. However, it is most unlikely that cell rupture of microbes will occur in environments by cavitation where there are larger amounts of gases present as seen with suspensions containing microbes.

The metabolism of microbes may involve aerobic respiration which depends on dissolved gases being present in the surrounding fluid. Even when the metabolism involves anaerobic reactions, one of the end products is always carbon dioxide which must be released into the surrounding liquid in dissolved form. The amount of dissolved gases can be often assessed by observing the nature of the cell suspension after homogenisation. This is because the dissolved protein acts as a surface active agent and stabilises the bubbles once formed such that a stable froth is often produced (Prescott 2008). It seems therefore unlikely that cavitation-like phenomenon could be sufficiently violent to cause cell rupture unless the surrounding liquid has undergone some treatment to remove dissolved gases, for instance, by increasing the pH to a very high value. In true cavitation, there are no dissolved gases

present. In view of this, it is strange that cavitation is so often suggested as an explanation for cell rupture in homogenisation. The cavitation inception number (Harrison 1992) is defined in terms of the vapour pressure of pure water and while it might be legitimately applied to different experimental setups (S. T. B. Balasundaram 2008), it is also applied to cell rupture work despite the fact that bubbles observed in regions of low pressure must consist almost entirely of dissolved gases. The remarks of Phipps (Phipps, "The fragmentation of oil drops in emulsions by a high-pressure homogeniser" 1975), (Phipps 1974a) about cavitation in a homogeniser were given in context of studies of oil droplet breakup and not for cell rupture. He stated that cavitation and separation flow effects are more likely to be found for square edge valve seats than rounded valve seats. Also the existence and extent of cavitation has been determined empirically by measuring the amount of iodine which has converted from dissolved potassium iodide (Shirgaonkar 1998) as a solution was passed through a homogeniser. However this can only be applicable for cell rupture analysis if steps are taken to exclude dissolved gases in microbial suspensions.

Because of the existence of large quantities of dissolved gases in cell suspensions in most of the studies of cell rupture, it would seem appropriate to modify the computational fluid dynamics model to allow for special effects which occur once the external pressure falls below atmospheric. Under these circumstances of reduced external pressure below atmospheric as stated previously, gas bubbles will begin to appear such that the flow characteristics are altered radically. While the pressure is above atmospheric, the continuity equation can be simplified to predict that there will be no change in the fluid density and that it is incompressible. Because of this, it is most unlikely that the pressure can fall to values approaching the vapour pressure of water and cause cavitation in the gap region where it could cause more extensive damage.

3.3.4 Wall Impact and Impingement

Kelly (W. M. Kelly 2004) considered the case of cell breakage in a homogeniser taking place at low operating pressure in liquids of low viscosity. His argument stated that the mechanisms of turbulence, pressure gradients and shear stresses could not be the cause of cell breakage because his analysis predicted that no breakage should occur under these

mentioned operating conditions. However cell breakage was observed under these conditions but Kelly (W. e. Kelly 2002) attributed it to impingement and believed that this could occur when the impact distance was small. The impact distance is the distance between the outside surface of the valve rod and the inner surface of the impact ring, and it can be small when an impact ring such as the CD-6 is used for the APV-Gaulin high pressure homogeniser.

It had been already proposed by Keshavarz-Moore et al (Keshavarz-Moore 1990) that impingement and impact are the two main causes of cell disruption in a high-pressure homogeniser. As normally understood, impact is the collision of two objects such as a microbe and the impact ring, whereas impingement is a special case of impact in which one object such as the impact ring is eroded gradually by large numbers of small impacts caused by numerous discrete solid objects such as microbes or solid impurities flowing in the liquid at high velocity. The empirical formula in equation 3.1 from Kelly attempted to predict the fraction of broken cells from impingement from values of the impact ring pressure (W. e. Kelly 2002) (W. M. Kelly 2004):

$$f_f = \begin{cases} 0 & P_r \leq 160 \\ 0.01P_r - 1.6 & 160 \leq P_r \leq 240 \\ 0.8 & P_r > 240 \end{cases} \dots\dots\dots(\text{Eqn.3.1})$$

The impact ring pressure is the impact ring wall pressure where the occurrence of impingement and stagnation are most likely (marked x in figure 4.6 (c)). In the homogeniser used by Kelly (W. e. Kelly 2002), when any other impact rings were used, the impact ring pressure became too low to allow cell breakage. This does not seem to be the case with the homogeniser used by Flourey et al (Flourey 2004). The geometrical arrangement of the homogeniser valve parts in both cases (W. e. Kelly 2002), (Flourey 2004) is different from the arrangement in the homogeniser studied in this thesis.

However there are a number of crucial differences between the classical description of the impact mechanism for the fracture of brittle solids, and the rupture of the cell walls of microbes found in a high pressure homogenizer. The most obvious of these is that the cell

wall consists mainly of soft materials which have the ability to absorb strong compressive pulses without fracture (Prescott 2008). The cells would resemble a tennis ball more closely than a delicate item of glassware. There may be some sections of the cell wall which are composed of crystalline materials which could be brittle, and other sections such as bud scars which are known to contain high proportions of chitin which also can be brittle (Prescott 2008). However these potentially brittle sections are considered to be very small components in the cell wall and, because most of the other parts are easily deformed, strong compressive pulses would be attenuated over very short distances. Thus, the probability of cell fracture by impact is minimal.

The other major difference is that any collisions in a water environment is in a normally functioning high pressure homogenizer whereas in the fracture of brittle solids the collisions almost always take place in air or a gaseous environment. Water differs from air with much higher viscosity and with incompressibility. Much more energy is needed to allow solid objects to move in water at a velocity which is different from the surrounding water. When a solid body is moved through water, because of the incompressibility, water must be transferred from a position in front of the object and to a position behind the object. There is thus a necessity for water to flow along the surface of the solid from the front to the back. The high viscosity involved in this flow forms a continuous drag on the object, making it very difficult to allow high velocity differences between water and free objects suspended in it, to continue over a significant distance. However in air, objects can maintain their velocities relative to the air over long distances.

A similar effect occurs when two objects move at high speed towards each other with the potential of a violent collision. Again, because of incompressibility, water between the two objects must be removed so that objects to approach one another. For highly stream-lined objects moving towards one another, there would be very little water to be removed between them. However for a spherical microbe approaching the almost flat inner surface of the impact ring, large quantities of water must be removed. In fact, as the object surfaces come within a few nanometres apart, the velocity of the water between them must be many multiples of the velocity of approach of the objects. Because of this, the water provides a “cushioning” effect, where potential collisions between solid objects are often suppressed,

and when collisions occur, they are much less violent. This is not the case for potential collisions in air, because air is easily compressed with much less resistance to the movement of two objects towards each other. Despite these considerations, it would be incorrect to conclude that impact, or impingement, can never be the cause of cell rupture. Commonly, a groove develops on the inside surface of the impact ring, after operating the equipment many times. This must be due to erosion, due to water jets striking the surface. If erosion by water jets is the case, solid objects in the jet of water must also strike the impact ring with considerable force. The impact ring is usually fabricated using a material with good wear resistance properties, and, except in the case of impact fracture, described above, soft-bodied materials such as microbes, will incur damage much more readily than very hard surfaces. It is also accepted that once a groove has formed, further cell rupture is more likely. Any microbe on the flow path towards the inner surface of the impact ring exactly on the edge of the groove, will be easily cut into two pieces as it collides.

Therefore, cell rupture due to collisions with the impact ring cannot be ruled out for all situations. The question to ask is if the rupture by impact is a common event, or a comparatively rare event. The answer to this question depends on whether there are other mechanisms which are more likely to cause cell wall rupture in homogenisation. Also it is worth noting that the valve geometry setup can play a part in this, particularly at the exit of the gap, where many designs implement chamfers often at different angles to streamline the flow in a curvilinear motion. If this is the case, it would be more appropriate to state that the microbes graze or abrade off the impact ring. Microbes would be expected to break upon abrading but not a great population of microbes are expected to make sufficient contact with the impact ring, especially on one valve pass. The streamlines for impact velocities are covered in section 4.2.4 and verify that there is not a need to place in a short impact distance.

3.3.5 Shear Stress

It has been considered that shear stresses might arise on the surfaces of a microbe in the operation of the homogeniser, and if these stresses were significant, cell rupture could occur. However, there are other reports denying shear stress as a significant source of microbial

breakage in a low viscosity suspension such as that encountered with microbes in water. It was stated by Kelly et al (6), (17) and Millar et al (16) that at low viscosity, channel shear stress is an unlikely factor of cell disruption based on the gap size range of 1-11 microns, viscosity of 1-5 cp (1-5 mPas) and pressure of 2-14 kpsig (0.138 – 0.965 MPa). Only at high values of viscosity, did these researchers consider channel shear to be the main cause of cell breakage. Ayazi Shamlou et al (Ayazi Shamlou 1995) analysed shear stresses which might arise purely as a cause of turbulence without taking into consideration any ordered movements of the liquid in bulk as it passes through the equipment.

Unless a microbe is so small that its movements exactly match the movements of the liquid in a small eddy, there will be some microbe and liquid relative motion. If the microbe is much larger than the average eddy size, a number of eddies will be influential, and since the velocity of the liquid in each eddy will follow a different and random pattern, there must be considerable relative movement between the liquid and various sections of the surface of the microbe. These relative motions cause shear stresses to form on sections of the cell wall of the microbe. It will be appreciated, therefore, that there is a probability of two adjacent eddies swirling in opposite directions acting to produce a section of the cell wall which is in tension. If tensile stresses are great enough, rupture of the cell wall could occur. Making some assumptions about the turbulent intensity, Ayazi-Shamlou (Ayazi Shamlou 1995) calculated that a tensile force of 540 μN could be generated along the cell wall of a 5 μm microbe in a liquid with density and viscosity similar to water. It was proposed that this is sufficient to cause rupture. The description above applies only to shear stresses developing purely by the turbulent magnitude in the homogenizer operation.

However there are some other effects which could also produce shear stresses independently. Because of the high liquid homogeniser gap velocities, shear stresses must form on the walls of the valve parts. Various assumptions must be undertaken to calculate these stresses mathematically. An assumption must be made as to whether the flow is turbulent or laminar. Then, before computational fluid dynamics became available, a further assumption had to be made about the gap size. This provided an estimate for the average fluid velocity through the gap region. Assuming laminar flow, a parabolic velocity distribution provided values of the velocity gradient close to the valve part walls. Only the

velocity component parallel to the surface is of interest for these calculations. The velocity gradient is a measure of this velocity component as the point of reference moves from the wall (0 m/s) a short distance into the flow normal to the valve wall. The velocity gradient at the wall is the shear rate, and for Newtonian liquids, the shear stress is obtained by multiplying the shear rate by the liquid viscosity (constant).

This simple geometry can be extended for what happens when there is a surface imperfection, such as a protrusion. In this case the fluid must travel around the protrusion, and there will be a build-up of pressure upstream and lower pressure down-stream of the protrusion. As a result the protrusion will experience bending moments with tensile stress on the upstream side and compressive stress on the downstream side. If the liquid velocity is significant, the tensile stress will exceed the modulus of rupture of the material so that the protrusion will be broken off. It follows in general that where a high liquid velocity exerts a high shear stress on a solid surface, any surface imperfections cause a magnification of the stress and this may be enough to cause fracture with the result of the removal of the surface imperfection and the creation of a smoother surface. This description about shear stresses and surface imperfections on valve parts must now be applied to the surfaces of the microbes. However, to undergo this, it is essential to assess any situations where there is a difference in velocity between the microbes and the surrounding fluid. It is only in these circumstances of velocity differences that shear stresses will develop and cell rupture by this mechanism can take place.

A large amount of data has been compiled on the force exerted on a spherical solid body when it is mounted in a fixed position in a tube containing a liquid which is moving horizontally. The data was originally compiled by Lapple and Shepherd (Lapple 1940) who published a table showing the relationship between a coefficient and the Reynolds number, and it has recently been reduced to a set of equations in Perry's Chemical Engineers Handbook (Perry 2008). Strictly speaking the data refers to steady state conditions where the velocity profile does not change across a cross-sectional area many times greater than the exposed cross-sectional area of the spherical solid. Therefore the data cannot be applied in the gap region or too close to the gap region. It is also much more complicated to use computational fluid dynamics because there are two solids, the stationary valve parts and the

accelerating microbes. However by making a number of assumptions, the data can be applied to give approximate indications of the forces experienced by microbes. One of these assumptions is that the forces acting on the microbe depend on the microbe and liquid relative velocity. Therefore, it makes no difference to shear force calculations whether the solid is stationary and the fluid is moving, or the solid is moving and the fluid is stationary. Another assumption is that the concentration of microbes is small enough so the flow around one microbe does not affect the flow around the neighbouring microbes. The forces acting on the solid sphere will cause it to accelerate. If the solid is stationary the forces will cause it to accelerate so that its velocity increases and so that eventually it approaches the velocity of the liquid. Further, if the dimensions of the solid sphere (the microbe) are known and an assumption is made that its density is 1.1 times that of water, its mass can be calculated. In this way the magnitude of the forces estimated using the data of Lapple and Shepherd (Lapple 1940) can be used to estimate the acceleration of the microbe as it passes through the homogenizer, based on data on the changes in velocity of the liquid as it passes through the homogenizer also.

The analysis shows therefore that there are indeed grounds for estimating a large difference in velocity between the microbes and the surrounding fluid at the beginning of the gap region. Therefore it follows that there is the possibility of high shear stresses occurring on the surfaces of the microbes in this region.

Three further factors need to be taken into account at this point. *Firstly*, the surfaces of the microbe are unlikely to be smooth. The cell wall is understood to have a fibrous structure, being composed of an arrangement of micro-fibrils of carbohydrate polymers wound together (Prescott 2008). It is expected that various branching members in these molecular chains will allow minute hair-like structures to protrude outwards beyond the cell wall into the surrounding liquid. A cell wall structure like this would be very vulnerable to fracture caused by high shear stresses. *Secondly* the cells of microbes are not rigid structures, but are believed to resemble very small bags of fluid. Most of the mass of the microbe is located in the central cytoplasmic liquid section, while the walls are comparatively thin. For purposes of description the microbe can be thought of as composed of two hemispheres joined together. The front hemisphere which has the leading surface is joined to the rear

hemisphere which has the trailing surface. The shear stresses, due to the high relative velocity of the surrounding liquid will reach a maximum intensity on the band where the two hemispheres meet. Under this situation the whole of the cell wall which surrounds the rear hemisphere will be under a tensile stress. This is a result of the shear stress along the band forcing the whole microbe to accelerate. This is resisted by the mass of the microbe, which, because of momentum, exerts a pressure on the rear hemisphere, reaching a maximum at the part of the cell wall which is at the rear of the microbe. The whole of the cell wall surrounding this rear hemisphere is under tension, so that if there is a weak part, the fracture of the whole cell wall will begin at that point. *Thirdly*, outside the front hemisphere the liquid forms a number of vortices which are shed at regular intervals. The frequency of shedding depends on the relative velocity between the liquid and the solid, and it is very high when the microbe is entering the gap region. A number of vortices are shed each time a microbe passes through this region. The result of this is that the microbe will experience a violent recoil as the shed vortex accelerates away. The tensile stress, which is established in the cell wall around the rear hemisphere, therefore does not build up gradually and then decrease gradually. It is applied as a series of jolts as a result of the vortex shedding. *Finally* in this description of possible mechanisms of fracture, attention needs to be drawn to the fact that shear stresses can occur in a homogenizer, not only in the region at the entrance to the gap, as the fluid accelerates, but also in other parts of the equipment. At least two other situations should be mentioned. There is firstly the region at the other end of the gap where a jet of liquid enters a much wider volume of liquid which is almost stationary, close to the inner surface of the “impact” ring. In this region the liquid in the jet decelerates rapidly and seems to divide into two streams with slightly curved pathways (see figure 4.6). It is expected that microbes within that jet stream will also decelerate abruptly, but the analysis carried out during the acceleration stage using the data of Lapple and Shepherd (Lapple 1940) would suggest that there is a lag in the deceleration also. In addition to this, the momentum possessed by the microbes as they exit from the gap will cause them to follow slightly different flow paths in comparison with most of the liquid. Both of these factors would indicate that the microbes will enter a region where there is a large difference in velocity between them and the surrounding liquid. This provides another opportunity for shear stresses to form on the surfaces of the cell walls.

1. Get Velocity gradient 1 μm from the microbe wall at N number of equally placed locations around the circumference of the wall.
2. Multiply the velocity gradient by the dynamic viscosity of the fluid flowing to obtain the shear stress for each location.

$$\sigma_{s_{N-(N+1)}} = \mu * \frac{\Delta V}{\Delta s} \dots \dots \dots (\text{Eqn. 3.2})$$

3. Multiply the shear stress by the area of each face to find the force on each microbe wall location.

$$F_{N-(N+1)} = \sigma_{s_{N-(N+1)}} * A_{Loc_N} \dots \dots \dots (\text{Eqn. 3.3})$$

It is accepted by many researchers that increasing the pressure drop across the valve gap increases cell breakage (Kleinig A.R. 1996), (Siddiqi 1996), (Ramanan 2009). Taking the above explanation on how shear stress may break cells, increased operating pressure would increase gap velocity (due to smaller gap size) and also increase shear forces. If this is the case, then results of increasing shear stress would also closely agree with results of pressure versus fractional protein release by Kleinig et al. (Kleinig A.R. 1996) Results from Siddiqi et al. (Siddiqi 1996) found particle size distribution to decrease with increased operating pressure also. An optimum cell disruption homogeniser design based on the above premises would be one that could obtain higher velocity differences between phases (water and microbes) but with a lower pressure drop. Work was carried out in this thesis to determine such a design with aid of the above equations 3.2 and 3.3 as outlined in chapter 5.

It is interesting that the conditions which maximize the opportunity for shear stress to cause cell rupture in this deceleration zone are a short “impact” distance and a high “impact” pressure. It was been observed by many workers that when these conditions are met there is an increase in cell rupture. However this does not prove that impact is a valid mechanism of fracture of the cell wall, because the same conditions will also maximize shear stresses at this point, and the observed rupture could be attributed to this effect. Since the shear stress phenomenon depends on the relative velocity between the solid and the surrounding liquid the same set of features will occur whether the liquid is accelerating or decelerating. Therefore in this case also there will be the tensile stress developing in the cell wall, but this

time in the front hemisphere. There will also be the vortex shedding phenomenon, and this time the vortices will be shed behind the microbe into the stationary liquid.

3.3.6 Others (Number of passes, Separation)

Siddiqi et al. (Siddiqi 1996) have believed that pressure and number of passes are the two greatest factors of disruption. It is believed that total protein release occurs after 5 passes and only debris is produced for subsequent passes. Results from figure 3.4 (b) show that increasing the pressure decreases the size of the particles and thus increases the rate of protein release. The same may be said for nutrient release in cells that are passed through the homogeniser. From the experimental data, it was found that below pressure of 115 bar (11.5 MPa), no cell breakage was found. Therefore the results of the study conclude that cell disruption could be considered as a function of number of homogeniser passes and operating pressure. (Siddiqi 1996)

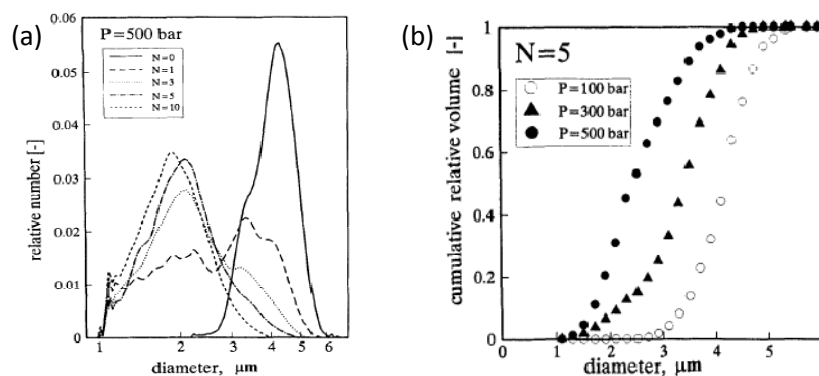


Figure 3.4: Particle size distribution data (Siddiqi 1996) for packed baker's yeast cells obtained for (a) Constant pressure 500 bar with number of passes variable and (b) 5th pass at various pressures

Separation was also a possible cause noted by Phipps (Phipps, "The fragmentation of oil drops in emulsions by a high-pressure homogeniser" 1975) but this was limited to the study of milk globules. It is believed that exit velocity would have to be extremely high to undergo sufficient forces to pull apart a cell or microbe in the same occurrence. A disruption model was proposed by Hetherington (Hetherington 1971) which related the fraction of cells disrupted (R) to temperature (k), operating pressure (P) and number of passes (N). Also, a is a pressure component constant and b is a linear variable relating to cell concentration.

$$\ln\left(\frac{1}{1-R}\right) = kN^b P^a \dots\dots\dots (\text{Eqn. 3.4})$$

3.3.8 Measuring Breakage

A reasonable assumption was made by Agerkvist and Enfors (Agerkvist 1990) that cell breakage only releases protein for yeast when total cell breakage occurs. This assumption is also supported by (Siddiqi 1996). It was also noted by Agerkvist and Enfors (Agerkvist 1990) that protein release and enzyme release were independent of method of cell breakage but the particle size distribution was strongly dependant on it. So if the same can be applied to nutrient release from cells, then a measure of cell breakage could be made by the particle size distribution in the homogeniser. However, Kopp et al (Kopp 1997) considered disruption of cells to be poorly detected by means of particle size distribution measurement.

3.4 Finite Volume Analysis of homogeniser

Finite volume analysis can be achieved using the program Fluent 6.3.26. Before a model containing microbes can be included, it is important that a simplified model is made first. This simplified model makes use of only water passing through.

Table 3.1: Overview of previous CFD works carried out on homogeniser

	Kleinig	Stevenson and Chen	Miller, Kelly, Muske et al	Floury et al	Casoli et al
Code	Phenics 2.1	FLOW 3D	Fluent 5.3	Fluent 6.3	Fluent 6.3
State	steady	steady/unsteady	Steady	Steady	Unsteady
Solver	laminar	STD K-epsilon (laminar before gap entry)	KE realizable (laminar before gap entry)	RNG KE turbulent	K-Realizable
Phases	water	water	water and air	water	water / air
Flow rate (m³/s)	0.000046	-	-	2.60E-06	n/a
Inlet velocity (m/s)	-	2.841	1.724	pressure inlet based on experimental data	pressure inlet based on experimental data

	Kleinig	Stevenson and Chen	Miller, Kelly, Muske et al	Floury et al	Casoli et al
Pressure outlet (Pa)	fixed pressure BC	fully developed	fixed pressure	fixed pressure 0	variable pressure - increases to experimental value at end of simulation using exponential UDF
Wall BC	no slip	near-wall	no slip	no-slip	near wall
Other BC's	Axi-symmetric	Axi-symmetric	-	Turbulent intensity 1% at inlet	-
Cells	5852	20000	45000-65000	350000	350000
Regions solved	Inlet only	All	All	All	All
Gap sizes covered	8-25 microns	3-55 microns	1-25 microns	2-4.74	not specified
Convergence criteria	none	1% for large gaps (20-30) and 3-5% for small gaps (less than 20)	e-4 as well as <1% change for 5000 extra iterations	double number of cells in mesh and check	not specified
Iterations	n/a	1500-3000 per run (12-36 hours)	15000-25000 per run (24 hours)	not specified	not specified
Relaxations factors	none	0.3-0.7 momentum; pressure 0.9-1.0, k and e 0.1-0.3 at start and 0.5-0.8 near end of simulations	not specified	less than 10% turbulent intensity at pressure drop 26MPa to above 35% at 340 MPA	not specified
Measurements made	Pressure and velocity	Pressure contours and drops, velocity fields	Pressure inlet, pressure wall (vs. gap space and vs. impact distance)	Velocity profiles in gap, cavitation, pressure drop	cavitation, flow rate vs. pressure
empirical formulae created	$h = 37P^{-0.35}$	Kin		one taken from Poiseuille for cavitation	
Novel features	first CFD model of homogeniser flow	3 regions covered	Proposed cell breakage inversely proportional to impact distance square and gap spacing squared with results	validated velocity profile in gap by comparison with Poiseuille, measurement of cavitation	C-Program UDF to reduce the outlet pressure over time to ensure steady solution.

	Kleinig	Stevenson and Chen	Miller, Kelly, Muske et al	Floury et al	Casoli et al
Limitations	Inlet region covered only	Only 10 cells across gap width, individual pressure drops not taken into account	steady state	small range of gap sizes	Often the introduction of a cavitation model in CFD produces a vapour region in fluid regions without reason or warning which greatly affects results
		also laminar solving only - therefore channel shear stresses and turbulent intensities could not be taken into account accurately			Setting inlet boundary conditions based on experimental measurement was not helpful as the solution fails close to beginning of solving due to flow inconsistency.
					Even if the cavitation model is begun after initial iteration, negative values of pressure occurs instantaneously

3.5 Suggestions from Other Works

The ideas from the following works were used in the computational work carried out through the validation and optimisation processes outlined in chapter 4 and chapter 5. For the homogeniser, it has been believed that an impact ring is necessary for cell disruption but this is not the case for the gas saturation system of Nakamura et al (Nakamura 1994) and the high-pressure system of Constant Systems Ltd (Foster 1995). This suggestion was later validated in section 4.2.4. Vortex shedding is likely to occur in the positions covered by the microbes as outlined in section 4.3 because in order to suppress vortex shedding the critical gap ratio (see figure 3.5) must not exceed 0.25 for Bosch and Rodi (Bosch 1996) and between 0.2 and 0.3 for Lei et al. (Lei 1999). However, Lei (Lei 1999) reported that if the boundary layer of the cylinder increases, the critical gap ratio also increases. However the critical gap

ratio for the microbes at position 1-4 as shown in figure 4.7 was found to be at least 2.0. Thus vortex shedding is expected in the homogeniser for the microbes unbroken.

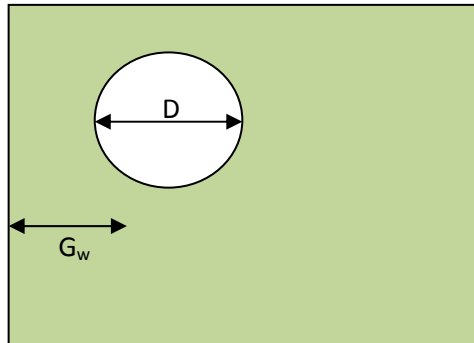


Figure 3.5: Critical gap ratio (G_w/D)

Baker's yeast cells were assumed to 5 μm in diameter for theoretical calculations by Ayazi-Shamlou (Ayazi Shamlou 1995). This is considered a reasonable assumption as yeast cells has been recently estimated as 3 - 8.5 μm with a slight cylindrical shape (Charinpanitkul 2008). Another paper was found that theoretically determined that by using 3.5° chamfers, reverse flow after the main opening on a valve could be minimised (Gibson 1910). This paper has been recently referenced by (Sparrow 2009) and (Jana 2008).

But as the fluid enters the gap at such high velocities and pressures, cavitation is highly unlikely to occur there. However just after the gap exit corners (for square edged seats), there may be some cavitation. However, the extra expense required by using a multiphase model in a computational fluid dynamics model would not be necessary considering that higher computational accuracy would be required in the exit region. Note that in the gap region, over 70% of pressure drop is found as from computational experiments carried out as outlined in validation work carried out in chapter 4 for the gap size versus pressure measurements. Breakage of cells is believed to be maximised in the gap entrance as explained in further detail in as in “section 3.3.5 shear stress”. As turbulence suppression will be maximised by the high gap pressure in the gap region (M. C. Stevenson 1997) where cell breakage is maximum, highest computational accuracy is priority at this location and not at the exit region where vapour may emerge. Previous work carried out by Casoli (Casoli 2005) suggested a method that can include a cavitation model but with the use of unsteady simulations. There is also a requirement of using a User Defined Function (UDF) that gradually increases the fluid pressure difference over time. However, there were still air

pockets appearing without reason during the simulation. As cavitation is a random phenomenon as outlined in section 3.3.3, it would appear favourable to leave out for reasons of inaccuracy in computational solvers to deal with random air pockets occurring as well as unnecessary computational expense.

3.6 Chapter 3 Summary

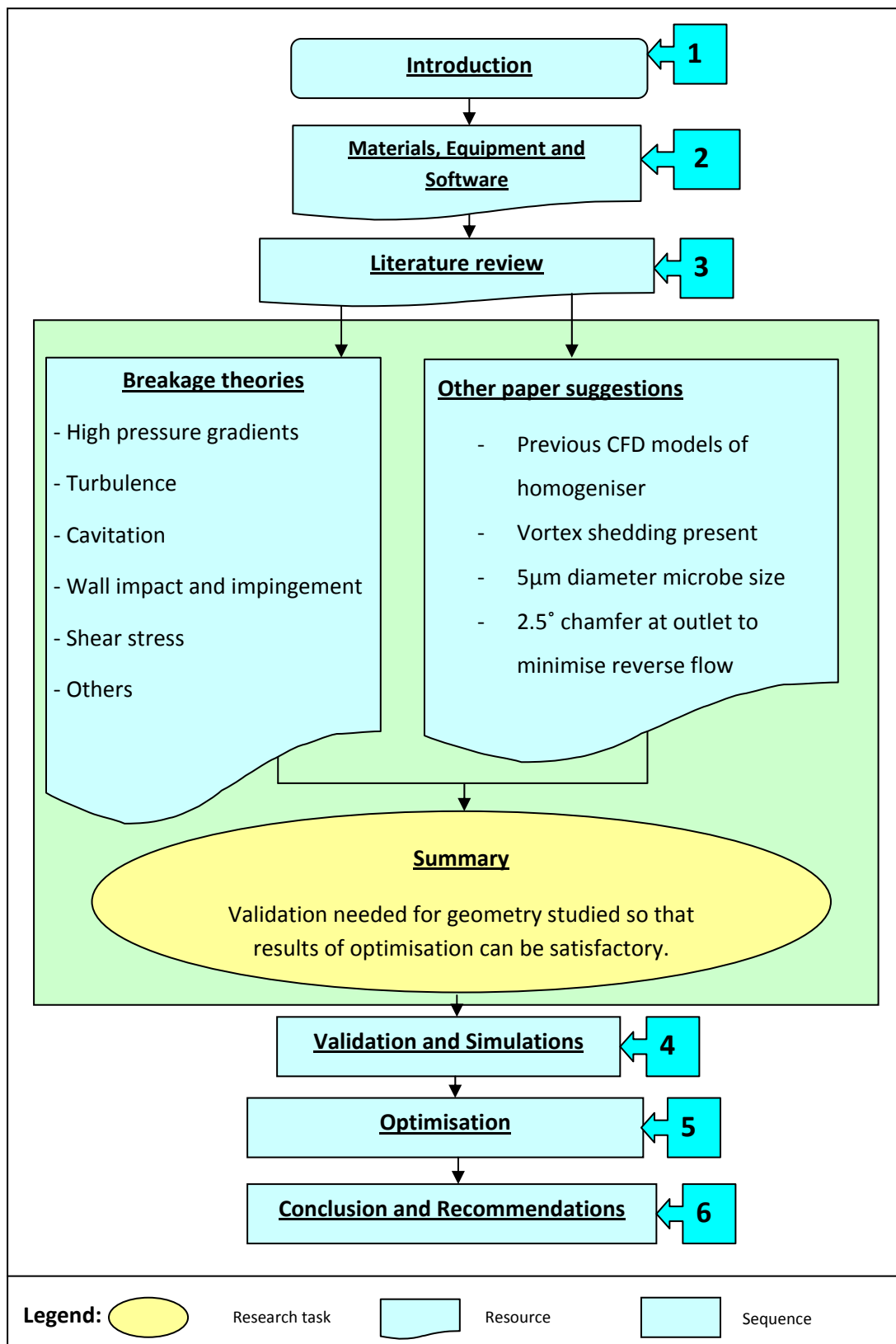


Figure 3.6: Summary of the research process in chapter three

Chapter 4 – Validation and Simulations

4.1 Introduction

Fluent is a Finite Element (FE) Computational Fluid Dynamics (CFD) software code that is used to resolve equations of continuity, momentum and other flow equations for user defined models. This software package has many advantages over experiments in terms of detailed flow and pressure field description as well as increased understanding of turbulent development that cannot be quantified easily by experimental means. Recent versions of *Fluent* have made great advancement in describing the flow of separate phases as well add on modules that can describe chemical reactions.

However, accuracy of results is highly dependant on computer performance. For example, in multiphase models, there is computer performance limitation by means of describing all levels of variation in the model while keeping the model solutions stable. For these reasons, all attempts must be made to find a way of comparing computational results with theory, formulae or experimental results as often as possible to ensure accuracy and reliability.

The main aim of the Biowell project is to come up with a means to increase the methane yield and yield rate of maize silage and sewage sludge with anaerobic digestion. The main problems that were originally encountered was that total yield and yield rate was low. One such possible cause of low yield rate was that the reactant surface area of the maize was too low. A mechanical pre-treatment design was used to break up the maize silage to increase the reactant surface area. The work carried out with the maize mechanical pre-treatment is outside the scope of this study and hence will not be covered in more detail. As for the low yield, a probable cause is that the microbes from the secondary sewage waste used to produce methane cannot be broken down by anaerobic digestion. There are large tough microbes that add to digester volume without greatly increasing methane production cannot be broken down by anaerobic means alone. One of the most effective ways to release these nutrients is to break them up. The method that will be used in this study to achieve this breakage is the homogeniser. The original homogeniser valve used in this work appears to be not very efficient in carrying out this objective as the valve was originally adapted for the dairy industry. In order to compare different geometries, it is necessary to understand the flow fields within the homogeniser. This is not possible with experimental measurement so

therefore the flow fields must be estimated by means of finite element software (Fluent 6.3.26). Once the measurements obtained using Fluent can be validated, then geometries of the finite element model can be made and compared in terms of flow efficiency for the size of microbe desired. Such desirable outcomes would be to have higher velocity gradients causing shear forces which may break open the cell walls easier. Also recirculation, reverse flow and vena contracta effects would need to be minimised as much as possible.

4.2 Validation

4.2.1 Introduction to validation

Before optimisation can begin, the solver and grid settings that obtain results closest to expected experimental conditions must be carried out to ensure that computational measurements are accurate enough. The pressure drop across the homogeniser valve will be compared with previous empirical formulae obtained from experimental work as a means of validating the computational work. K- ϵ realizable solving was used as this solver copes well with axi-symmetric spreading jets after the gap exit and stagnant regions at the impact ring (Fluent Inc 2007).

4.2.2 Pressure drop validation

Both of the pressure drops from the computational model and empirical formulae were obtained based on the geometry obtained from the homogeniser valve used in the laboratory. The dimensions of the valve seat were obtained using a CMM (Co-ordinate Measuring Machine). This apparatus was needed to measure the valve seat especially as it was not possible to measure chamfer angles physically as seen in figure 4.1. The valve head had a diameter of 4.75 mm. The impact ring had an inside diameter of 5.55 mm. The other geometries of the valve seat are shown in figure 4.1.

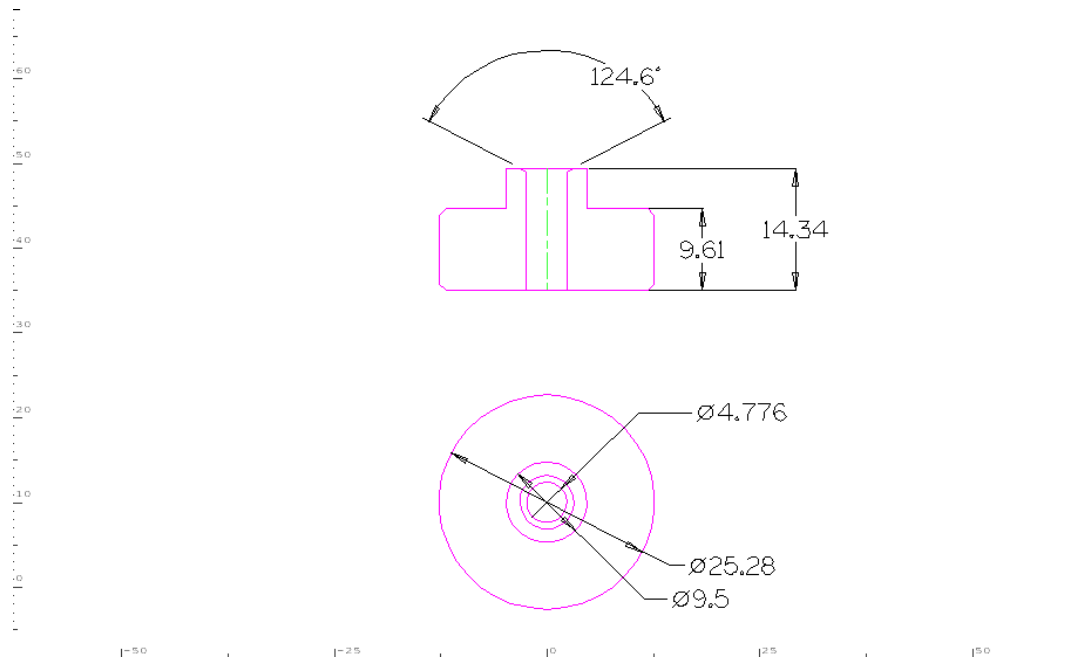


Figure 4.1: Valve seat geometries

These geometries were then created in Gambit 2.1 by means of an axisymmetric model. The mesh was refined close to the wall and in regions of high total pressure gradients as specified in “Section 4.2.3 Convergence methods for residuals and mesh”.

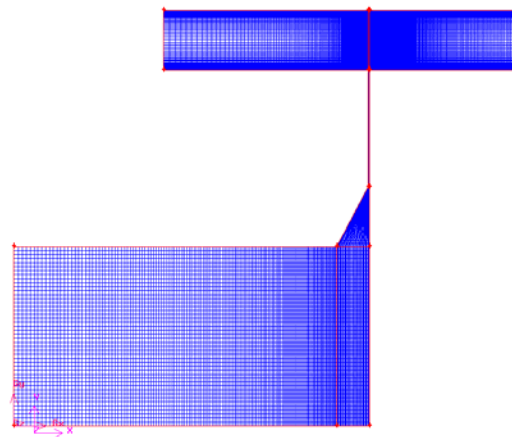


Figure 4.2: Axi-symmetric model created in Gambit 2.1 for the homogeniser valve with 20 μm gap.

The converged grid was then imported into Fluent 6.3.26. The grid was scaled to mm for ease of plotting measurements (please refer to appendix B for extra information). The double precision solver was used due to the long and narrow gap region being present in the domain

as recommended in the Fluent user guide (Fluent Inc 2007). The K-Realizable discretisation scheme was used due to its ability to deal with regions of swirl and stagnation (Fluent Inc 2007) as seen in the homogeniser. A velocity inlet of 1.393 m/s was used based on experimental measurements carried out (table 4.1). The measurement was obtained by measuring the volume of water (m³) displaced by the homogeniser over 1 minute, and converting to SI units which worked out to be a median (excluding outlier of 1st measurement) of 0.025 m³/s.

Table 4.1: Water flow rates in homogeniser

Number	Pressure reading (MPa)	Water temperature (°C)	Flow rate (ml/min)	Flow rate (m ³ /sec)	Date
1*	5	27	1380	0.00023	02/07/2008
2	10	27	1472	0.00025	02/07/2008
3	5	27	1520	0.00025	02/07/2008
4	10	27	1550	0.00026	02/07/2008
5	10	27	1418	0.00024	03/07/2008
6	5	33	1500	0.00025	03/07/2008
7	5	33	1520	0.00025	03/07/2008
8	10	33	1500	0.00025	03/07/2008
9	10	33	1500	0.00025	03/07/2008
10	10	33	1490	0.00025	03/07/2008
11	10	33	1480	0.00025	03/07/2008
12	15	33	1490	0.00025	03/07/2008

**Outliers – maize residue left over from previous experiments too high in concentration to be considered. The residue increased viscosity higher than water and caused the flow rate to be reduced.*

Using the inlet radius of the 2.388 mm (0.002388 m), the flow rate (m³/sec) was divided by the cross sectional area to give a value of 1.395 m/s for the velocity inlet. Values of $K = 0.00389$ and $\varepsilon = 0.0001286$ were obtained based on the formulae provided by Stevenson and Chen (M. C. Stevenson 1997). The pressure outlet was set as 0 Pa and standard wall conditions were used. Each model was run for between 6-9 hours with mesh sizes found

between 50000 and 80000 cells. Second order solving was used for the residuals as flow in the domain is not aligned well with the grid due to curvilinear motion of the fluid entering and leaving the gap. In the case first-order solving would yield too high an error (Fluent Inc 2007).

Table 4.2: Boundary conditions for single phase water model used for preliminary validation

Fluid zone before gap entry and in gap	Water-liquid, Laminar
Fluid zone after gap expansion	Water-liquid, K-ε Realizable
Velocity inlet	1.393 m/s, normal to inlet, relative to adjacent cell zone
Turbulent kinetic energy	0.00389 m ² /s ²
Turbulent dissipation rate	0.001286 m ² /s ³
Pressure outlet	0 Pa
Wall	Standard wall
Discretization	PRESTO pressure Momentum 2 nd order upwind Turbulent kt. energy 2 nd order upwind Turbulent kinetic energy 2 nd order upwind Energy 1 st order upwind
Under-Relaxation factors	Pressure 0.2 Density 0.1 Body forces 1 Momentum 0.4 Turbulent KE 0.8 Turbulent dissipation rate 0.8 Turbulent viscosity 1 Energy 1
Pressure velocity coupling	SIMPLE

This model was implemented for gap sizes between 1 μm and 45 μm. The pressure drop was recorded for each gap size and compared to the empirical formulae of Phipps (Phipps, "The fragmentation of oil drops in emulsions by a high-pressure homogeniser" 1975) and

Nakayama (Nakayama 1964) as seen in Figure 4.3. Full details of the empirical formulae are provided in Appendix B.

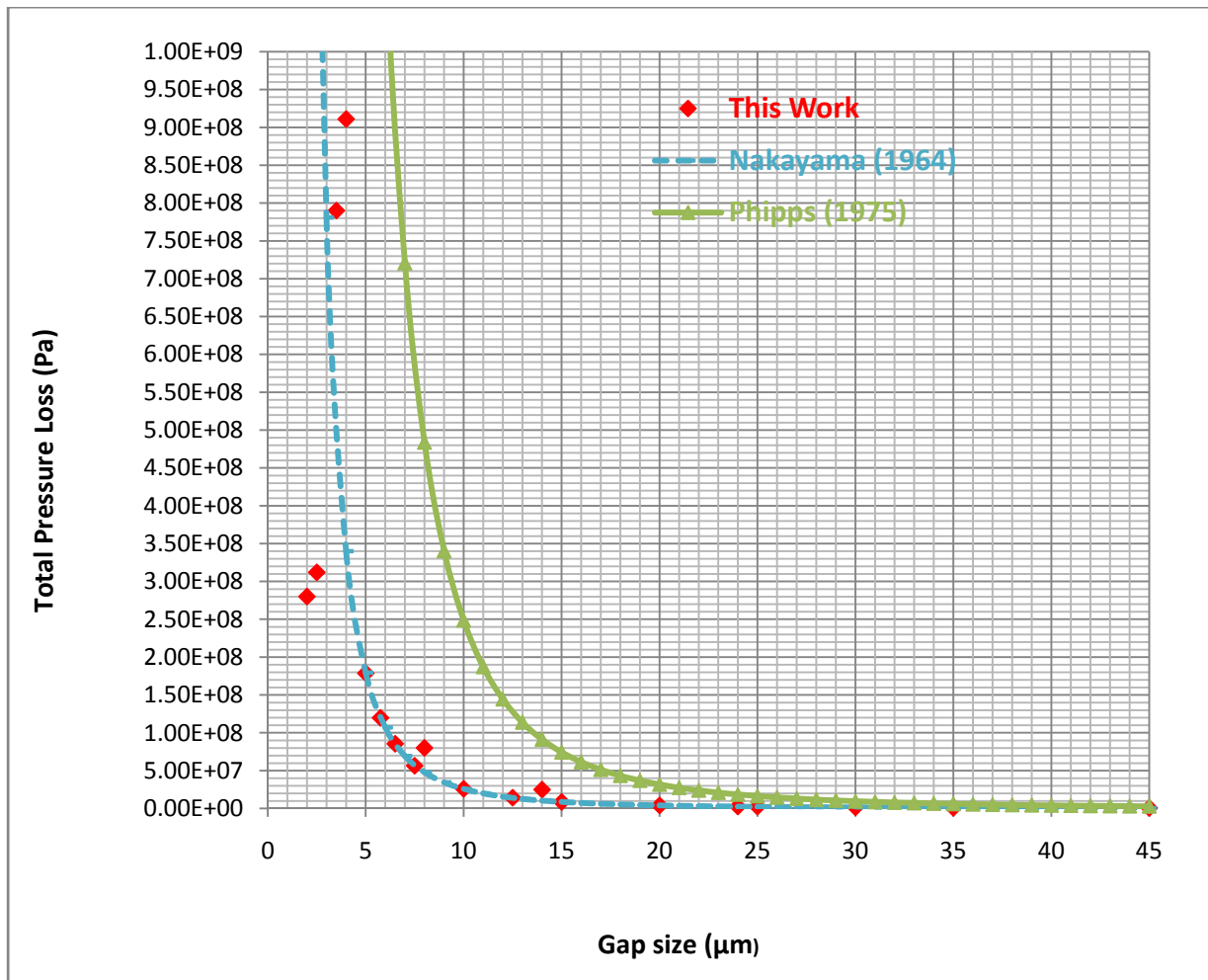


Figure 4.3: Pressure drop versus gap for computational model and empirical formulae

Therefore from the close correlation of empirical formulae (particularly Nakayama's) with the computational models, the computational setup as described in this section is sufficient to be used for later validation of the optimised homogeniser valve as described in Appendix B, particularly for gap sizes greater than 5 μm. It was noticed that almost all (73%) of the pressure drop was found across the gap for the original design as covered in appendix B. Detailed data of the different pressure drops and gap sizes can also be found in appendix B.

4.2.3 Convergence methods for residuals and mesh

To ensure that the residuals of each equation was sufficiently converged, the residuals were checked to see if there was not a drop of order of magnitude over 10000 iterations. After this, the model was iterated for the further 5000 iterations and if the maximum velocity of the domain did not change by more than 1%, then the residuals were considered converged.

For each mesh produced, the velocity profile located just downstream of the gap entry at grid locations along $y = 3.5$ mm was compared and examined. The mesh was refined close to the walls and in regions of high gradients of total pressure such that the total number of cells in the domain was increased by 10% approximately each time. This process was continued until there was no noticeable change in the velocity profile. This was further tested by doubling the mesh to see if the change in maximum velocity of the profile covered differed by less than 2%. Once the mesh fitted these criteria, mesh convergence could be confirmed.

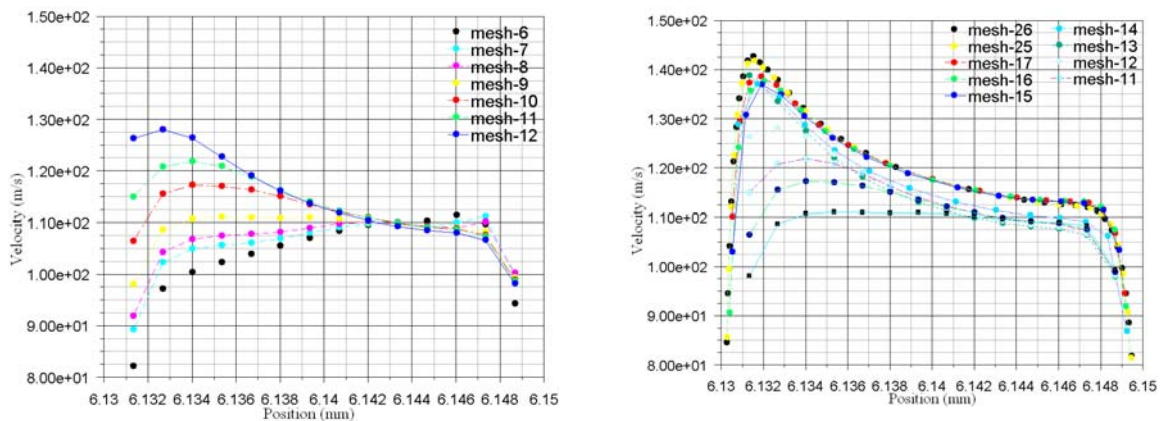


Figure 4.4: Mesh convergence of single phase water model for original dimensions (Meshes 18-24 and 27-28 were excluded for purposes of clarity)

4.2.4 Preferences for further work carried out

To determine which gap size would be the most suitable to work with computationally for optimisation, it is important to determine a gap size that would be small enough to generate comparable and non-negligible forces on cell walls while preventing the maximum velocity in the gap not to exceed one-third of the speed of sound. Once the velocity of a fluid exceeds one-third the speed of sound, compressibility effects cannot be ignored and a density-based solver would have to be used. A density-based solver would require much more

computational expense and hence would force the models to be oversimplified or incur too much time to solve. From examining maximum velocity values obtained from figure 4.5, a 20 μm gap obtained a maximum velocity of 79.94 m/s, which is well below 112 m/s (equals $336 \text{ m/s} \div 3$). This means that even with the extra contraction of the presence of a microbe of diameter 5 μm , the maximum velocity should not exceed this compressible threshold value. If the maximum velocity is found to exceed this value in the microbe models, then a density-based solver may have to be used.

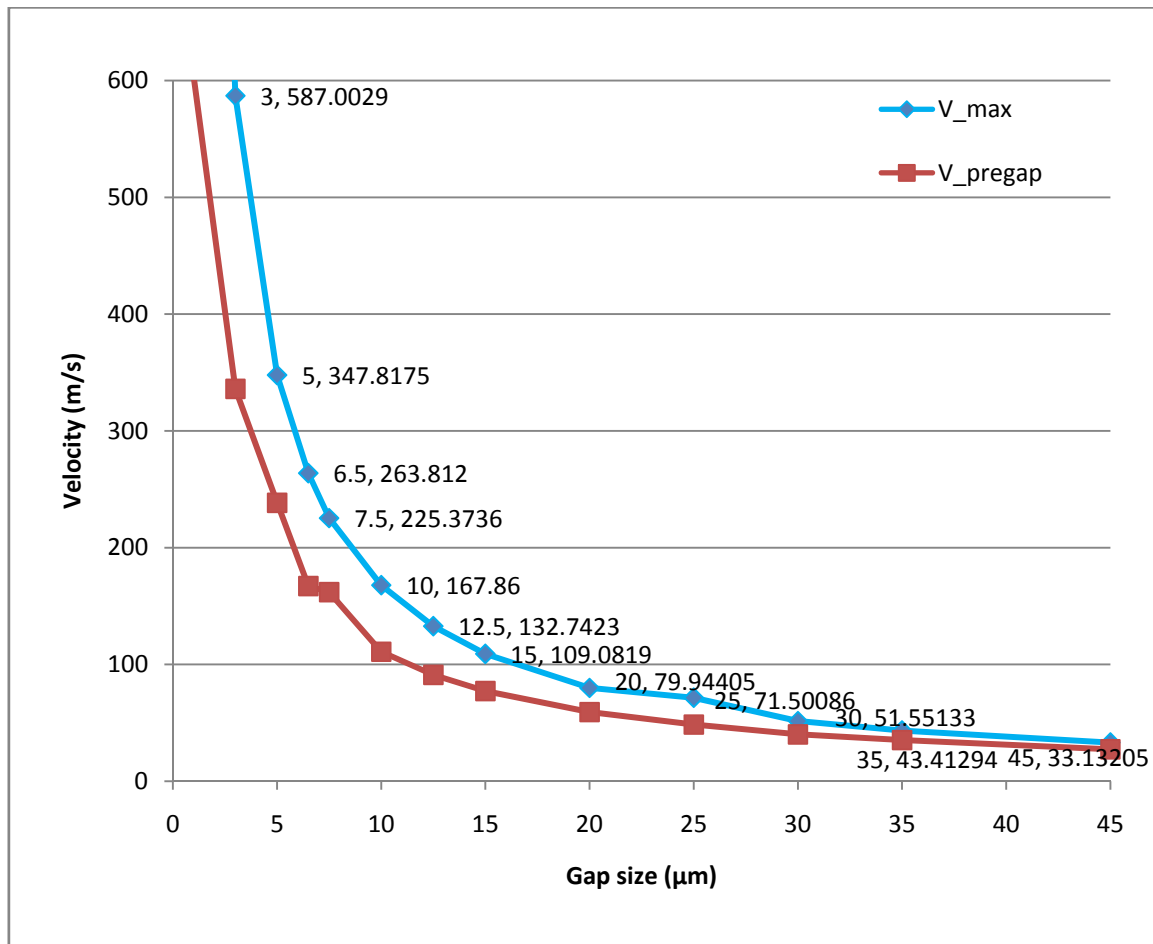


Figure 4.5: Maximum velocity and velocity at start of gap in terms of gap size

The radial jet issuing from the gap was investigated using Fluent 6.3.26 for this geometry (see figure 4.6). It can be observed that the liquid velocity close to the wall is between 0 and 8 m/s. The streamlines show that the jet divides into two and follows curved paths, eventually with the fluid moving parallel to the impact ring. If this analysis is correct, the low velocities and the change in direction of the liquid would suggest that wall impact or

impingement may not be major causes of microbe breakage. However the path of a microbe flowing through the homogenizer may be quite different from the pathway of the liquid.

While these details supply useful information about the conditions under which cell breakage occurs, they cannot be considered as pin-pointing the mechanism of fracture. The word “impact” suggests that the mechanism must be related to the fracture of brittle solids which occurs during a collision. In that case a compressive pulse is generated and passes through the solid. The actual fracture depends on the existence of flaws in the structure of the solid, and when a flaw exists with an orientation of 30 degrees to the direction of the pulse, a tensile stress is produced in the solid which may be sufficient to cause fracture. From the low velocity encountered as well as the non-direct impact of the impact ring with the radial jet, the impact ring should not cause major levels of microbe breakage travelling in water. Also the presence of water should act as a shock absorber. Therefore the impact will not be needed in aiding breakage of microbes with water passing through the homogeniser.

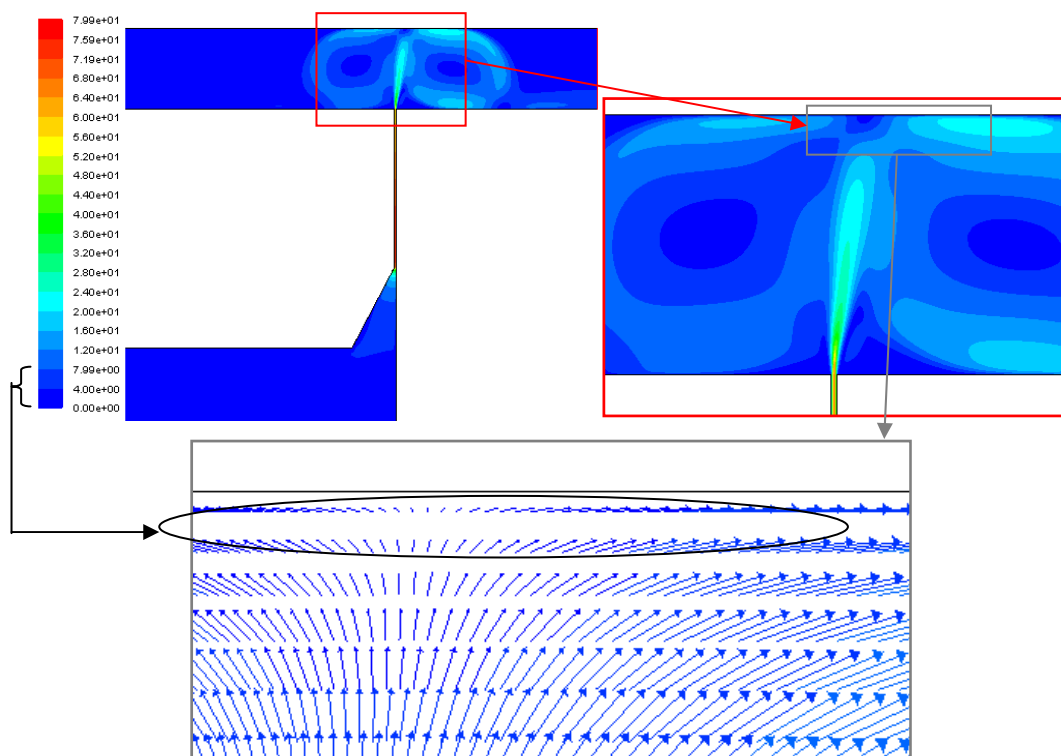


Figure 4.6: Velocity contours of (a) homogeniser gap and exit region, (b) exit region and (c) velocity vectors at impact ring with small velocity values.

The yeast cell diameter will be used as a template microbe in this study. It can be assumed as a diameter of 5 microns as specified in section 3.5. Therefore a microbe of 5 μm will be

looked at for the microbe breakage model. A 10 μm diameter micron model will also be covered briefly to see differences in values of shear when compared to the 5 μm models.

4.3 Microbe breakage model

4.3.1 Introduction

Microbes in waste water sludge are highly variable in size and properties. These microbes can occupy sizes from the nanometre range to millimetre range. As an axi-symmetric model is being used for the microbe model, the microbe representing the size of a yeast cell was chosen to be a 5 μm diameter. However with these settings, a circle of 5 μm in the 2d plane translates to a ring of 5 μm diameter in 3d space. There were problems obtaining a curvilinear trajectory of movement for the microbe entering the gap. This was because Fluent 6.3.26 does not allow a moving wall condition with both rotational and translational movement. A stationary microbe had to be adopted in steady state flow with the microbe located in different locations along one of the streamlines of water flow in the homogeniser instead. A 10 μm microbe was also used for comparative purposes.

4.3.2 Effective model used

The 5 μm microbe model consisted of the original homogeniser dimensions containing a singular microbe at 6 different locations along a flow streamline (table 4.3). Due to the irregularity of using a quad mesh around the microbe surface and extra cells required for sufficient accuracy, the mesh was changed to accommodate triangular cells throughout the domain for all microbe models. Triangular meshing also has lower computational expense so therefore more cells can be used in the same model.

Table 4.3: Microbe Positions

Microbe Number	Microbe Position X (mm)	Microbe Position Y (mm)
1	4.735	3.180
2	4.740	3.188
3	4.740	3.969
4	4.740	4.750
5	4.780	5.150
6	5.150	5.540

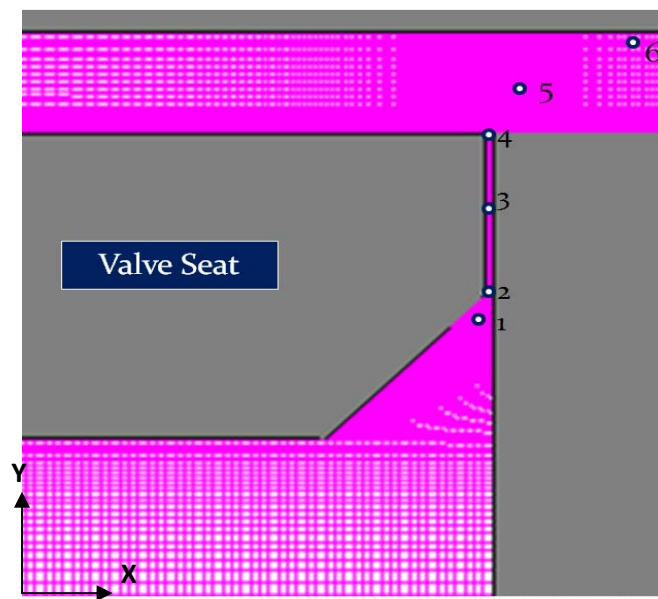


Figure 4.7: The axis-symmetric view of the six locations of microbes along the expected streamline of flow

By using the stationary microbe, velocity gradients and breaking forces will be greatly overestimated but the mechanisms should be to scale more sufficiently. However a problem still arises with overestimated wakes being produced in the simulations which are inherent of the solver used as well as the stationary microbe. Shear forces are produced by the fluid passing by the microbe wall. This has a tendency to pull the microbe wall in either a clockwise or anti-clockwise direction. It is believed by the author that the microbe wall may be pulled apart where these forces separate in opposing directions as seen in location A and B. It is expected that the separation force at location A will be much greater than B in figure 4.8. However, if excessive vortex shedding occurs at location B, then the separation force

could be greater. The measurement of vortex shedding will not be covered in this thesis due to the additional computational expense due to the use of a denser mesh and unsteady solving.

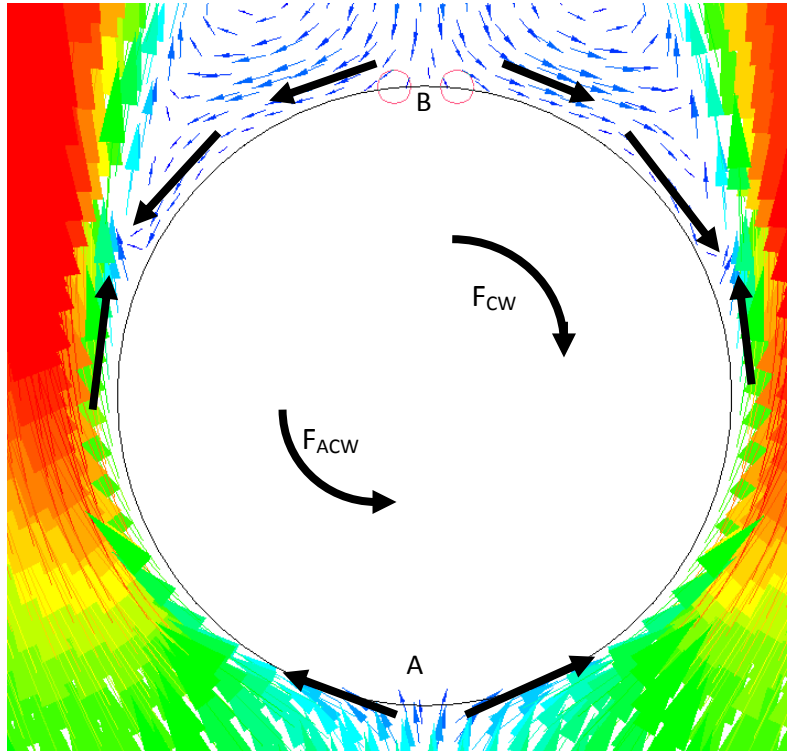


Figure 4.8: Clockwise force (F_{CW}) and anticlockwise force (F_{CW}) examples

So therefore the main limitations of the microbe model covered in this thesis are:

1. Stationary microbe: This will overestimate forces acting on the microbe when compared to a moving microbe
2. Axisymmetric modelling: If a 3d model was used, the microbe could be represented as a sphere. If the exact dimensions of a yeast cell were used, then a cylindrical-like shape could be used. However calculations as seen in appendix B would be very time consuming if 3d modelling was used.
3. Resolution: Due to the mesh being used, the circle in the 2d plane representing the microbe does not have a curved face but has many flat faces. Using 60 faces to represent a $5\ \mu\text{m}$ microbe should minimise this limitation sufficiently.
4. Does not take multiple microbes and collisions into consideration – therefore only viscous drag will be covered as a mechanism for breakage.

5. Microbes are variable in size and size can change the value of shear force greatly (see section 4.4 breakage results).
6. Simulation does not include rotational or translational effects of microbe.
7. Velocity at inlet found in water only from single phase experimental work without microbes present. The flow rate of may be expected to be less due to the constriction of the microbes especially near and in the gap. Also if large enough pieces of sludge are present in the water microbe-water mixture, then further flow rate constriction could occur, affecting results greatly.
8. No data is available for exact failure shear forces or stresses of the microbe.

It appeared from investigations in the literature review that viscous drag was to be the most common cause of cell breakage. Therefore, the viscous drag needs to be calculated to determine an estimate for the level of breakage at the point covered. Valve wall shear could also be a cause of breakage but this effect will not be covered due to only isolated and static microbes being studied. For purposes of investigation, if results show high velocity gradients between the microbe wall and the fluid passing, then microbe velocities in the gap should be greater as well as shear forces from viscous drag. This would mean that if the microbe happens to make contact with the valve seat or valve head by inter-particle collision, the contact of the microbe and the valve seat or head should be at a greater velocity also.

In order to estimate the viscous drag for shear forces, it is important that the velocity gradient is measured from each face of the rough sphere. The shear forces acting on the microbe surface are calculated using the following method. Lines projecting each face perpendicular to each face were created using Excel calculations and the Fluent line/rake create command. The lines created were used to measure the average velocity on each of these lines. The velocity difference between the centroids of each face and 1 micron projected line determined the velocity gradient. This velocity gradient was then multiplied by the dynamic viscosity to obtain the shear stress. The shear stress was multiplied by the acting surface area which is in this case assumed to be the measurement line length multiplied by 1.0 as a 2d model is being used. This obtains the shear force. Shear forces are divided according to the category selected. The four categories are the lead anticlockwise forces, lead clockwise forces, trailing clockwise forces and trailing anticlockwise forces as in figure 4.9. Flow that lies in between any of these four categories which also approach the microbe surface between 45° and 90° are assumed to flow at right angles to the microbe surface and hence do not exert shear

forces. As the location of a microbe causes vortices to form, the zone surrounding the microbe and the downstream zones must be turbulent even if in a zone which could be assigned laminar without microbes present. This is due to results from Bosch and Rodi (Bosch 1996), whose results found that for under 4% turbulent intensity, and a Gw/d ratio (D = cylinder ratio; Gw = distance from cylinder centre to nearest wall) of less than 0.3, vortex shedding can be suppressed. In the case covered at position 2, this ratio was found to be $^{10}/_5$ which is 2. Therefore vortex shedding should be present in microbes even in the gap region. Non-negligible velocity vectors were found to be in the opposite direction to the fluid initially hitting the microbe at location c in figure 4.9. This creates a shear force resistance which reduces the effect of shear on the microbe. Clockwise forces are the forces attempting to rotate the microbe clockwise and anticlockwise forces are the opposite rotational force. Full information on the procedure for calculating shear forces on the microbe can be found in appendix B.

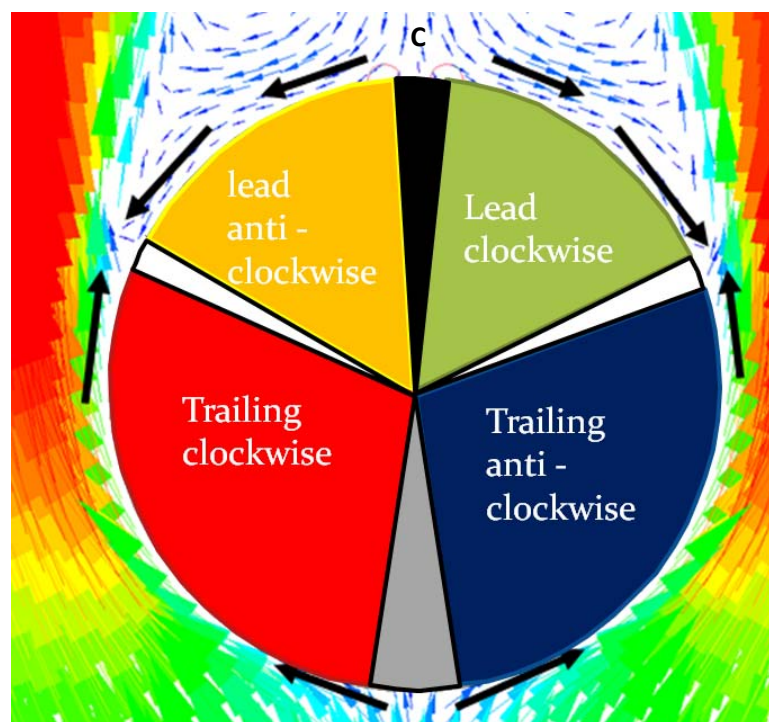


Figure 4.9: Shear force categories and null categories where flow approaches microbe surface near right angle

Table 4.4: Boundary conditions for microbe model

Fluid zones before zone surrounding microbe at nominated position	Water-liquid, Laminar
Fluid zones after zone surrounding microbe at nominated position	Water-liquid, K-ε Realizable
Velocity inlet	1.393 m/s, normal to inlet, relative to adjacent cell zone
Turbulent intensity	3% (position 1-3), 4% (position 4-6)
Turbulent length scale (based on 1/3 D_h)	0.0003 m ² /s ³
Pressure outlet	0 Pa
Wall	Standard wall
Discretization (see section 4.5)	<u>Stage one (<2000 iterations approx):</u> PRESTO pressure Momentum 1 st order upwind Turbulent kt. energy 1 st order upwind Turbulent kinetic energy 1 st order upwind <u>Stage two (>2000 iterations approx)</u> PRESTO pressure Momentum 2 nd order upwind Turbulent kt. energy 2 nd order upwind Turbulent kinetic energy 2 nd order upwind
Under-Relaxation factors	Pressure 0.2 Density 0.1 Body forces 1 Momentum 0.4 Turbulent KE 0.8 Turbulent dissipation rate 0.8 Turbulent viscosity 1 Energy 1
Pressure velocity coupling	SIMPLE

4.4. Breakage results

By using the methodology outlined above for the six microbes along the streamline flow of the homogeniser as outlined in figure 4.7, shear tearing forces caused by lead and trail fluid flow could be estimated.

5 μm diameter results:

Table 4.5: Trailing shear forces for the 5 μm diameter

Microbe position	CW shear force e-16 (N)	ACW shear force e-16 (N)	Total force e-16 (N)
1	51.38	55.75	107.13
2	57.27	51.97	109.24
3	51.84	51.97	103.81
4	47.37	46.90	94.27
5	15.67	15.94	31.61
6	6.20	7.02	13.22

Table 4.6: Lead shear forces for the 5 μm diameter

Microbe position	CW shear force e-16 (N)	ACW shear force e-16 (N)	Total force e-16 (N)
1	11.28	13.44	24.71
2	16.52	4.57	21.09
3	13.31	13.13	26.44
4	9.57	9.31	18.88
5	0.72	1.02	1.74
6	0.00	0.00	0.00

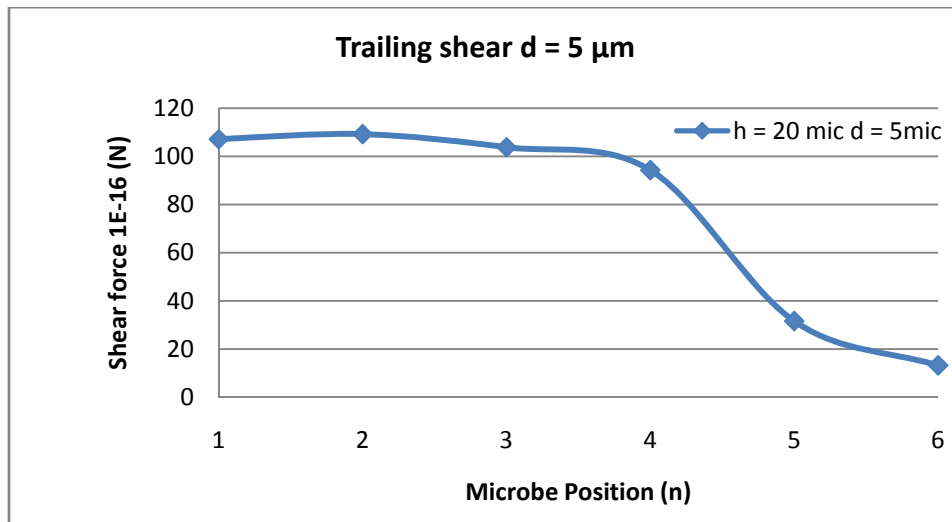


Figure 4.10: Trailing shear force profile for microbes at position 1 to 6 for the microbe of 5 μm diameter

As the gap width does not change along its length for the original concept, trailing shear forces does not change much. However the maximum trailing shear is found at position 2 (109.24 e-16 N). As there is currently no methodology available to accurately quantify the exact breaking force for the cell wall covered experimentally, there is no way of knowing the extent of microbe breakage at the positions covered.

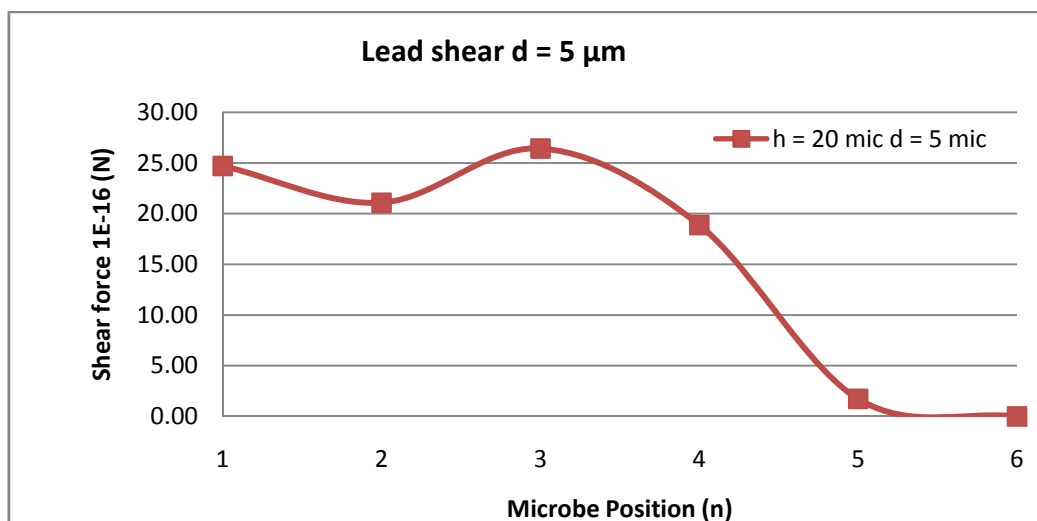


Figure 4.11: Lead shear force profile for microbes at position 1 to 6 for the microbe of 5 μm diameter

However lead shear forces (caused by vortex separation) do not follow such a regular pattern. This is because vortices are unsteady in nature. In order to capture vortex movement more accurately, unsteady solving with time steps would have to be carried out. This would increase hours required to solve as well as hours involved in statistical analysis considerably. Lead shear forces are found to be at least under one-quarter the value of trail shear forces which are caused by direct flow past the microbe.

Also from investigation from velocity vector plots, it is difficult to say if the vortices formed are realistic enough to be considered in calculations as seen in figure 4.11. For reasons of vector plots as well as irregular results, lead shear forces will not be considered in total shear force calculation for optimisation.

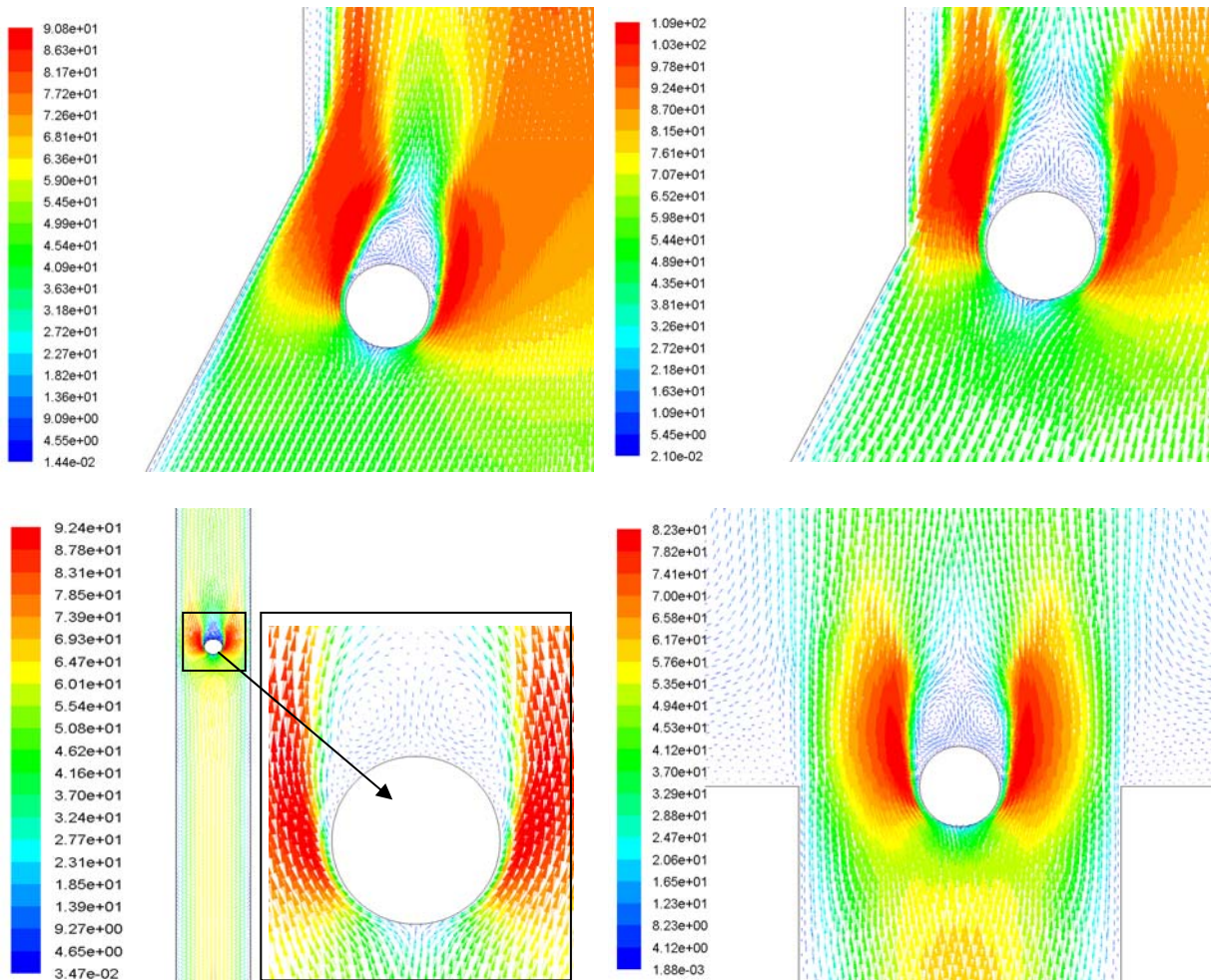


Figure 4.12: Water velocity past microbe at positions (a) 1 (b) 2 (c) 3 and (d) 4

The same procedure was repeated with microbes of 10 μm diameter. It was found that trailing shear was measured as between 31% and 63% greater with a 10 μm diameter. The largest increase in shear forces (62%) was found for the microbe at position 2 where maximum velocity is generally found in the homogeniser. So therefore doubling the diameter of the microbe in the homogeniser does not mean doubling the shear forces. Thus results for shear force magnitudes cannot be considered realistic even if one microbe at a time could pass through as the size of microbes changes greatly. However for optimisation, if the microbe size is kept at 5 microns diameter, equivalent measures of shear forces could be kept reasonably consistent.

5 μm diameter results:

Table 4.7: Trailing shear forces for the 10 μm diameter

Microbe position	CW shear force e-16 (N)	ACW shear force e-16 (N)	Total force e-16 (N)
1	51.38	142.62	150.33
2	57.27	168.98	177.73
3	51.84	153.73	146.87
4	47.37	131.87	124.30
5	15.67	29.67	1.21
6	6.20	8.21	21.64

Table 4.8: Trailing shear forces for the 10 μm diameter

Microbe position	CW shear force e-16 (N)	ACW shear force e-16 (N)	Total force e-16 (N)
1	17.49	12.79	30.27
2	18.71	14.49	33.21
3	16.65	11.51	28.16
4	16.57	9.24	25.81
5	2.85	27.53	30.38
6	18.03	6.28	24.31

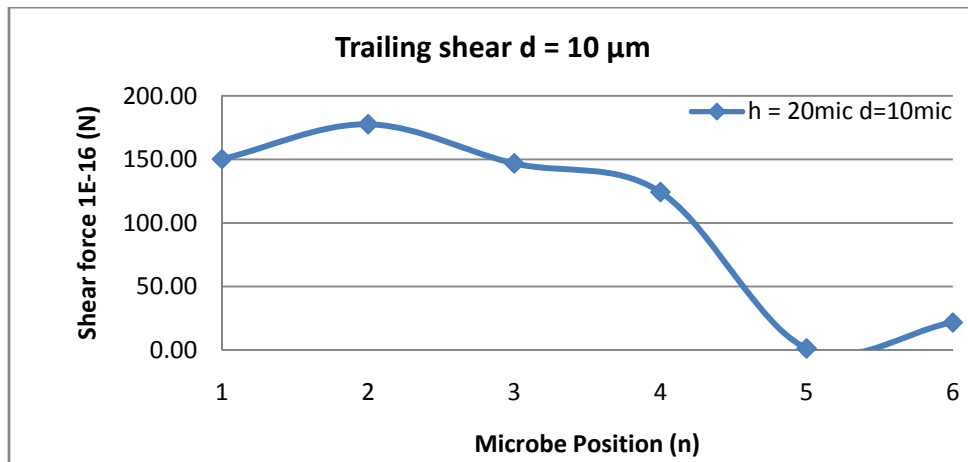


Figure 4.13: Lead shear force profile for microbes at position 1 to 6 for the microbe of 10 μm diameter

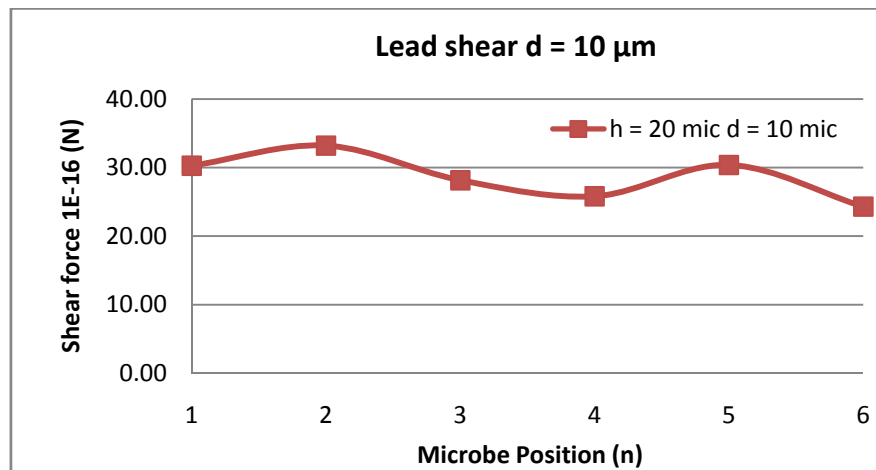


Figure 4.14: Lead shear force profile for microbes at position 1 to 6 for the microbe of 10 μm diameter

4.5. Optimal setup required

As the results for both trailing and lead shear were not very consistent for the exit region as well as being significantly less than near the gap entrance, only positions 1-4 will be compared for each concept for optimisation. Also as vortices cannot be considered reliable due to shear forces obtained as well as the fact that steady simulations are only being covered, lead shear values will not be considered for optimisation. The 5 μm diameter for the microbe will be used in the next part of the study as this size is closer to the yeast cell size that the microbe size is being based on. There was problems implementing the values of K

and ε for the velocity inlet in the microbe model based on Stevenson and Chen's formula (M. C. Stevenson 1997) due to instability. It was found that implementing 3-4% turbulent intensity with a turbulent length of 0.8 was more sufficient in keeping the model stable. Also to ensure stability, the first few thousand iterations was run with the 1st order standard K- ε standard model. As soon as the residuals stabilised (residuals did not change by 1% over 1000 iterations), the model was switched to the 2nd order K- ε standard. As soon as the residuals stabilised again, the model was switched to 2nd order K- ε realisable and the model was run for more iterations until the model fulfilled the convergence criteria as outlined in section 4.2.3 convergence methods for residuals and mesh. The method for determining lead shear forces remains unchanged as outlined in section 4.3.2.

4.6. Chapter 4 summary

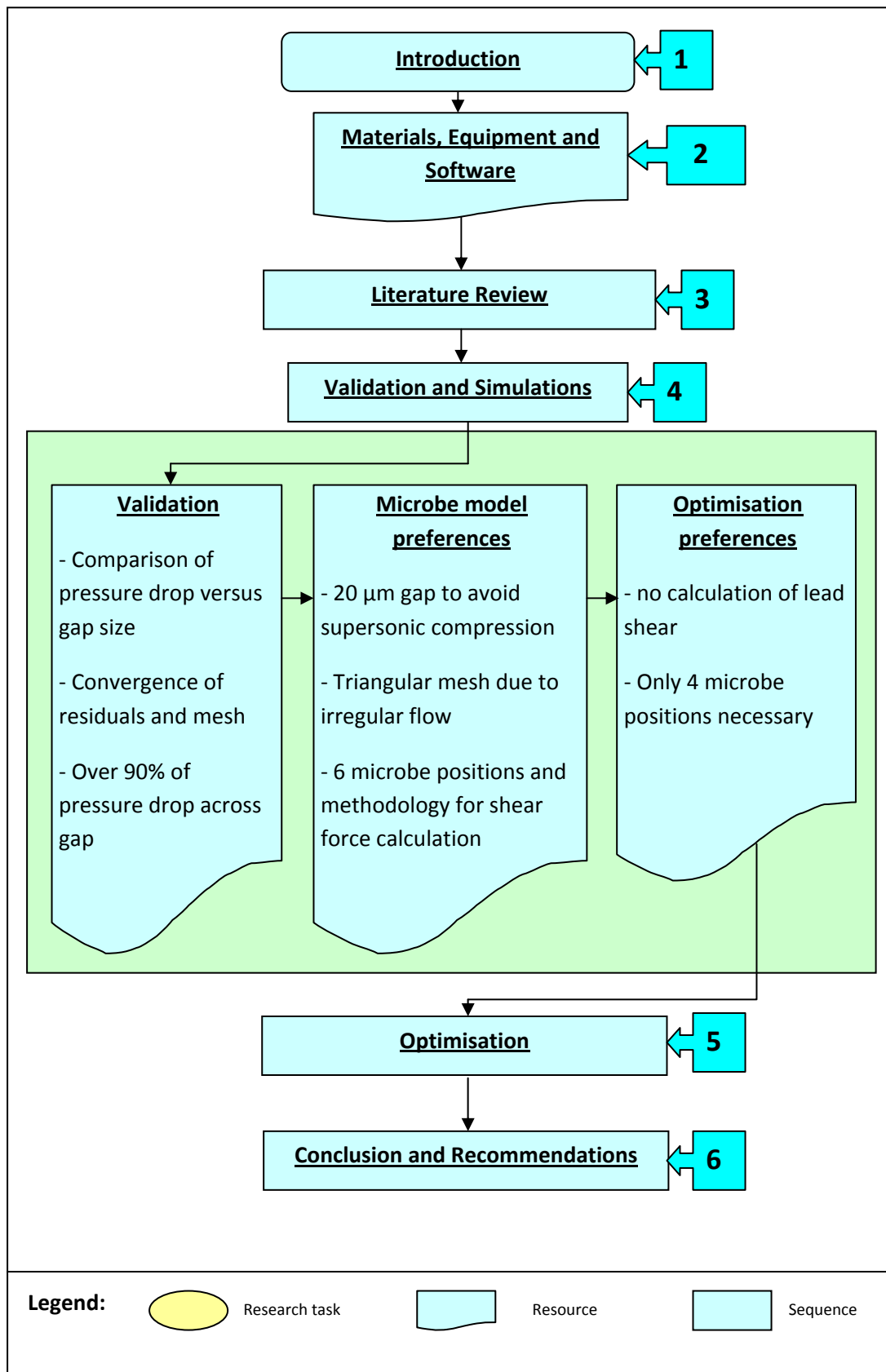


Figure 4.15: Summary of Chapter

Chapter 5 – Optimisation and results

5.1 Introduction

Due to the disagreements between basic theories such as causes of cell wall rupture, it is very important to carry out optimisation of specific geometrical parameters in the homogeniser. In this work, only chamfer angles will be covered. These chamfer changes (inlet and gap chamfers) will be changed one at a time. For all concepts, the parallel gap (between the valve seat and valve head) will extend only to the approximate length where max velocity is reached. It is believed that a gradual opening would reduce heat losses and allow sudden deceleration which may play a moderate part in microbe breakage. The impact ring will also be removed in the model as impact velocities were not significant enough to be considered as a source of breakage with agreement from results obtained from section 4.2.4, Floury (Floury 2004) and Foster (Foster 1995). As a crevice will now be present due to the impact ring removed, removal of homogeniser block material as instructed is recommended as seen in recommendation number 6 in chapter 6. The first seven concepts that will be covered in this chapter will concern optimisation of the gap exit angle to reduce reverse flow after the gap exit as seen in figure 5.3 as well as possible heat losses. Heat losses will not be covered in this study as it is considered outside the scope of study. However, heat losses would become a greater concern if the homogeniser would be in operation for a long period of time.

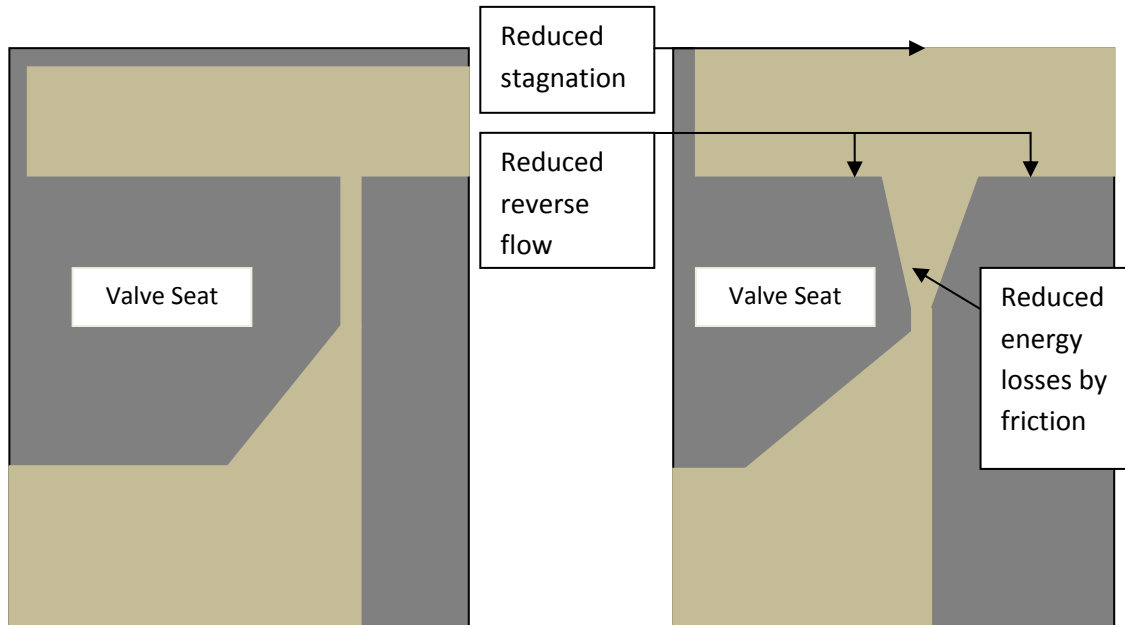


Figure 5.1: Change of original design towards optimising for cell disruption

5.2 Optimisation parameters

As specified in the introduction, only the chamfer angles of the valve head and valve seat will be considered in the study. The goal of changing the valve seat angle (θ_{8-17}) and valve head gap angle (θ_{1-7}) is to minimise reverse flow and reduce energy losses from friction thus reducing unwanted levels of heat. In the original model, the long gap would have been more prone to blockage when compared to a rounded outlet as seen in figure 5.1.

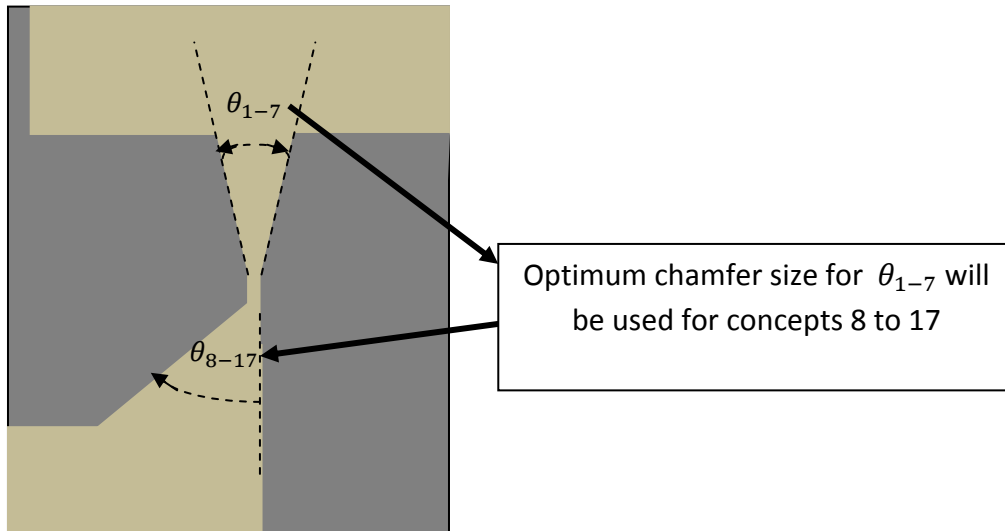


Figure 5.2: Sequence of chamfer size optimisation for concepts 1-17

The goal of changing in the gap entrance chamfer (θ_{8-17}) is to minimise the effects of vena contracta on the wall of the valve seat along the gap as shown in figure 5.3. If high levels of vena contracta is present, less direct flow space will be available at the entrance to the gap thereby reducing efficiency of flow. The effectiveness of each concept will be compared in terms of maximum shear force obtained using the methodology outlined in Appendix B.

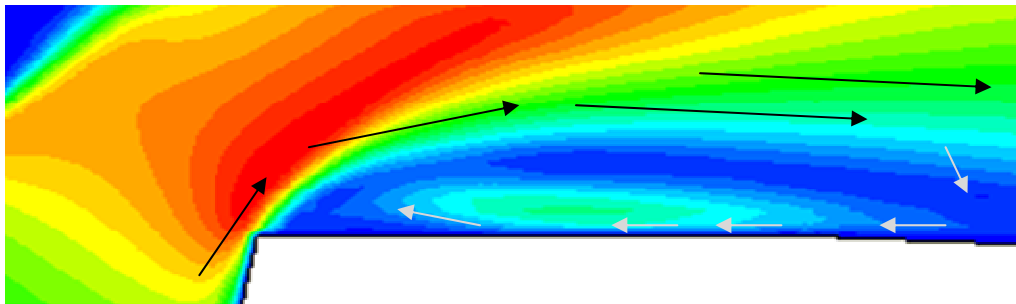


Figure 5.3: Vena contracta

5.2.1 Concepts

After reading the work of Gibson (Gibson 1910), it was decided that more increments of degree changes in the exit angle would be dedicated for the smaller angle range (i.e. 0-5 degrees). The first concept was to use an angle of 5 degrees. Total shear force breakage for

the microbe would be closely monitored as well as backflow velocity just downstream and each side of the outlet of the gap region as the optimum setup would maximise breakage and minimise backflow.

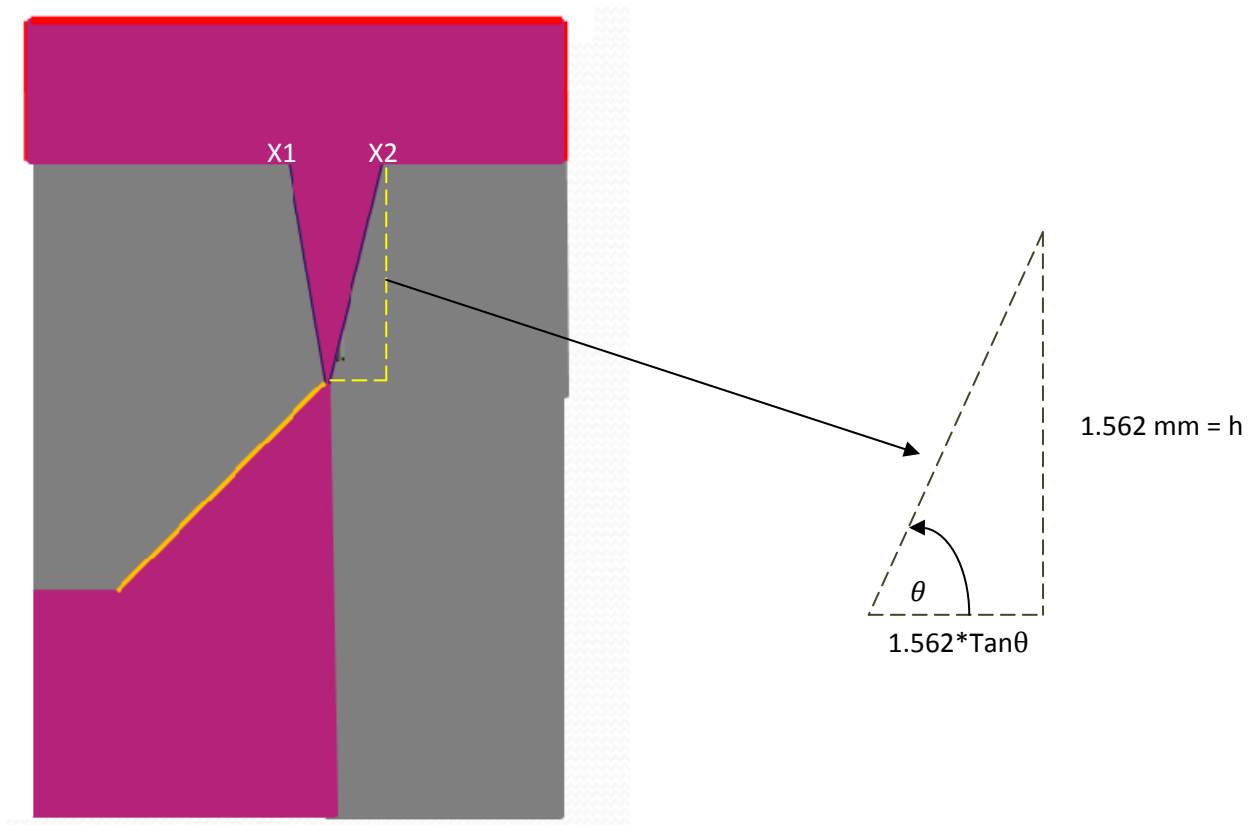


Figure 5.4: Creating coordinates to create angle

Concept 1:

Concept 1 was carried out based on recommendations after analysing the original homogeniser design. Due to reverse flow problems and lack of impact velocity observed, it has been decided that the impact ring will not be used in the following optimisation models. The gap will no longer be square with tapered exits of 5 degrees each side (10 degrees total value for θ_1) to help reduce fluid exit impedance due to strong reverse currents in the exit region. This angle will be changed accordingly as seen in figure 5.5.

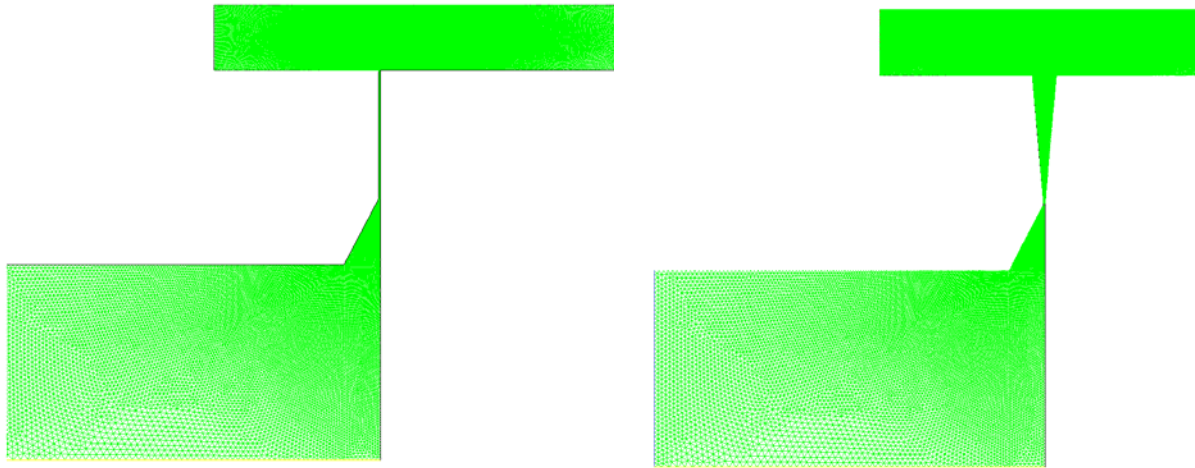


Figure 5.5 : Meshes of (a) concept 0 and (b) concept 1

It appears that despite the tapering out of the gap region, trailing shear force from direct flow appeared to change little around the gap inlet. However shear forces were greatly reduced from the gap entrance to the mid-gap position ($8.62\text{e-}16$ N for C1 and $103.808\text{e-}16$ N for the original model) as vortex shedding influence increased greatly due to increased turbulence. This is due to the fact that in the original model, the gap was still restricted at this point and much of the turbulence was suppressed but with expansion occurring at the gap exit (position 4) instead. The case of the constricted parallel gap suppressing turbulence has already been reported by Chen and Stevenson (M. C. Stevenson 1997). This was not the case with concept 2 due to gap opening occurring here.

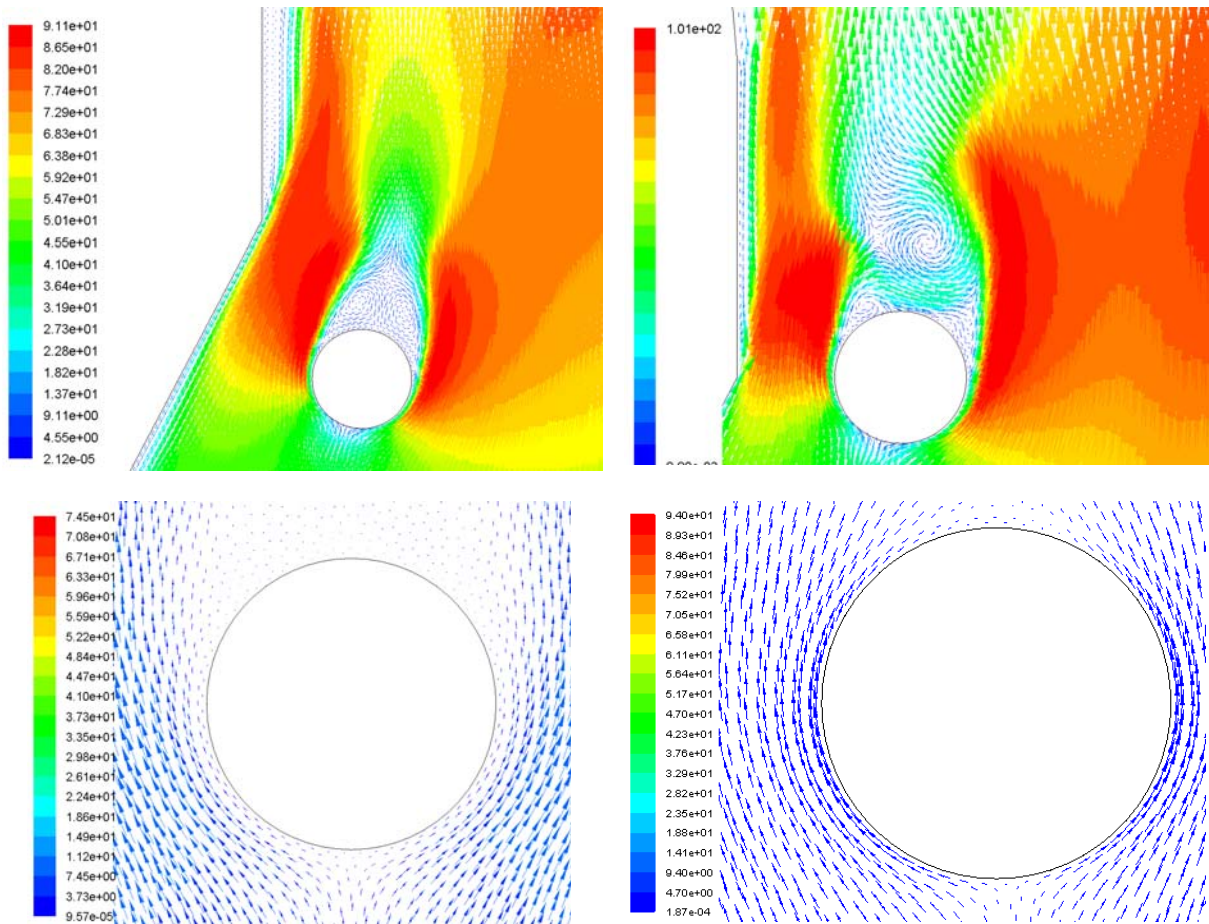


Figure 5.6: Water velocity around microbes for position (a) 1, (b) 2, (c) 3 and (d) 4

At Position 2 as seen in Figure 5.6 (b) and Figure 5.7, there was highly unusual vortex shedding compared to the original design where vortex patterns did not change much in the gap. As the vortex changes direction suddenly from position 1 to position 2, there would be a high possibility of breakage by the sudden change of the vortex. However as K- ϵ realizable viscous modelling is used, it cannot be certain that this occurs experimentally as the μ_t term as seen in the RNG viscous model is not part of the K- ϵ realizable K and ϵ equation (Fluent Inc 2007). This may cause vortices to be overemphasised for the setup used in this study.

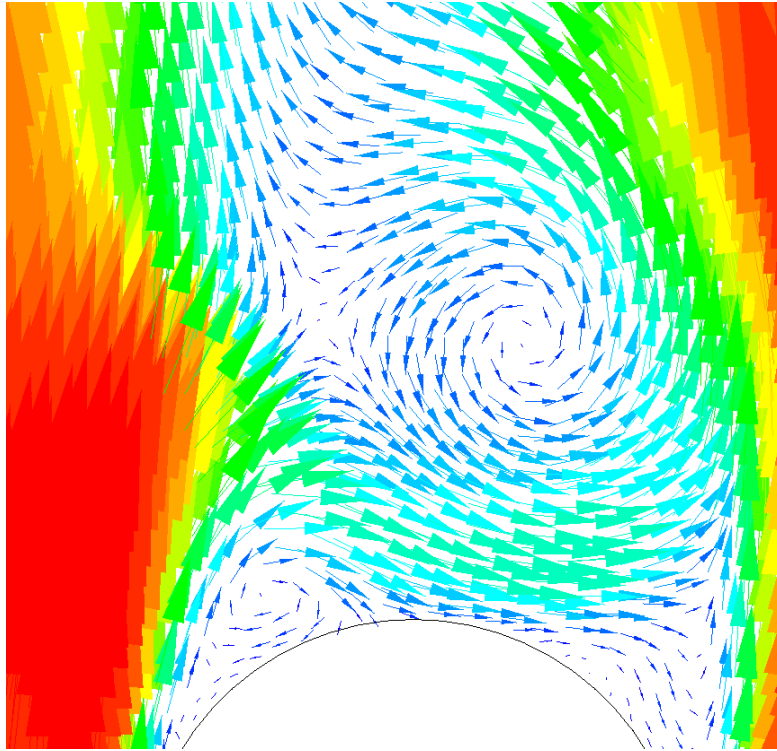


Figure 5.7: Position 2 - Sudden change in microbe pattern at position 2 for concept 1

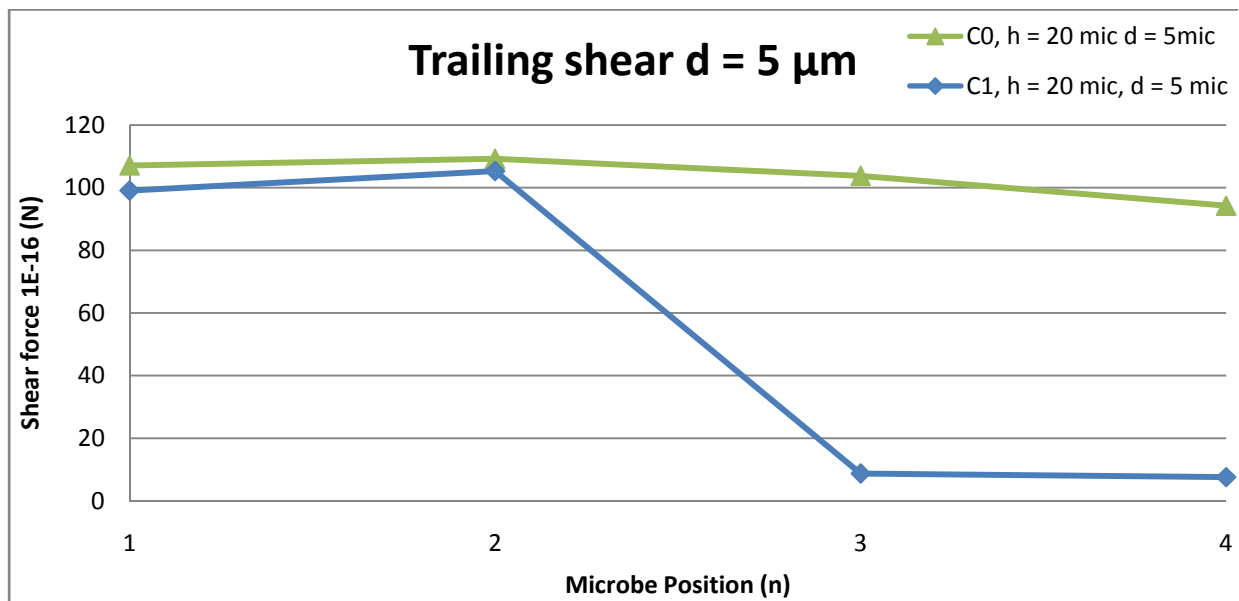


Figure 5.8: Comparison of lead shear for concept 1 and original

Summary of Concept 1

- Changes Made:
 - No impact ring

- Gradual opening from after max velocity in gap to exit
- Opening angle equal both sides with 5 degrees angle
- Observations of setup
 - Velocity gradients approach zero before the gap exit because angle is too steep (i.e. gap needs more constriction)
 - High reverse flow in exit region due to high levels of separation. This reverse flow occurring left and right of the gap also causes problems for the KE solver as turbulent intensities approach very close to maximum allowed values for turbulent viscosity.
 - Sudden vortex change was found.
- Recommendations
 - Reduce angle of chamfer to 2 degrees on the left and 3 degrees on the right to help streamline the flow
 - Extend gap wall at valve seat beyond the gap exit. This will reduce the stagnation caused by 2 flow path options for the fluid exiting the gap. This will also streamline the exiting fluid to leave as a jet. Some reverse fluid will be expected to come from the far end of the valve head downstream of the gap exit. However, this is not expected to be very strong as stagnation regions are no longer present. This is due to the impact ring being removed.
 - Shorter grid exit region in simulation of concept: This is purely to aid quick solution times and also reduce turbulent viscosity problems.

Concept 2:

Following the recommendations from concept 1 results, concept 2 was carried out. The left exit region was removed which would be expected to reduce separation just after leaving the gap. From velocity readings at the gap exit, separation is highly unlikely to be a cause of breakage. Therefore separation effects are undesirable for this purpose of microbial breakage. Two different angles were used for left and right chamfer angles to simulate a 5 degree opening as suggested (Gibson 1910). As in concept 3, 2 equal angles will be formed to make a 5 degree opening also.

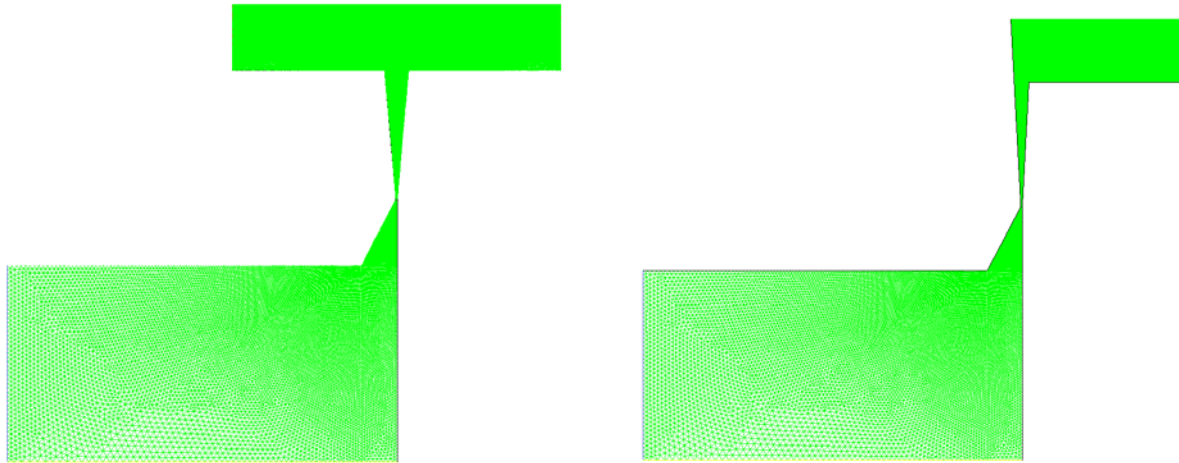


Figure 5.9 : Meshes of (a) concept 1 and (b) concept 2

Even though backflow is somewhat less than in concept 2 than in concept 1, no sudden change in vortex shedding was observed. However consistent increases were observed in trailing forces in comparison to concept 1 and 0. Therefore it is difficult to decide if concept 1 or 2 is a better setup. Reverse flow is reduced as separation no longer occurs as seen in concept 0 and 1. There is still some reverse flow occurring but as the exiting jet is stronger than in concept 1, reverse flow interfering with the exiting jet will be less for concept 2.

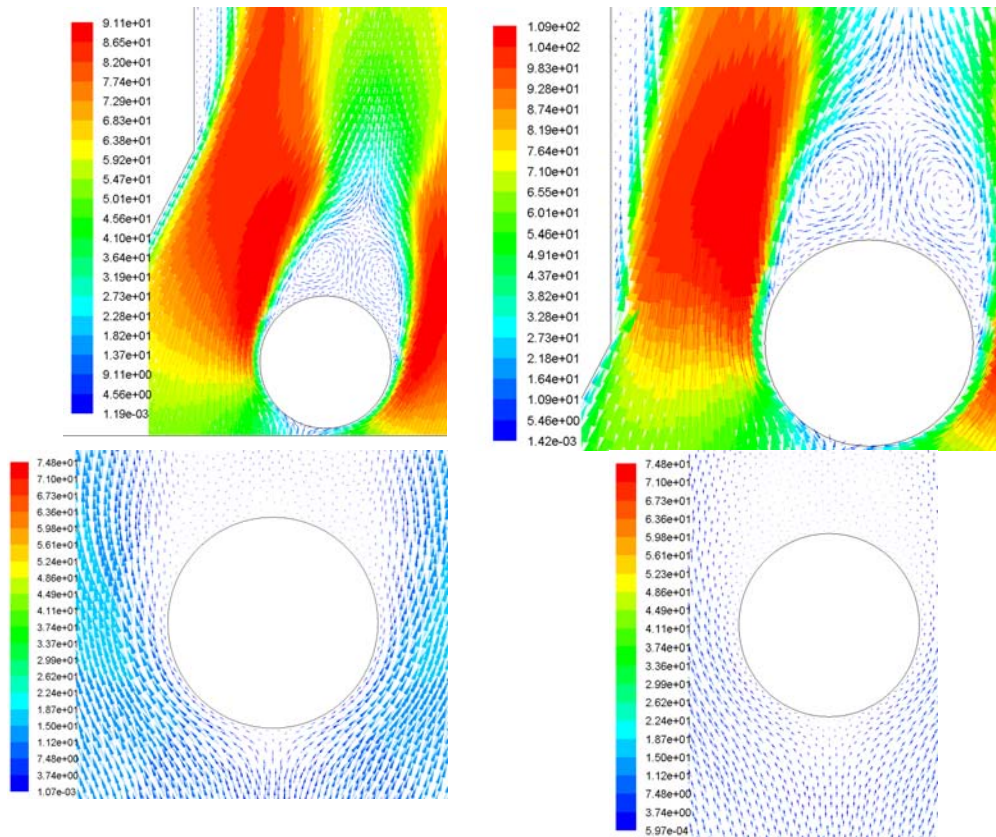


Figure 5.10: Water velocity around microbes for position (a) 1, (b) 2, (c) 3 and (d) 4

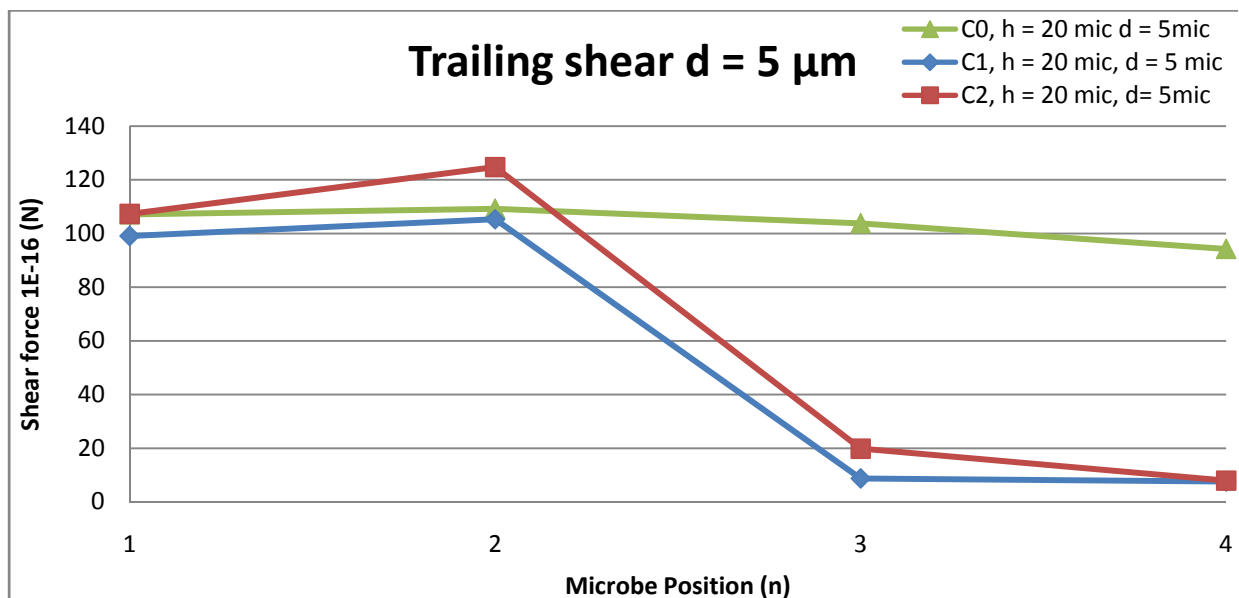


Figure 5.11: Comparison of concept 2 to previous concepts.

Summary of Concept 2

- Changes Made:
 - Removed left exit region
 - Fully extended valve seat wall along gap region
- Gap exit chamfer angle 3° on left, 2° on right
- Observations of setup
 - Higher peak shear forces than found with concept 0 or 1.
 - Velocity gradients approach zero before the gap exit because angle is too steep (i.e. gap needs more constriction)
 - Reduced reverse flow.
 - Stronger gap exit jet than concept 1 but weaker than concept 0.
 - Sudden vortex change at gap entrance was not found as seen in concept 1
- Recommendations
 - Change angle of chamfer to 2.5° on both sides

Concept 3

For concept 3, the chamfer was changed to 2.5° . No other major changes were applied to the geometry.

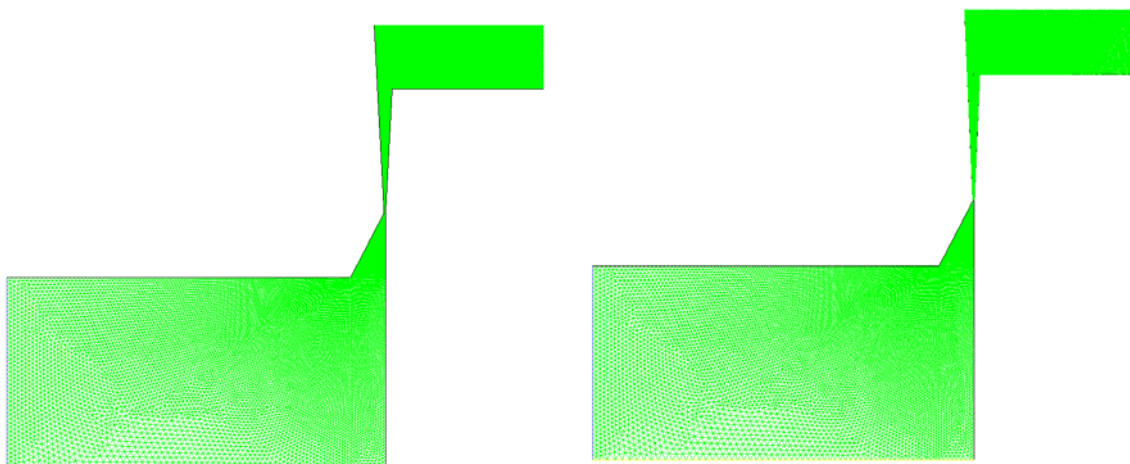


Figure 5.12 : Meshes of (a) concept 2 and (b) concept 3

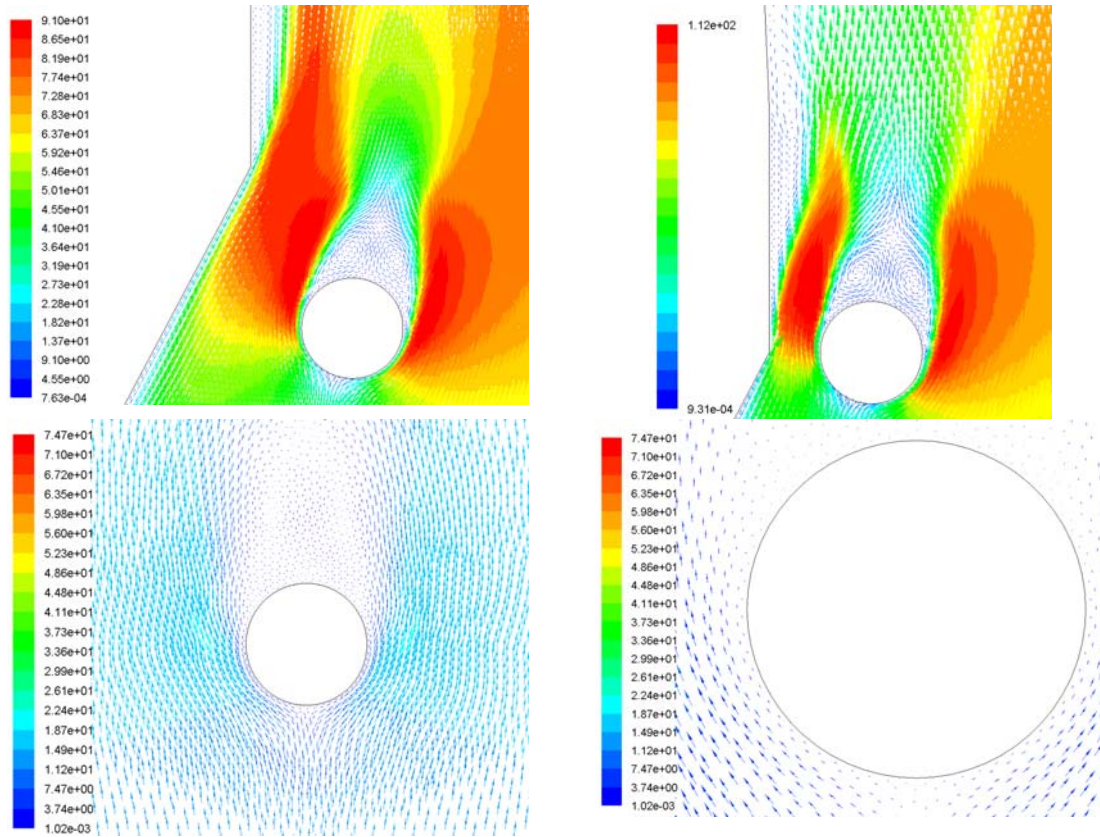


Figure 5.13: Water velocity around microbes for position (a) 1, (b) 2, (c) 3 and (d) 4

Vortices remained regular enough but in position 2, a circulation region was found to form at the beginning of the gap expansion as seen in figure 5.14

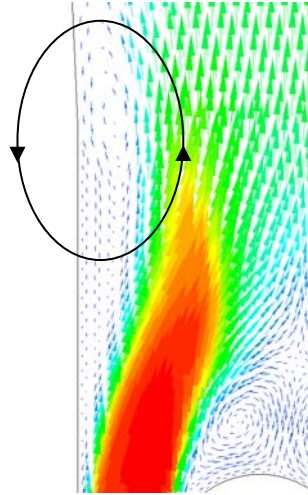


Figure 5.14: Circulation downstream of microbe at position 2.

Once again, the trailing shear forces increased further but this time by 22.4%. It seems that a less sudden expansion gives higher max velocities for the microbe shear force.

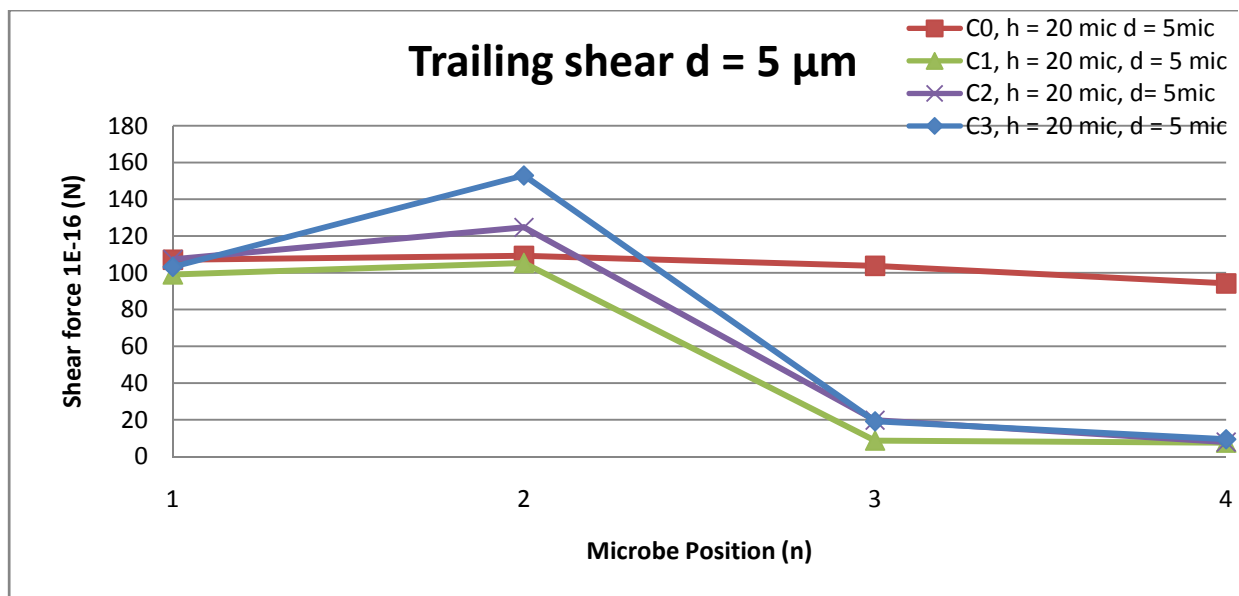


Figure 5.15: Comparison of concept 3 to previous concepts.

Summary of Concept 3

- Changes Made:
 - Gap exit chamfer angle 2.5° on both sides
- Observations of setup
 - Much higher shear forces (22.4% greater) than concept 2.
 - Small circulation region found at gap expansion when microbe was at position 2.
- Recommendations
 - Decrease angles of chamfer to 2° both sides.

Concept 4

For concept 4, the chamfer was changed to 2° for both sides. No other major changes were applied to the geometry.

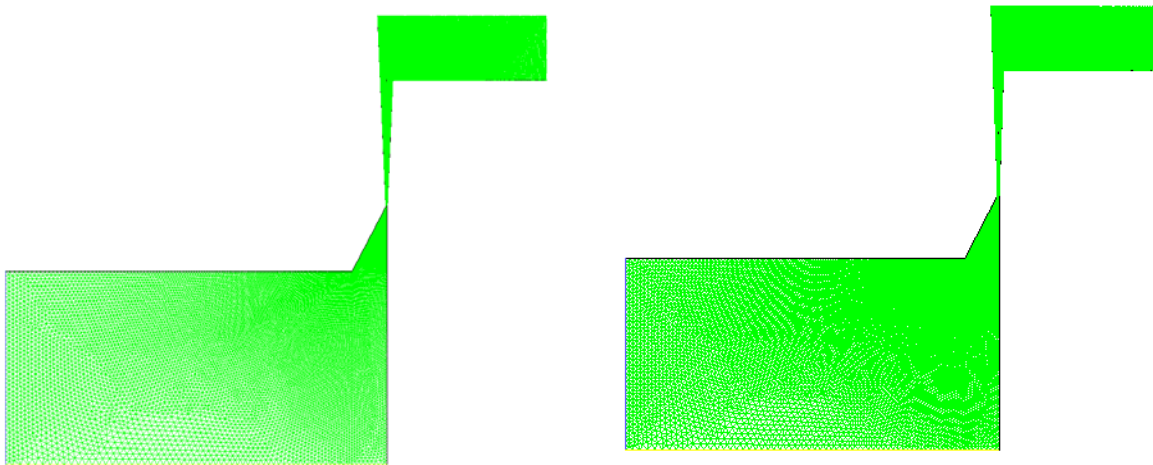


Figure 5.16 : Meshes of (a) concept 3 and (b) concept 4

High levels of vena contracta were noted in concept 4 for when the microbe was located at position 2 (marked “c” in Figure 5.17 (B)).

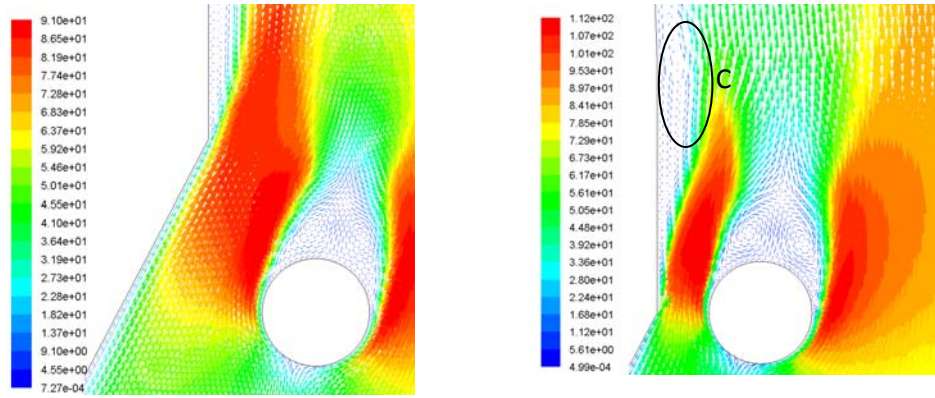


Figure 5.17: Water velocity around microbes for position (a) 1, (b) 2

However using an outer chamfer angle of 2 degrees was found to have lower shear forces than using the 2.5 degree chamfer.

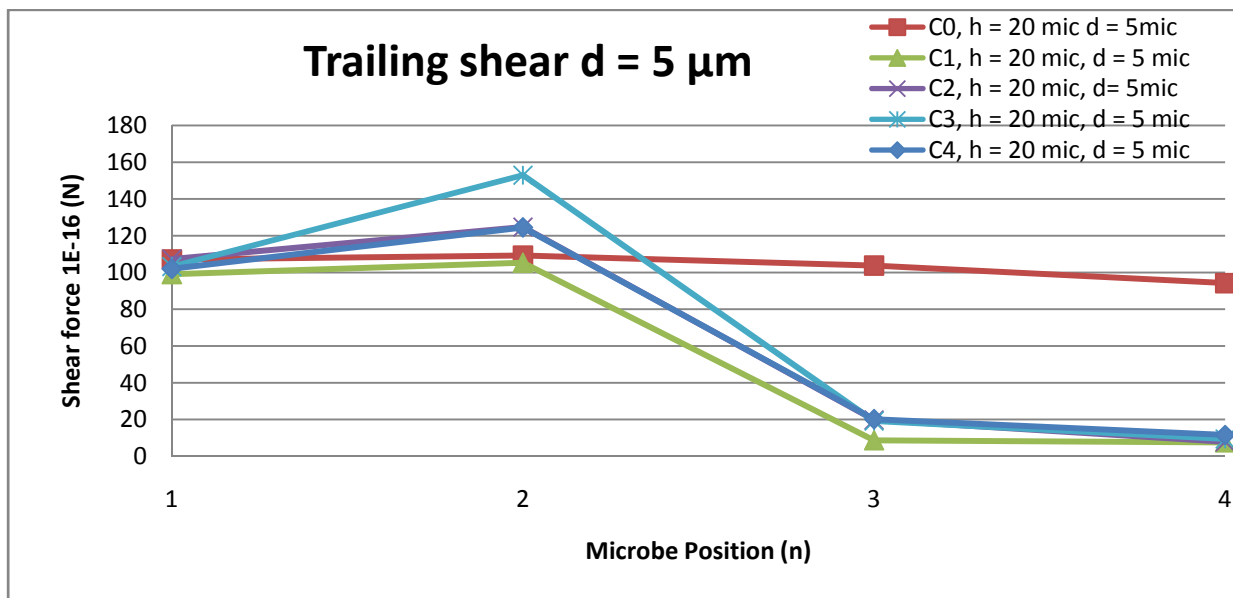


Figure 5.18: Comparison of concept 4 to previous concepts.

Summary of Concept 4

- Changes Made:
 - Gap exit chamfer angle 2° on both sides
- Observations of setup
 - Reduction of shear forces
- Recommendations
 - 3 degrees each side

Concept 5-7 (3.0, 2.25 and 2.75 degree chamfers)

The chamfer angle at the gap exit was changed to 3, 2.25 and 2.75° to see how variations in angles around the value of chamfer angle where maximum shear was achieved is affected. Circulation regions at position 2 were found for these remaining three configurations as seen in concept 3 and 4. Flow patterns did not change greatly when compared to the previous concepts 3 and 4. Values of near microbe velocity gradients and hence shear forces were less than when a 2.5 degree chamfer was used as seen in concept 3.

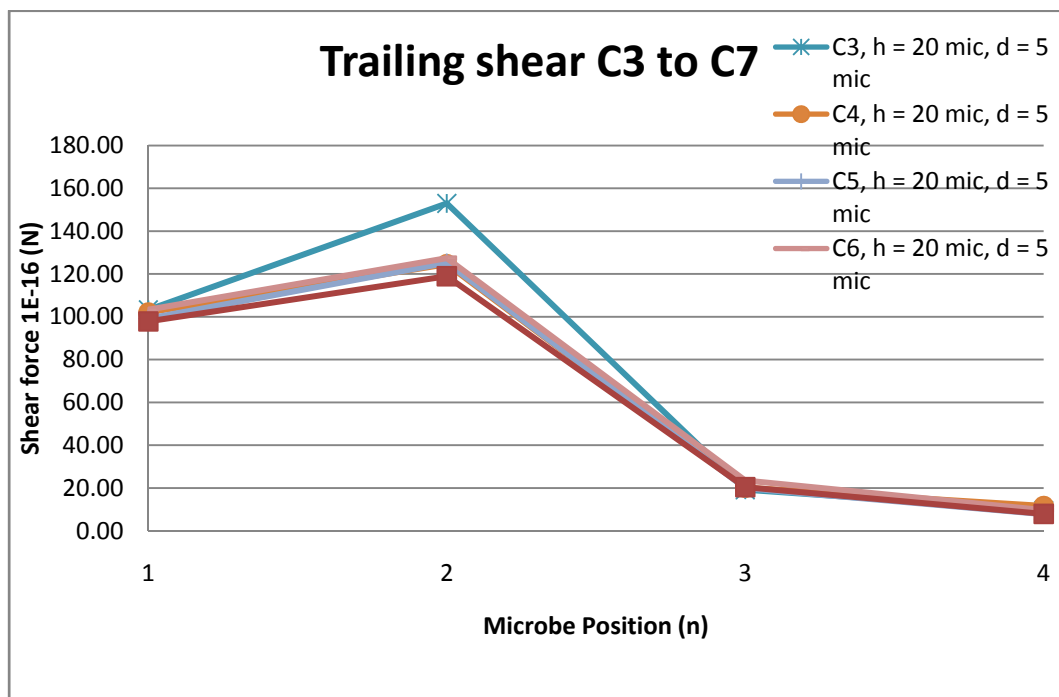


Figure 5.19: Comparisons of concept 3 with subsequent concepts in terms of shear force profiles from microbe position 1-4

Overview of concept 1-7:

Table 5.1: Chamfer angles used for concept 1-7

Concept (n)	left chamfer angle (°)	right chamfer angle (°)
0	0	0
1	5.77	5.77
2	3	2
3	2.5	2.5
4	2	2
5	3	3
6	2.25	2.25
7	2.75	2.75

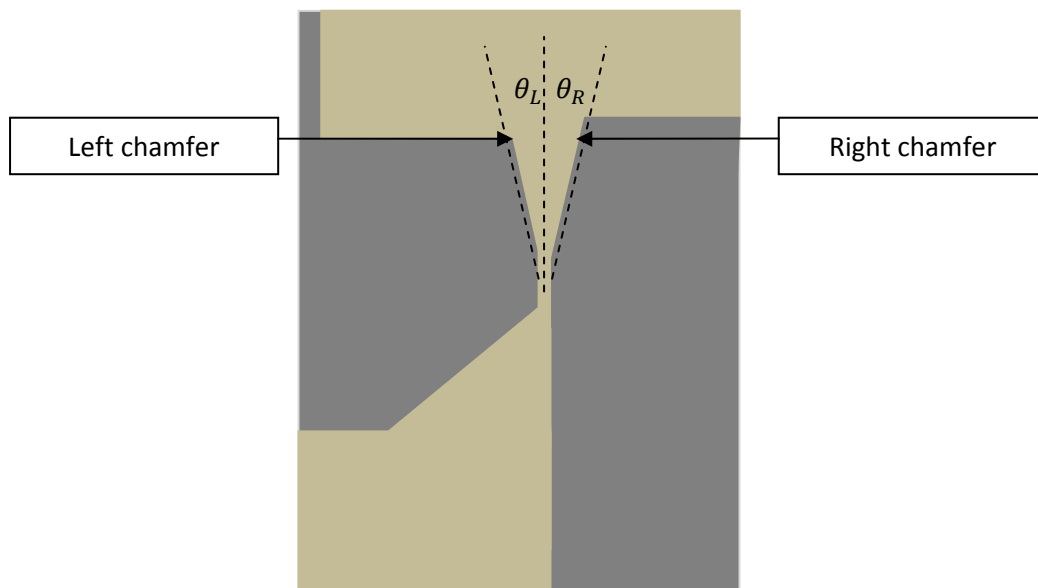


Figure 5.20: Left chamfer angle and right chamfer angle

Table 5.2: Shear forces for concept 1-7

Concept (n)	Shear force 1 (N)	Shear force 2 (N)	Shear force 3 (N)	Shear force 4 (N)
0	107.13	109.24	103.81	94.27
1	99.10	105.33	8.72	7.57
2	107.32	124.77	19.84	7.93
3	103.25	152.98	19.23	9.47
4	102.01	124.54	20.20	11.64
5	99.12	125.19	19.94	7.76
6	103.21	127.35	23.51	9.74
7	97.84	118.96	20.42	7.96

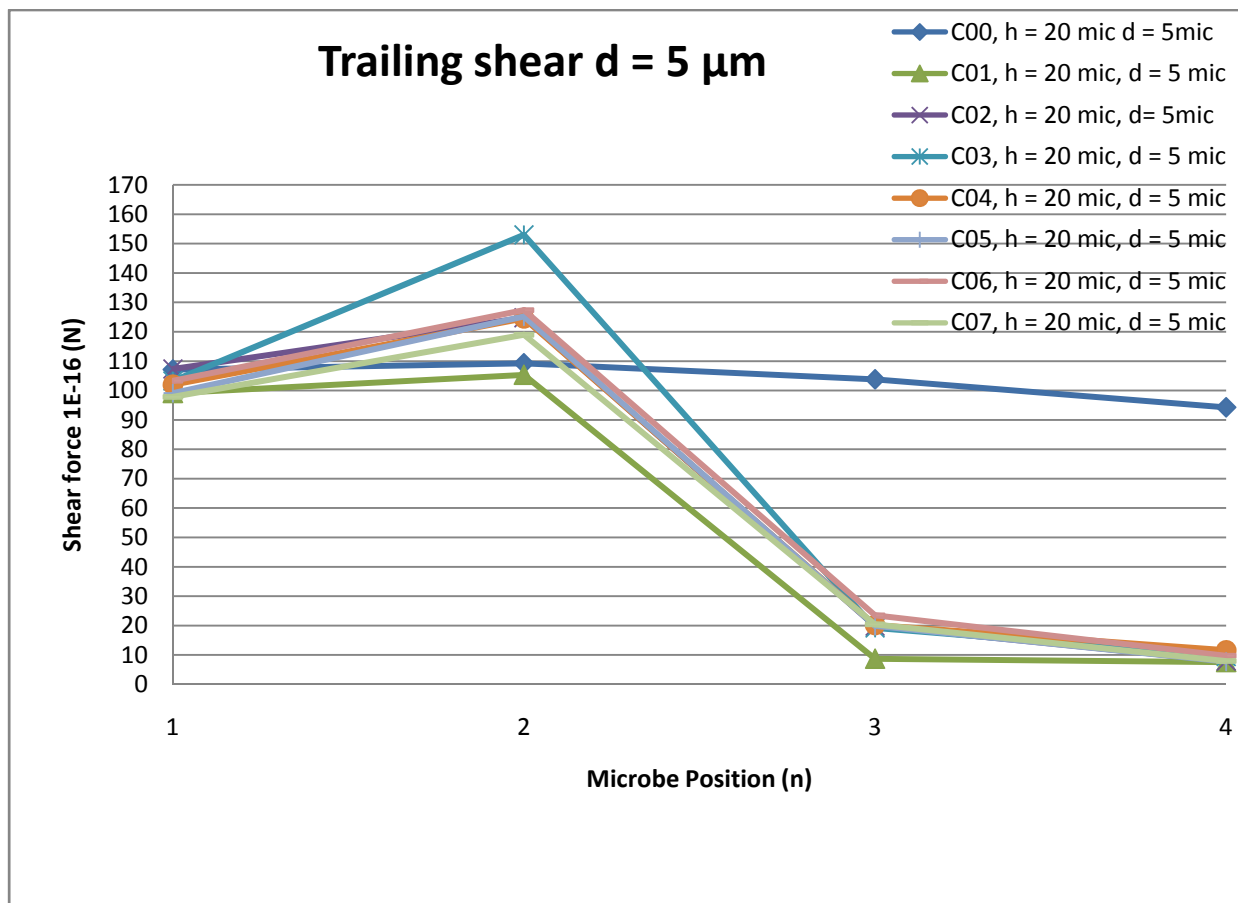


Figure 5.21: Comparison of shear force profile from microbe position 1-4 for concept 1-7

Concept 8-15: Inner chamfer change in steps of 10 degrees

For these concepts, the inlet chamfer was changed in 10 degree increments to determine the optimum chamfer angle for cell disruption and breakage.

There was a evolution of a vena contracta found as the chamfer angle was increased from angles exceeding 30 degrees. When the chamfer angle was 30 degrees, vena contracta phenomena was only more noticable as the microbe entered the gap region. This behaviour became noticeable even when the microbe had not entered the gap region.

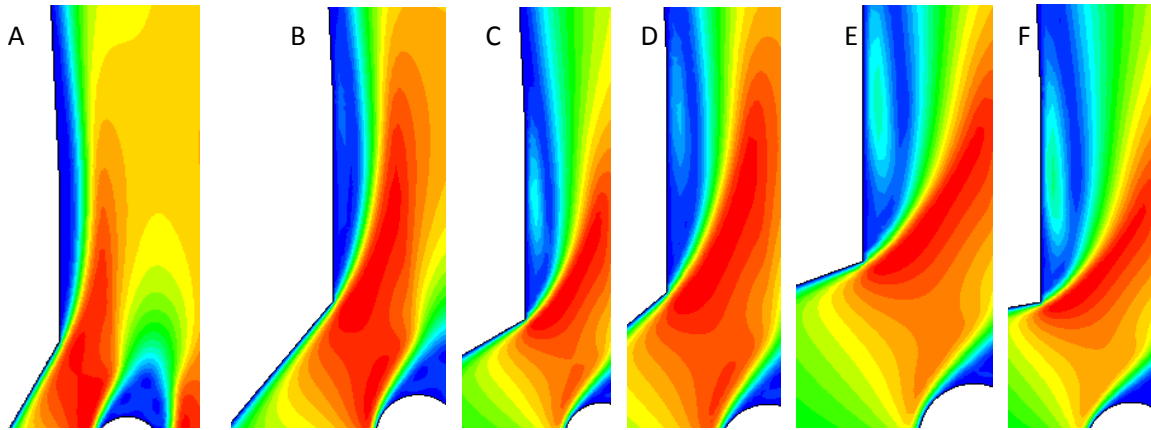


Figure 5.22: Evolution of vena contracta with left and right chamfer change for (a) concept 10 (30°), (b) concept 11 (40°), (c) concept 12 (50°), (d) concept 13 (60°), (d) concept 14 (70°), (d) concept 15 (80°) for the microbe at position 1

Again there was a steady increase of vena contracta as the inlet chamfer angle increased.

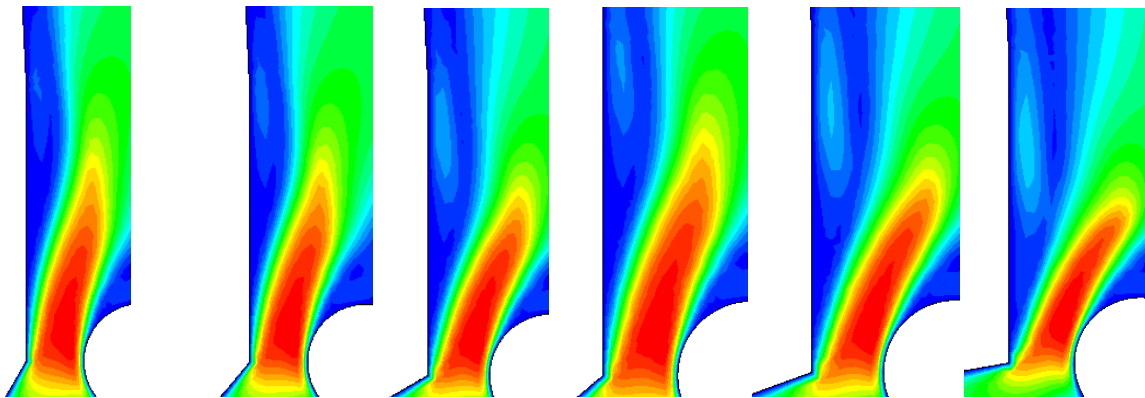


Figure 5.23: Evolution of vena contracta with left and right chamfer change for (a) concept 10 (30°), (b) concept 11 (40°), (c) concept 12 (50°), (d) concept 13 (60°), (d) concept 14 (70°), (d) concept 15 (80°) for the microbe at position 2

Vena contracta is not favourable for efficient flow. Even if velocity gradients and leading shear forces are increased, much higher energy inputs would be required to force the fluid mixture through a smaller space. There was no noticeable vena contracta behaviour for all microbe positions when the inlet chamfer was 27.69° as seen in the original design provided. Therefore this could have been one of the aspects the original designers wanted to minimise.

Again, the shear forces were compared and it was found that maximum shear forces were found at the gap entrance when the inlet chamfer angle was retained.

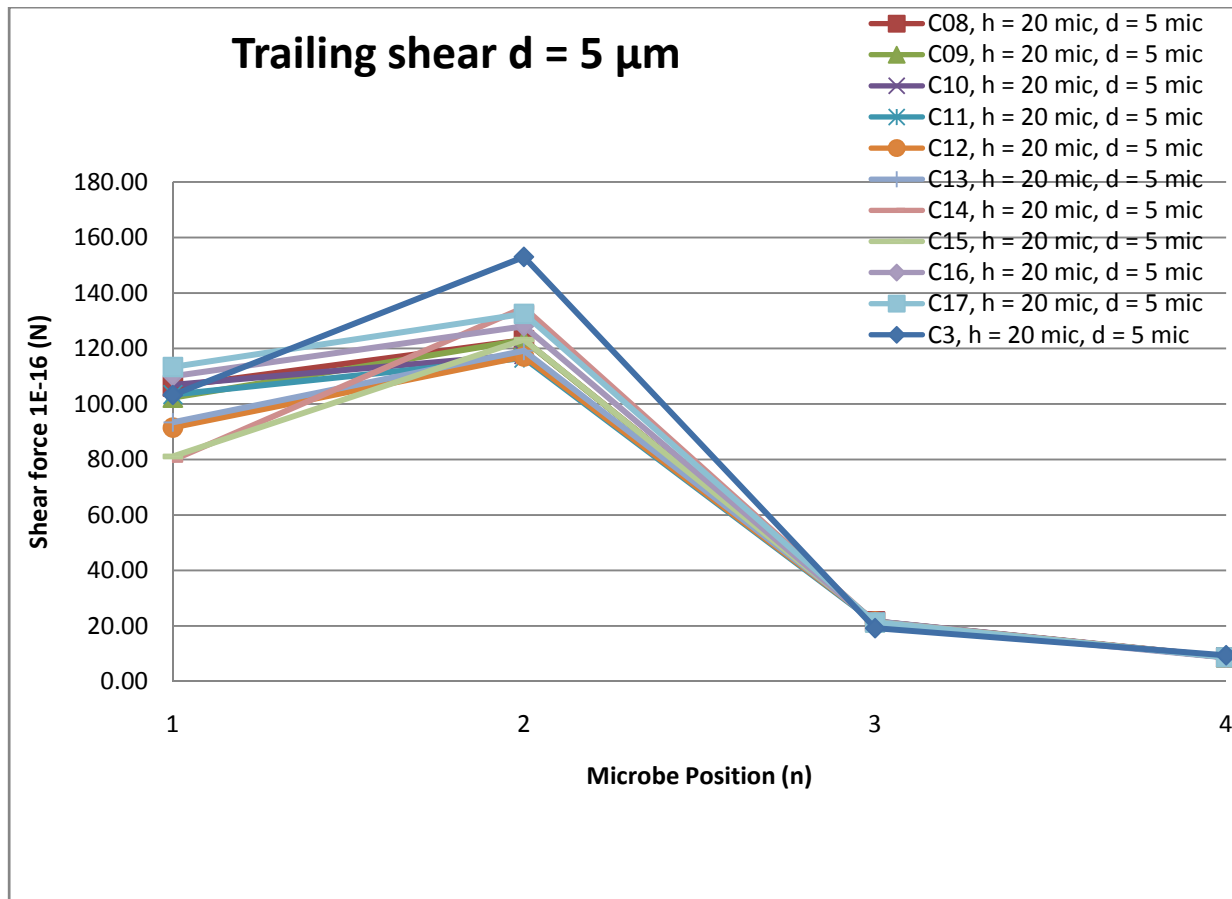


Figure 5.24: Shear forces for concept 8 – 17 and for concept 3

Overview of concept 8-17:

Table 5.3: Chamfer angles used for concept 8-17

Concept (n)	inlet chamfer angle (°)
8	10
9	20
10	30
11	40
12	50
13	60
14	70
15	80
16	27
17	28

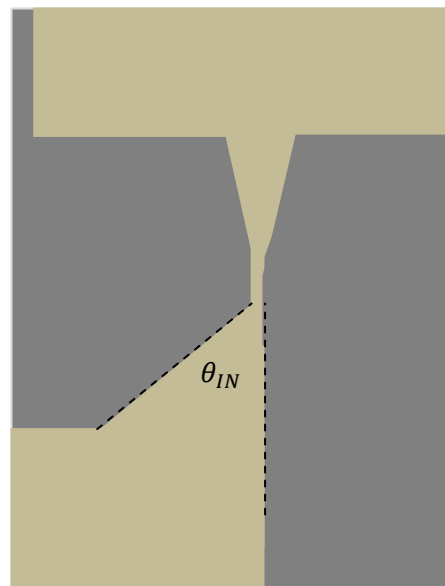


Figure 5.25: Chamfer angle for concept 8 – 17 and for concept 3 (not to scale)

Table 5.4: Shear forces for concept 8-17 in comparison to concept 3

Concept	(n)	Shear force 1 (N)	Shear force 2 (N)	Shear force 3 (N)	Shear force 4 (N)
8		106.29	123.02	21.70	8.76
9		102.27	123.02	21.40	8.79
10		106.92	117.78	21.73	8.86
11		103.38	116.55	21.31	8.81
12		91.53	117.13	21.64	8.78
13		93.38	119.19	21.65	8.68
14		79.80	134.70	21.32	8.93
15		81.10	123.18	21.32	8.89
16		110.12	128.02	20.88	8.67
17		113.34	132.49	21.31	8.75
3		103.25	152.98	19.23	9.47

5.2.2 Optimised setup

The optimised design of concept 3 can be seen in appendix C. The extended valve seat face along the gap helps to streamline the flow towards the outlet. No impact ring was needed in the optimal setup as explained in section 4.24. Therefore for the optimised model, the single phase water model had to be carried out to compare the pressure drop with the original design.

5.2.3 Optimised setup versus original design in terms of pressure drop

Both models were measured for static pressure at equivalent points in the domain. Both models implemented the same settings as specified in Appendix B.2.2.

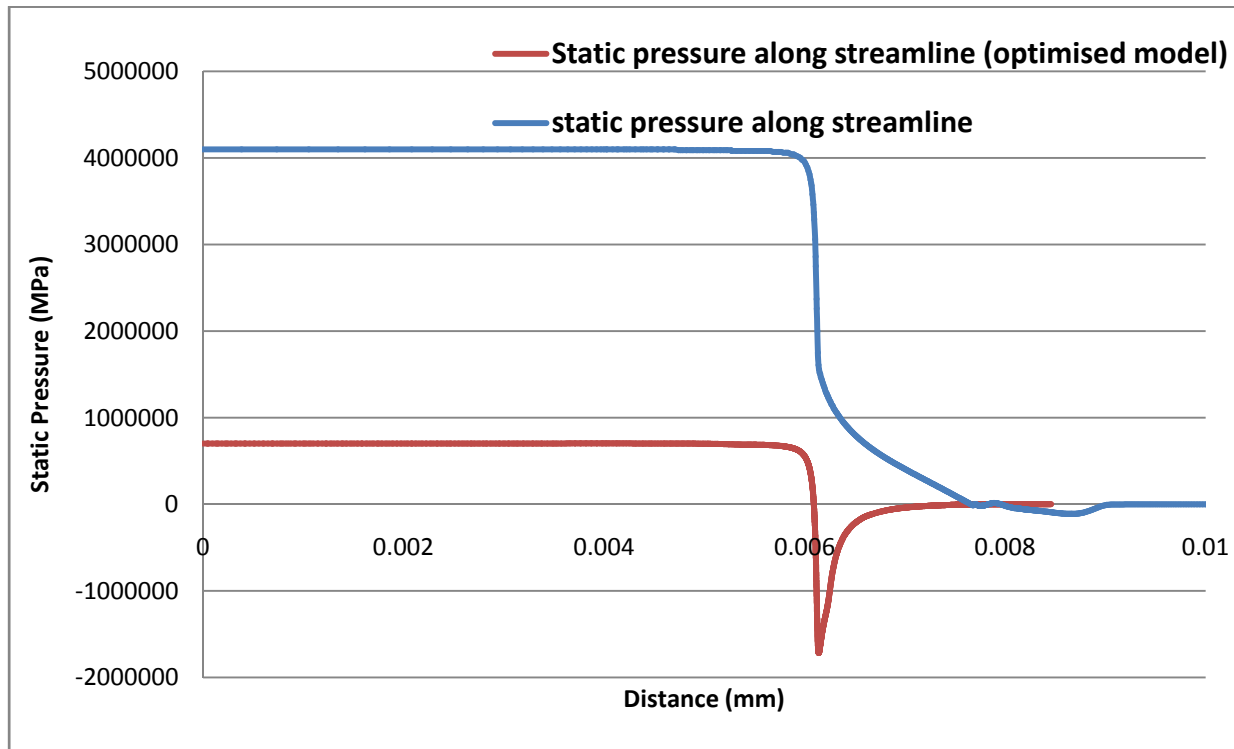


Figure 5.26: Comparison of pressure drop of original concept against optimised concept

It was found that for the same flow rate that there was a 95% difference between the pressure drop of the original design and the optimised design. Therefore, as the optimised design reported a lower pressure drop for the same gap size, the optimised design could be deemed more efficient for flow as seen in figure 4.26. This is because kinetic energy conversion heat and friction energy would be reduced with less chances of constriction and blockage of flow. Also, as the same pressure drop is made with greater velocity gradients, this makes the new valve design even more efficient than the original one.

Summary of improvements in design for mechanical disruption of microbes by homogenisation:

1. Shorter average streamline length due to repression of separation regions that were caused by the presence of an impact ring. The streamline path covered in the original design was 88 mm. In the new design the streamline selected covered a path of only 22 mm.
2. There are smaller pressure drops across the valve for the new design by 90% with the same flow rate which translates to less unwanted energy losses such as kinetic energy to friction and heat energy.
3. There was an increase of peak shear force formed by velocity gradients at the gap entrance by 40% by using the new optimised design when compared to the original design.
4. There is a quicker drop off of fluid velocity and shear force after the gap entry for the new optimised design. This may cause some additional microbes to be broken by rapid decompression as well as reduced heat and friction losses as mentioned in point 2 above.
5. There is less reverse flow due to optimal gap departure angles and no impact ring. Vena contracta effects are maintained to the same low quantity as the inlet chamfer remained unchanged.

5.3 Chapter 5 summary

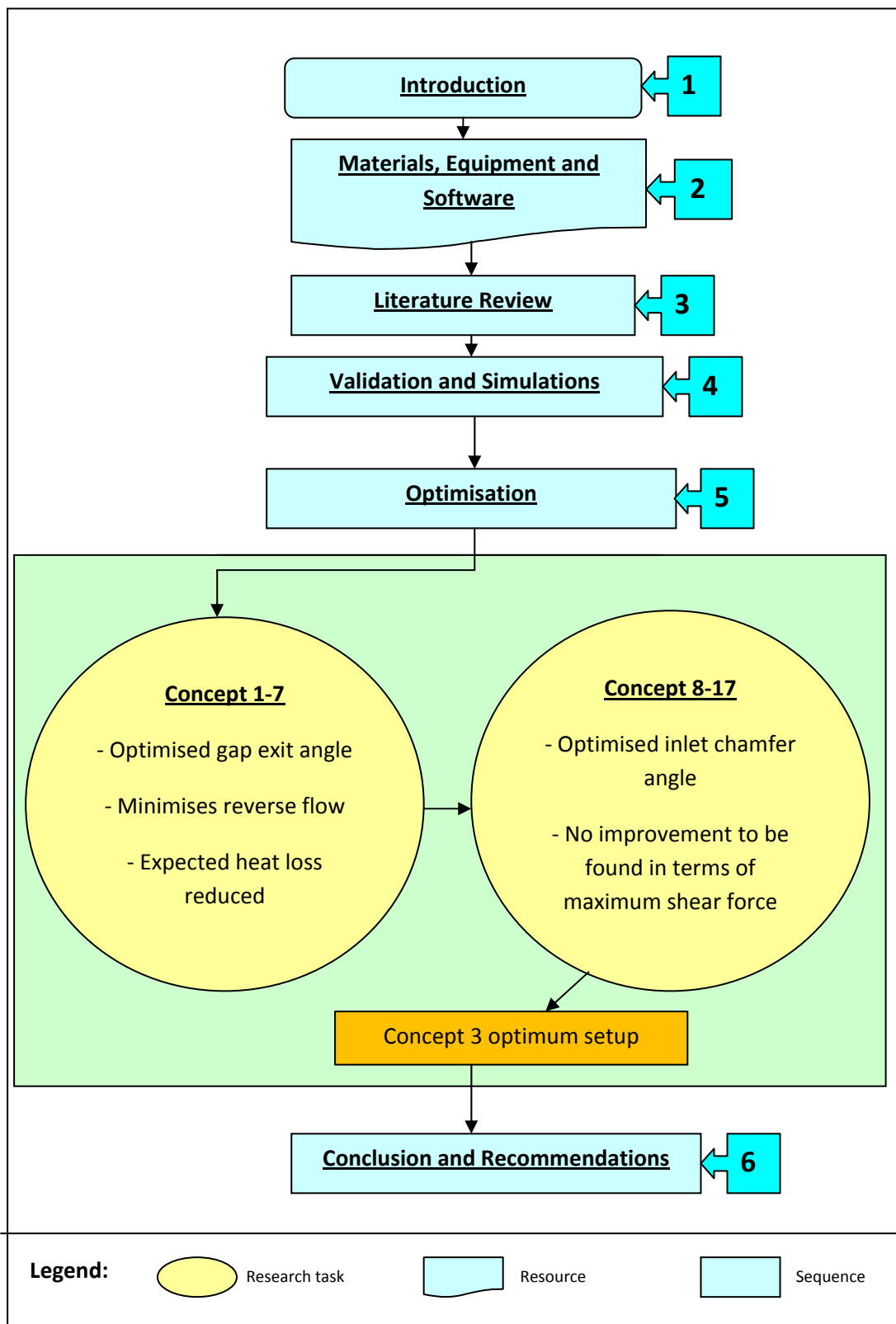


Figure 5.27: Summary of the research process in chapter five

Chapter 6 - Conclusion and recommendations

6.1 Conclusions

In order to make use of the valve design and setup, it is very important that the angles of the chamfers recommended are maintained in production of the optimised valve. As this valve is optimised for shear force on a microbe diameter of 5 microns constant size, this setup could be very useful for breakage of most yeast cells. Yeast is used in many industries such as in the food and brewing industries. Improvement in yeast cell breakage could help extend shelf life, improve flavour and content consistency and improve reusability of yeast for further processing hence reducing cost of ingredients. For the case of microbes in general, the increase of breakage of microbes can allow more nutrients to be released for possible increase in methane production of maize silage with waste water sludge.

The main conclusions of this thesis are:

1. There is no inherent advantage of implementing an impact ring for cell disruption or breakage from investigation of literature survey and computational results. Stagnant regions are eliminated with this approach. If an impact ring is absolutely necessary due to the use of an abrasive material being passed, then the impact distance should be maximised as far as possible.
2. A gradual gap opening of 5° (2.5° each side) between the valve head and valve seat with extended valve seat wall greatly reduces reverse flow and circulation in the exit region, thus improving flow efficiency.
3. The gradual gap opening of 5° degrees also allows lower pressure drops with the same flow rate while also increasing maximum microbe wall shear when compared to the original design of parallel valve seat and valve head faces at the gap.
4. No changes to the inlet chamfer were necessary to improve the original design.
5. Doubling the microbe diameter from 5 μm to 10 μm increases the peak shear stress by 62%.

The main contributions of this thesis are:

1. Verified pressure drop versus gap size and identified separate pressure drops.
2. Estimated values of shear force from direct flow and vortex shedding.
3. The rejection of the need for an impact ring for cell and microbe breakage.
4. Maximum microbe wall shear force increased by 40% with optimised valve geometries when compared to original design.
5. Reduced pressure drop by 90% with same flow rate for optimised setup.

6.2 Recommendations

1. As materials passing through the homogeniser may be corrosive and may be used in food products, steel would not be recommended as found in the original design. Zirconium would be a more recommended material as zirconium does not rust and also is highly scratch resistant. Zirconium is used in the homogeniser for the Ashtown National Food Centre. Tungsten Carbide is used in the MicroSludgeTM valve parts to extend life of the valve (US *Patent* No. 6013183). These two materials could be compared in future works.
2. To carry out simplified experiments with parallel plates, circular obstacles and rapid photography to compare the velocity vectors obtained in simulations against flow patterns observed based on a scaled up process. Miniature pressure sensors could be used on experimental circular obstacles to quantify forces of pressure on the microbes. The velocity of the passing fluid could be determined by passing some micron sized colour particles through and with use of rapid photography. There is definitely a need to determine validated minimum microbe breakage forces based on various dimension characteristics to know how much the microbe breakage forces are.
3. It would be also recommended by the author to improve capturing of vortex shedding using unsteady simulations (with time steps) to improve capturing of vortex shedding. The RANS viscous model may achieve better capturing of vortices but a user defined function that can rotate and translate the microbe according to predicted trajectory with each time step (would need to be very small $>10^{-6}$ s) may be more suitable. It is also worth mentioning that unsteady simulations may be able to capture pressure

fluctuations (with microbes larger than eddies) and velocity fluctuations (with microbes smaller than the smallest eddy).

4. Further analysis of microbe breakage with multiple microbes in the domain at the same time. If Discrete Phase Method (DPM) would be used, a new methodology would have to be implemented to determine levels of cell wall breakage by shear forces. It could be useful to carry out an unsteady simulation with cavitation where the pressure falls below the cavitation pressure over time to see its effects as there. However, this would require computational performance greater than desktop computers available today. Supercomputers would be required.
5. Manufacture the optimised valve seat and valve head for further use.
6. Passing yeast cells with water through the homogeniser with original valve design and new valve design and compare breakage levels using SEM (Scanning Electron Microscope). Also it would be recommended to repeat this experiment with sludge and filtered maize after 12 days anaerobic digestion to see if yield can be maintained beyond 15 days when re-introduced into anaerobic digestion.
7. Further optimisation based on results obtained on new design (change of gap length, valve seat outer diameter, other flow regions before the inlet region and after the exit region with optimised rounding). Also it would be recommended to round off regions that may generate significant turbulence and inefficiencies (figure 6.1). If this is not possible, a smaller thickness impact ring could be used to fill the space in the valve block.

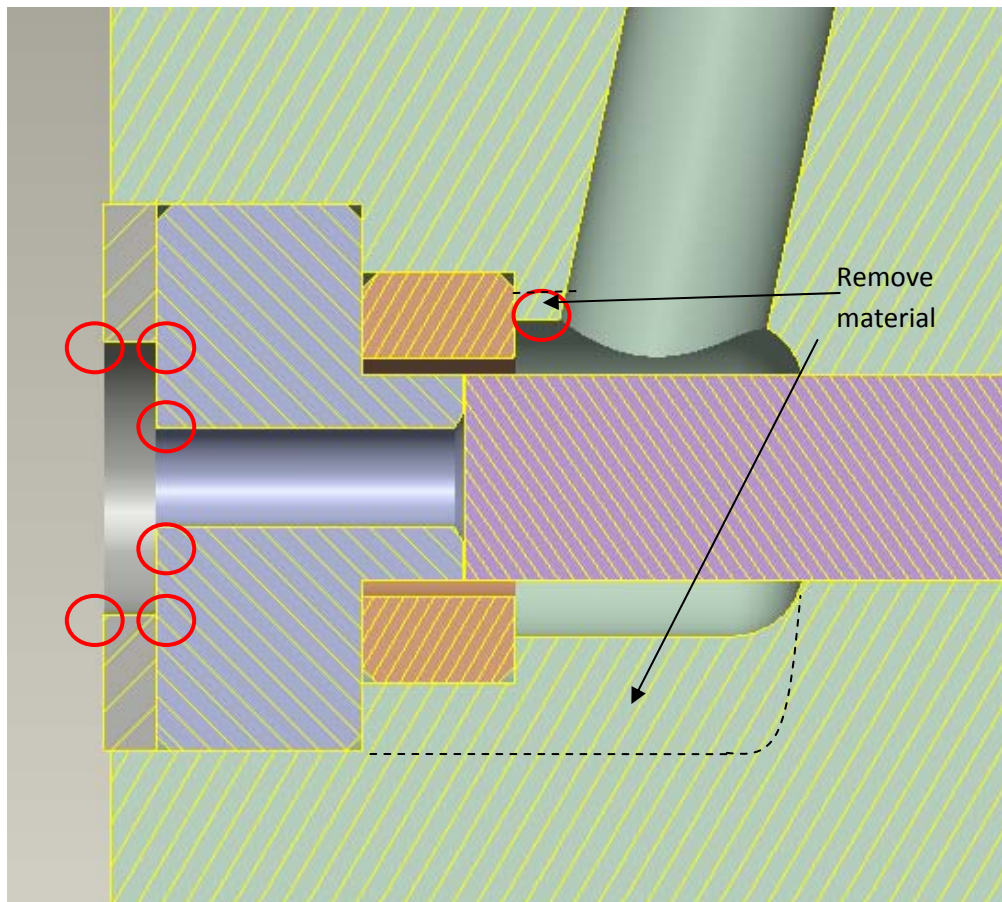


Figure 6.1: Instructions of material removal with dotted lines and rounding at red circles

8. Repeat work carried out with other materials other than maize such as grass, manure etc.

Appendix A – Equipment Specifications

A.1. Main Features of the Homogeniser

Some of the main features include the inlet funnel, the valve region, the discharge piping (return lines), turn wheel, the feed pump (motor) and the plunger. These features are displayed in figure A.1 (a). The inlet funnel is where material to be processed is introduced to be circulated. This is where the material is also recirculated. The valve region consists of the valve seat, valve head and the impact ring as shown in figure A.1 (d). The narrow space between the valve head and the valve seat (gap) can be changed by turning the turnwheel.

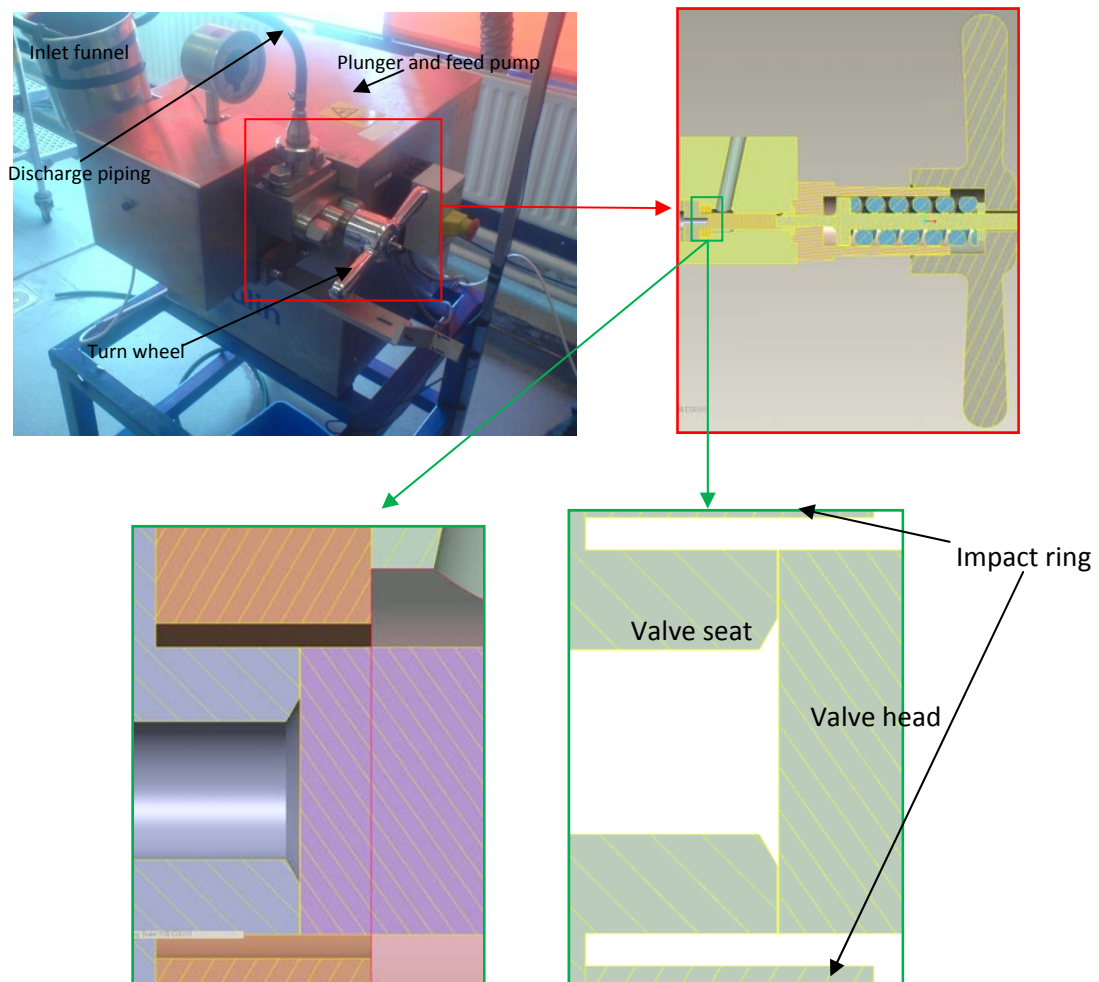


Figure A.1: The homogeniser (a) full assembly, (b) X-section of valve and turnwheel, (c) axi-symmetric view of valve region and (d) 2-d view of valve region

A.2. Recommendations for Installing the Gaulin High-Pressure Homogeniser

All information is sourced from the APV-Gaulin operation and service guide (APV Gaulin 1998).

1. Feed tank recommendations
 - a. Design such as to avoid turbulent conditions. Air can cause unwanted pressure fluctuations, loud knocking and shorten gauge life of the homogeniser. Therefore air inclusions should be avoided.
 - b. If a fluid of high separation of mixtures is used, a stirrer would be recommended.
 - c. A fluid level indicator with a connected alarm or automatic shut down mechanism would be very important if the homogeniser is not continually being monitored.
2. Suction and discharge piping
 - a. Keep as short as possible with radius as large as possible.
 - b. Keep radius of piping to fit well with connections and fittings of the homogeniser
3. Feed Pump
 - a. A feed pressure is recommended to be at least 2 bar (0.2 MPa) but for higher viscosity fluids and fluids which evaporate at operating temperature, higher pressures must be implemented but below the maximum pressure for fittings.
 - b. Once a month, if not in use, please turn the pump wheel slightly to reduce corrosion by static and trapped product in the homogeniser.
4. Feed pressure gauge: The pressure gauges are damped heavily and therefore the operating pressure must be increased gradually.
5. Return lines
 - a. Designed such that the return pipe does not have trapped air inside to be included with the product just passed through the homogeniser.

A.3. Starting Up Procedure

1. Check the homogeniser to ensure that there is enough lubrication and that all screws and fittings are firmly tightened with no foreign material already in the homogeniser.
2. Open the homogeniser hand-wheel to the maximum open position
3. Open the supply of cooling water from the mains to the plunger region and open the product supply valve
4. Start the homogeniser to start feeding the fluid.
5. Once the homogeniser operating pressure levels off, start to turn the hand-wheel gradually (as pressure gauge is heavily damped) until the desired operating pressure is obtained.

A.4. Shut Down Procedure

1. Open the valve gap using the hand-wheel until the operating pressure is reduced as far as possible
2. Pass water through the homogeniser for repeated passes until the homogeniser is sufficiently cleaned out for further use
3. Switch off the homogeniser and feed supply to the valve.
4. Close the main that provides cooling water to the plunger region.

A.5. Specifications

The following information is taken from the information plate on the homogeniser motor.

Type: APV-Gaulin High Pressure Homogeniser

Code: 98L35204

Max Pressure: 700 Bar (70 MPa) – However it is not possible for the homogeniser to exceed 20 MPa due to the type of belt being used on the motor which slips at this operational pressure.

Flow Rate: 60 L/hr (Later found to be 100 L/hr in experiments)

Motor Power: 2.2 KW

Appendix B – Calculations and procedures

B.1 Empirical validation

B.1.1. General Expression of Formulae to be Used:

$$\frac{2\Delta p}{\rho u_i^2} = k_i + k_g + k_e$$

$$\Delta p = \frac{\rho u_i^2}{2} [k_i + k_g + k_e]$$

$$\Delta p = \frac{\rho u_i^2}{2} (k_i) + \frac{\rho u_i^2}{2} (k_g) + \frac{\rho u_i^2}{2} (k_e)$$

$$\Delta p = \Delta p_i + \Delta p_g + \Delta p_e$$

B.1.2. Model Descriptions:

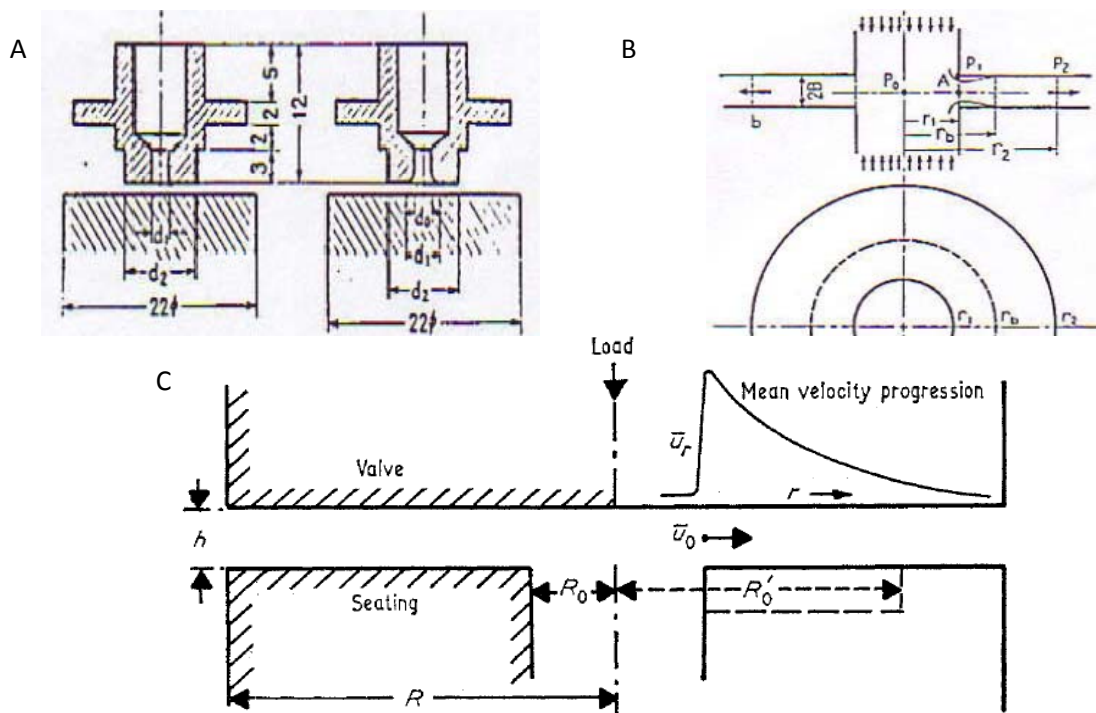


Figure B.1: Valve geometry of (a) Nakayama straight and round edge nozzle (Nakayama 1964), (b) Kawaguichi parallel disc setup (Kawaguichi 1971) and (c) Phipps cross section of plane faced valve (Phipps, "The fragmentation of oil drops in emulsions by a high-pressure

homogeniser" 1975).

B.1.3. Inlet Region Losses

Nakayama (Nakayama 1964) has nominated 0.18 inlet loss for the round edge nozzle (see figure B.2). However no figure has been nominated for the straight edge nozzle which may be closer to the homogenizer used in this study. However, it has been stated by Kleinig that as the gap size gets smaller, the inlet loss coefficient approaches 0.18 (Kleinig A.R. 1996). Therefore an inlet loss coefficient of 0.18 will be implemented for numerical calculations.

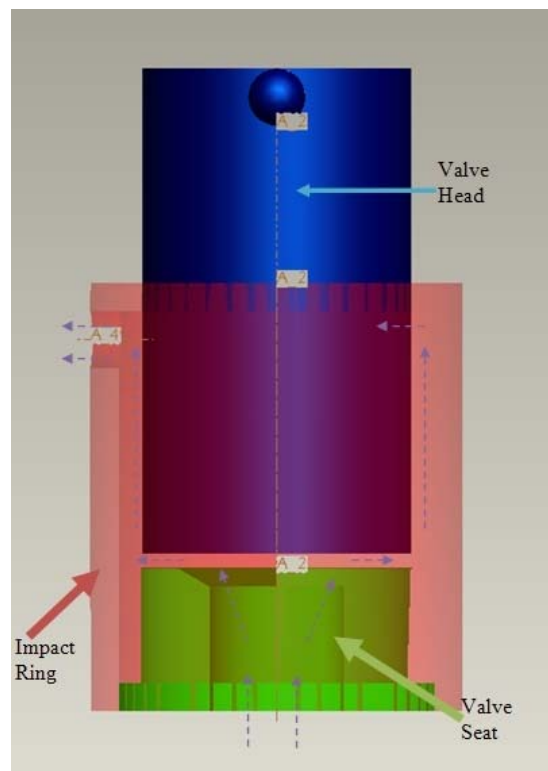


Figure B.2: Homogeniser Geometry

Clearly from investigation of the different models, none seem to match very closely the homogeniser used in the study (figure B.2). In terms of geometry, Nakayama's (Nakayama 1964) straight edged nozzle appears to be most similar to the homogeniser. However laminar conditions throughout the model have been assumed. The geometries displayed for Kawaguichi (Kawaguichi 1971) and Phipps (Phipps, "The fragmentation of oil drops in emulsions by a high-pressure homogeniser" 1975) both seen in figure B.1 do not contain inlet chamfers as seen in Nakayama (Nakayama 1964) or in the homogeniser model studied. Thus

it is probable that results from these two models are based on much larger vena contracta for the same pressure than for the homogenizer studied. However, turbulent effects are taken into account in this model. The model of Kawaguchi (Kawaguchi 1971) has two velocity inlets. However this seems to serve as an equivalent valve head for each inflow from each velocity inlet and may not affect results greatly unless flow rates in each entrance differs. It is also important to note that the initial velocity (u_0) in figure B.1 (c) occurs at the gap entrance and not the valve entrance as seen in other models including the homogenizer model covered. It appears that K_i does not change for turbulent or transitional flow. This could be because flow is always laminar at the inlet under operating conditions due the damping effect of the small gap size as reported by Stevenson and Chen (M. C. Stevenson 1997).

B.1.4. Gap Region Losses

It appears that the gap region is where the three formulae differs the most in terms of derivation and form. This may be due to the fact that pressure losses are clearly greatest here and hence most sensitive to change.

Nakayama (1964):

$$\begin{aligned}
 \Delta p &= \frac{\rho u_i^2}{2} [k_g] \\
 &= \frac{\rho u_i^2 \cdot 12}{2 \cdot m \cdot Re} \ln \left(\frac{R_e}{R_i} \right) & k_g &= \frac{12}{m Re} \ln \left[\frac{R_e}{R_i} \right] \\
 &= \frac{6 \rho u_i^2 \cdot (2R_i) \cdot (v)}{(h) \cdot (u_i \cdot h)} \ln \left(\frac{R_e}{R_i} \right) & m &= \frac{h}{2R_i} \text{ and } Re = \frac{u_i h}{\nu} \\
 &= \frac{12 \mu \cdot R_i \cdot u_i}{h^2} \cdot \ln \left[\frac{R_e}{R_i} \right] \\
 &= \frac{12 \mu \cdot R_i \cdot Q}{h^2 \cdot 2\pi \cdot R_i \cdot h} \cdot \ln \left[\frac{R_e}{R_i} \right] & u_i &= \frac{Q}{A_i} = \frac{Q}{2\pi R_i h} \\
 &= \frac{6 \mu Q}{\pi h^3} \cdot \ln \left[\frac{R_e}{R_i} \right]
 \end{aligned}$$

Kawaguichi (1971):

Using the 1/7 power law for velocity distribution ($u_i/U = (Z/B)^{1/7}$) and the empirical expression for shear stress ($\tau_0 = 0.0225(v/BU)^{1/4}$) subbed into the momentum balance equation ($\frac{1}{r} \frac{d}{dr} \left(r \int_0^B u_i^2 dz \right) = -\frac{\tau_0}{\rho} - \frac{1}{\rho} \frac{dp}{dr} \int_0^B dz$), the following expression for gap losses was obtained (Kawaguichi 1971):

$$\begin{aligned}
 k_g &= \frac{0.076}{m(Re/2)^{1/4}} \cdot \left[1 - \left(\frac{R_i}{R_e} \right)^{\frac{3}{4}} \right] \\
 \Delta P_g &= \frac{\rho u_i^2}{2} [k_g] \\
 &= \frac{\rho u_i^2}{2} \frac{0.076}{m(Re/2)^{1/4}} \cdot \left[1 - \left(\frac{R_i}{R_e} \right)^{\frac{3}{4}} \right] \\
 &= \frac{\rho u_i^2}{2} \frac{0.076 \cdot (2R_i)}{h(u_i h/2 v)^{1/4}} \cdot \left[1 - \left(\frac{R_i}{R_e} \right)^{\frac{3}{4}} \right] & m = \frac{h}{2R_i} \text{ and } Re = \frac{u_i h}{v} \\
 &= \frac{0.076(\rho \cdot u_i^{7/4} R_i) \cdot (2v)^{1/4}}{h^{5/4}} \cdot \left[1 - \left(\frac{R_i}{R_e} \right)^{\frac{3}{4}} \right] \\
 &= \frac{0.076\rho \cdot u_i^{7/4} \cdot R_i \cdot (2v)^{1/4}}{h^{5/4}} \cdot \left[1 - \left(\frac{R_i}{R_e} \right)^{\frac{3}{4}} \right] \\
 &= \frac{0.076\rho \cdot R_i \cdot Q^{7/4} \cdot (2v)^{1/4}}{h^{5/4} \cdot (2\pi R_i h)^{7/4}} \cdot \left[1 - \left(\frac{R_i}{R_e} \right)^{\frac{3}{4}} \right] & u_i = \frac{Q}{A_i} = \frac{Q}{2\pi R_i h} \\
 &= \frac{0.076\rho \cdot R_i \cdot Q^{7/4} \cdot (2v)^{1/4}}{h^{5/4} \cdot (2\pi R_i h)^{7/4}} \cdot \left[1 - \left(\frac{R_i}{R_e} \right)^{\frac{3}{4}} \right] \\
 &= \frac{0.076\rho \cdot R_i \cdot Q^{7/4} \cdot v^{1/4}}{h^{5/4} \cdot (2^{6/4})(\pi R_i h)^{7/4}} \cdot \left[1 - \left(\frac{R_i}{R_e} \right)^{\frac{3}{4}} \right] & \text{Constants combined} \\
 &= \frac{0.0036\rho \cdot v^{1/4} \cdot Q^{7/4}}{h^3 \cdot R_i^{3/4}} \cdot \left[1 - \left(\frac{R_i}{R_e} \right)^{\frac{3}{4}} \right] & 2^{6/4} = 2.828 \\
 & & \pi^{7/4} = 7.413
 \end{aligned}$$

$$= \frac{0.0036\rho \cdot v^{1/4} \cdot Q^{7/4}}{h^3} \cdot \left[\left(\frac{1}{R_i} \right)^{\frac{3}{4}} - \left(\frac{1}{R_e} \right)^{\frac{3}{4}} \right]$$

Phipps (1975):

$$\Delta p = \frac{\rho u_i^2}{2} [k_g]$$

$$= \frac{\rho u_i^2}{2} \cdot \frac{5}{m \cdot Re^{3/5}} \cdot \left[1 - \left(\frac{R_i}{R_e} \right)^{\frac{2}{5}} \right]$$

$$= \frac{\rho u_i^2}{2} \cdot \frac{5(2R_i) \cdot v^{3/5}}{h \cdot u_i^{3/5} \cdot h^{3/5}} \cdot \left[1 - \left(\frac{R_i}{R_e} \right)^{\frac{2}{5}} \right]$$

$$= \frac{5\rho \cdot u_i^{7/5} \cdot R_i \cdot v^{3/5}}{h^{8/5}} \cdot \left[1 - \left(\frac{R_i}{R_e} \right)^{\frac{2}{5}} \right]$$

$$= \frac{5\rho \cdot Q^{7/5} \cdot R_i \cdot v^{3/5}}{h^{8/5} \cdot (2\pi)^{7/5} \cdot (R_i)^{7/5} (h)^{7/5}} \left[1 - \left(\frac{R_i}{R_e} \right)^{\frac{2}{5}} \right]$$

$$k_g = \frac{5}{m Re^{3/5}} \cdot \left[1 - \left(\frac{R_i}{R_e} \right)^{\frac{2}{5}} \right]$$

$$m = \frac{h}{2R_i} \text{ and } Re = \frac{u_i h}{\nu}$$

$$u_i = \frac{Q}{A_i} = \frac{Q}{2\pi R_i h}$$

$$= \frac{5\rho v^{3/5}}{h^3} \cdot \left[\frac{Q}{2\pi} \right]^{7/5} \left[\left(\frac{1}{R_i} \right)^{\frac{2}{5}} - \left(\frac{1}{R_e} \right)^{\frac{2}{5}} \right]$$

← Combine and rearrange terms

Summary of gap losses.

Nakayama (1964)	Laminar	$\frac{6\mu Q}{\pi h^3} \cdot \ln \left[\frac{R_e}{R_i} \right]$
Kawaguici (1971)	Turbulent	$\frac{0.0036\rho \cdot v^{1/4} \cdot Q^{7/4}}{h^3} \cdot \left[\left(\frac{1}{R_i} \right)^{\frac{3}{4}} - \left(\frac{1}{R_e} \right)^{\frac{3}{4}} \right]$
Phipps (1975)	Turbulent	$\frac{5\rho v^{3/5}}{h^3} \cdot \left[\frac{Q}{2\pi} \right]^{7/5} \left[\left(\frac{1}{R_i} \right)^{\frac{2}{5}} - \left(\frac{1}{R_e} \right)^{\frac{2}{5}} \right]$

Where m= Inside radius/ inside chamfer radius = R_o/R_i

B.1.5. Exit Region Losses

$$K_e = C \left(\frac{r_i}{r_e} \right)$$

Nakayama (1964)	Laminar	$C = 54/35$ or $K_e = 54/35$
Kawaguichi (1971)	Turbulent	$C = 64/63$
Phipps (1975)	Empirical	$C = 1.0$

It is mentioned in many texts that these coefficients for the exit change with valve geometry considerably. However, a square edge for the chamfer outlet is used for the homogeniser covered. Another inconsistency may lie here. It appears from looking at these empirical formulas that highest exit losses are found with laminar conditions. Despite these formulas not being in close agreement, they serve as a sufficient guiding estimate for validation.

B.1.6. Total Pressure Drop:

$$\Delta p = \Delta p_i + \Delta p_g + \Delta p_e$$

Nakayama

$$\Delta p = k_i \cdot \frac{\rho}{2} \left[\frac{Q}{2\pi r_i h} \right]^2 + \frac{6\mu Q}{\pi h^3} \ln \left(\frac{r_e}{r_i} \right) + \frac{54\rho}{70} \left[\frac{Q}{2\pi r_i h} \right]^2$$

Kawaguichi

$$\Delta p = k_i \cdot \frac{\rho}{2} \left[\frac{Q}{2\pi r_i h} \right]^2 + \frac{5\rho v^{3/5}}{h^3} \cdot \left[\frac{Q}{2\pi} \right]^{7/5} \left[\left(\frac{1}{R_i} \right)^{2/5} - \left(\frac{1}{R_e} \right)^{2/5} \right] + \frac{\rho}{2} \left[\frac{Q}{2\pi r_i h} \right]^2$$

Phipps

$$\Delta p = k_i \cdot \frac{\rho}{2} \left[\frac{Q}{2\pi r_i h} \right]^2 + \frac{0.0036\rho \cdot v^{1/4} \cdot Q^{7/4}}{h^3} \cdot \left[\left(\frac{1}{R_i} \right)^{3/4} - \left(\frac{1}{R_e} \right)^{3/4} \right] + \frac{64\rho}{126} \left[\frac{Q}{2\pi r_i h} \right]^2$$

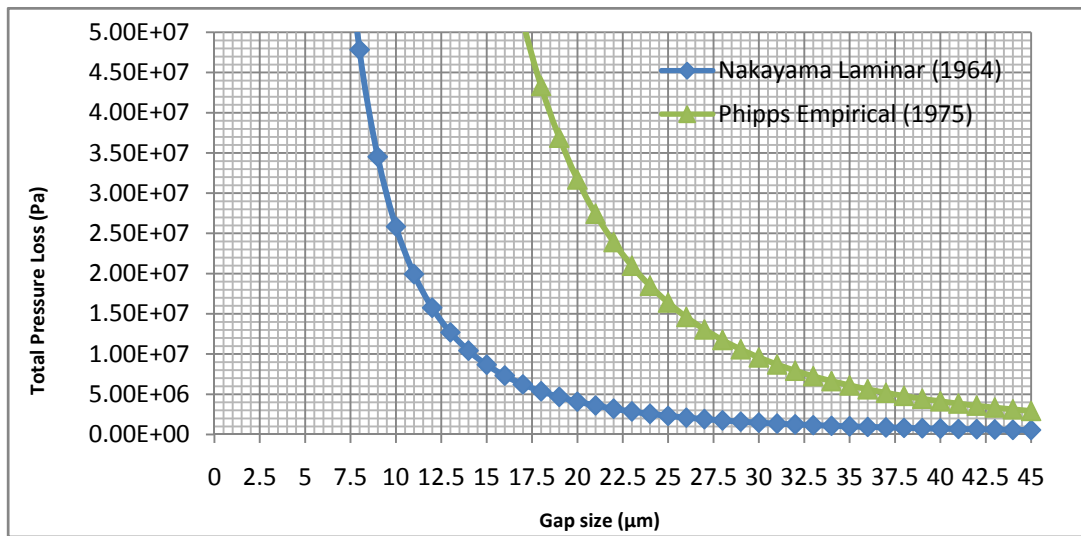


Figure B.3: Total pressure loss versus gap size calculated based on homogenizer setup used in laboratory

B.2 Pressure drop validation

B.2.1 Introduction

This pressure drop validation has already been explained in detail in section 4.2.2. Additional information of the exact procedure carried out is disclosed in the following section.

B.2.2 Steps Involved in Pressure Drop Validation

1. Scale grid to mm
2. Pressure based, Implicit, axi-symmetric, steady, absolute, green gauss cell based, superficial velocity solver selected
3. Energy turned on
4. Viscous → k-epsilon realizable, standard wall functions

The screenshot displays the 'Modelling setup' dialog box in ANSYS Fluent. It is divided into several panels:

- Model:** Radio buttons for Inviscid, Laminar, Spalart-Allmaras (1 eqn), **k-epsilon (2 eqn)**, k-omega (2 eqn), and Reynolds Stress (5 eqn).
- k-epsilon Model:** Radio buttons for Standard, RNG, and **Realizable**.
- Near-Wall Treatment:** Radio buttons for **Standard Wall Functions**, Non-Equilibrium Wall Functions, Enhanced Wall Treatment, and User-Defined Wall Functions.
- Options:** A checkbox for **Viscous Heating** which is currently unchecked.
- Model Constants:** Text input fields for C2-Epsilon (1.9), TKE Prandtl Number (1), TDR Prandtl Number (1.2), and Energy Prandtl Number (0.85).
- User-Defined Functions:** A dropdown for Turbulent Viscosity set to 'none', and a group of dropdowns for Prandtl Numbers (TKE, TDR, Energy) all set to 'none'.

Figure B.4: Modelling setup

5. Water nominated as material from material selection and later applied to fluid zones in boundary conditions
6. 2 separate fluid zones – one for laminar region and the other for turbulent

7. Velocity inlet – 1.395 m/s, $k = 0.00389$, $\epsilon = 0.0001268$
8. Pressure outlet – 0bc

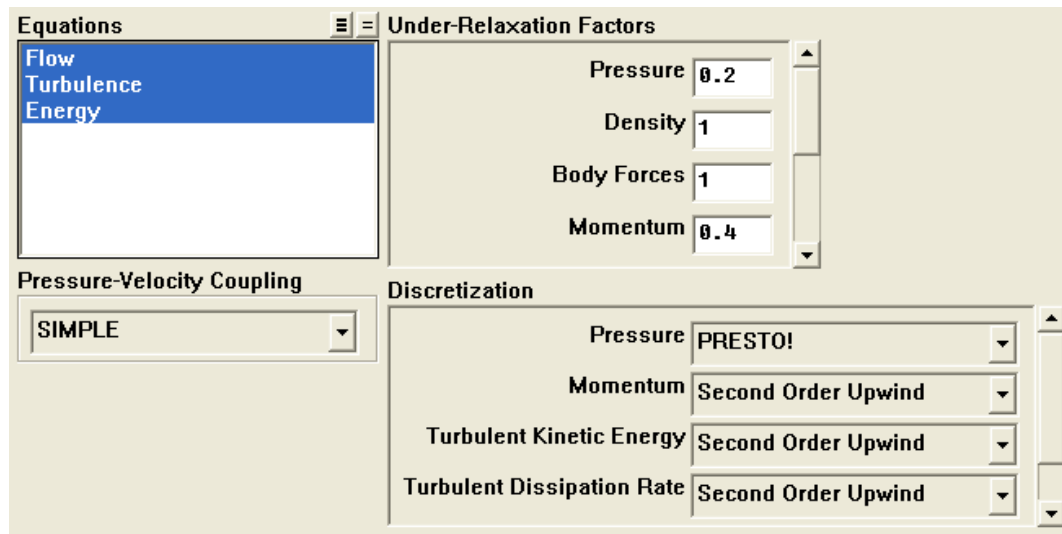


Figure B.5: Solver setup

9. $1e-6$ convergence criteria except energy which is $e-8$.
10. After simulation has converged, a line is created across the velocity inlet and across the exit at $x = 6$ mm (2 mm from the pressure outlet) to determine the pressure drop. This pressure drop is recorded for each gap size change.

B.3 Microbe Breakage Model ("10D_POS1_m20")

B.3.1 Introduction

The 10 μm microbe passing through the original design at position 1 is used for an example showing the method used in calculating the microbe breakage force. Faces that were angled between 0 and 90° were situated in the 1st quadrant. Faces between 90° and 180° were in the second quadrant with 4 quadrants in total as displayed in figure B.6. Please note that full spreadsheets of the microbe force calculations could not be included due to space restrictions.

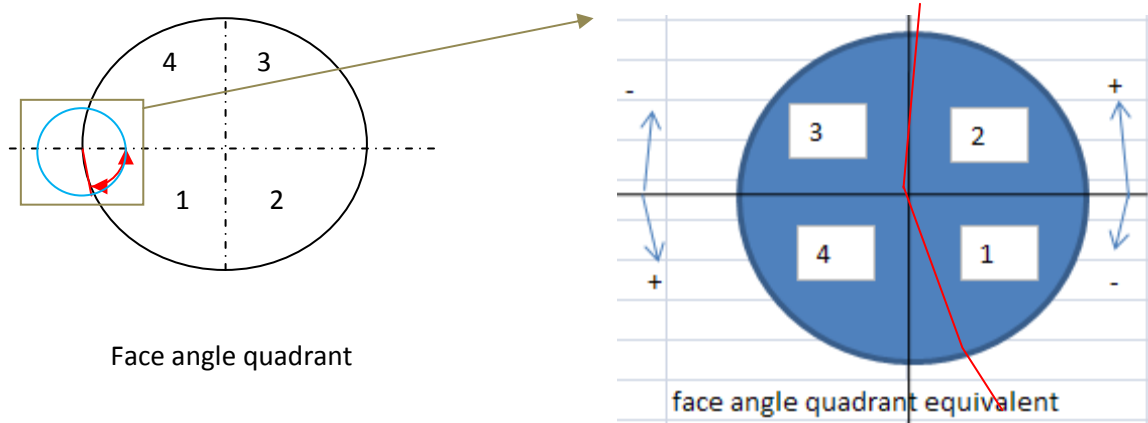


Figure B.6: Example of face defined as a 1st quadrant face as (a) part of a microbe and (b) defined as 1st quadrant

B.3.2 Shear force calculation steps

Step 1: Export microbe wall X and Y co-ordinates from Fluent 6.3.26 into MS-Excel. Work out the change of the X and Y co-ordinate change from node 1 to 2.

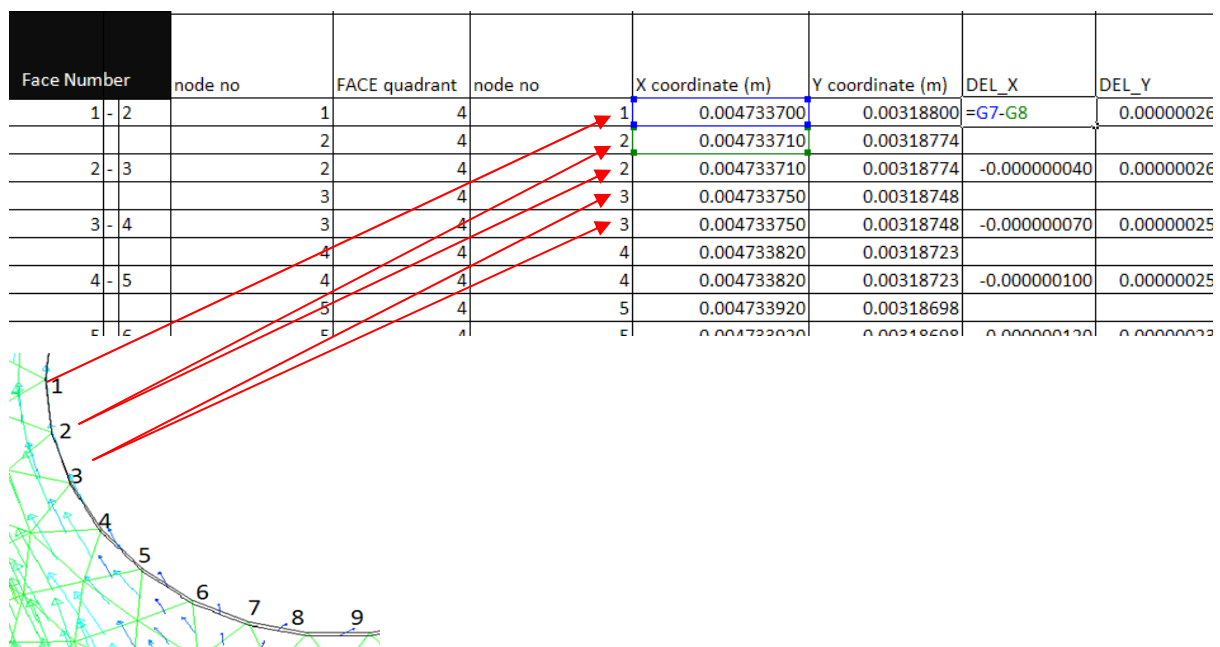


Figure B.7: Step 1

Step 2: The length of each discrete flat face that makes up the circle defining the microbe wall is calculated by absolute value of the X and Y co-ordinate change calculated in step 1.

X coordinate (m)	Y coordinate (m)	DEL_X	DEL_Y	length face (m)	Theta face (degrees)	Theta vector (degrees)	Theta vector (rads)
0.004733700	0.00318800	-0.000000010	0.000000026	$=\text{SQRT}((I7^2)+(J7^2))$		2.202598	0.038443
0.004733710	0.00318774			2.60192E-07			0.038443
0.004733710	0.00318774	-0.000000040	0.000000026	2.63059E-07	-81.2538377	8.746162	0.152649
0.004733750	0.00318748			2.63059E-07			0.152649
0.004733750	0.00318748	-0.000000070	0.000000025	2.59615E-07	-74.3577535	15.64225	0.273009

Figure B.8: Step 2

Step 3: The angle of each face is calculated using the inverse tan of the ratio of the change of Y values against X values.

DEL_X	DEL_Y	length face (m)	Theta face (degrees)	Theta vector (degrees)	Theta vector (rads)	Xnew (m)	Ynew (m)
-0.000000010	0.000000026	2.60192E-07	$=\text{DEGREES}(\text{ATAN}(J7/I7))$	0.038443	0.038443	0.004733	0.003188
		2.60192E-07			0.038443	0.004733	0.003188
-0.000000040	0.000000026	2.63059E-07	-81.2538377	8.746162	0.152649	0.004733	0.003188
		2.63059E-07			0.152649	0.004733	0.003187
-0.000000070	0.000000025	2.59615E-07	-74.3577535	15.64225	0.273009	0.004733	0.003187

Figure B.9: Step 3

The angles are converted from the angle measuring system implemented in Fluent 6.3.26 to the MS-Excel system as seen in figure B.10 and figure B.9.

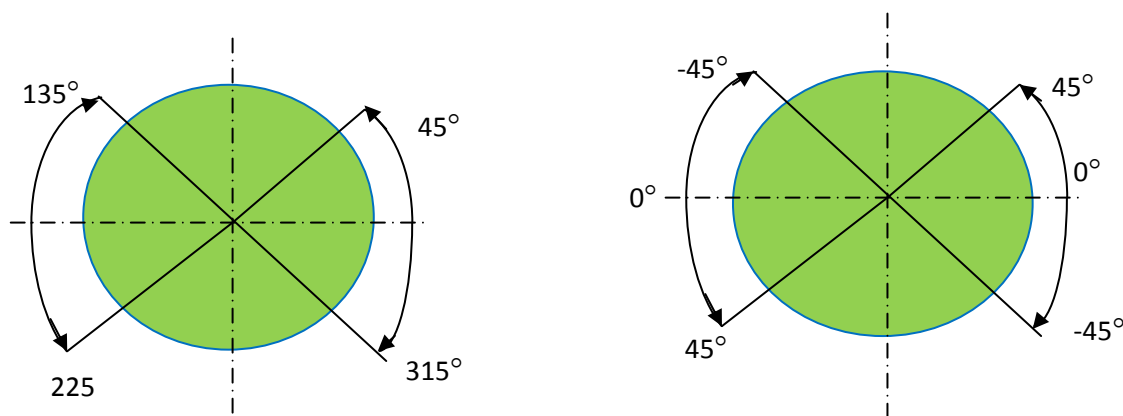


Figure B.10: Angle measurement system in (a) general engineering mathematics and (b) Microsoft Excel

Step 4: The direction of the vector of the right angle projection for each face was calculated. If the angle of the face lied between 0° and 180° , then 90° was added to the angle of the face direction as seen in figure B.11. Also if the angle of the face is greater than 180° and less than 360° (as in the 3rd and 4th quadrant faces), then 180° is added.

length face (m)	Theta face (degrees)	Theta vector (degrees)	Theta vector (rads)	Xnew (m)	Ynew (m)	Xnew (mm)	Ynew (mm)
2.60192E-07	-87.7974018	=90+L7	0.038443	0.004733	0.003188	4.732701	3.187962
2.60192E-07			0.038443	0.004733	0.003188	4.732711	3.187702
2.63059E-07	-81.2538377	8.746162	0.152649	0.004733	0.003188	4.732722	3.187588
2.63059E-07			0.152649	0.004733	0.003187	4.732762	3.187328
2.59615E-07	-74.3577535	15.64225	0.273009	0.004733	0.003187	4.732787	3.187210
2.59615E-07			0.273009	0.004733	0.003187	4.732857	3.186960
2.69258E-07	-68.1985905	21.80141	0.380506	0.004733	0.003187	4.732892	3.186859
2.69258E-07			0.380506	0.004733	0.003187	4.732992	3.186609
2.59422E-07	-62.4471884	27.55281	0.480887	0.004733	0.003187	4.733033	3.186517
2.59422E-07			0.480887	0.004733	0.003186	4.733153	3.186287

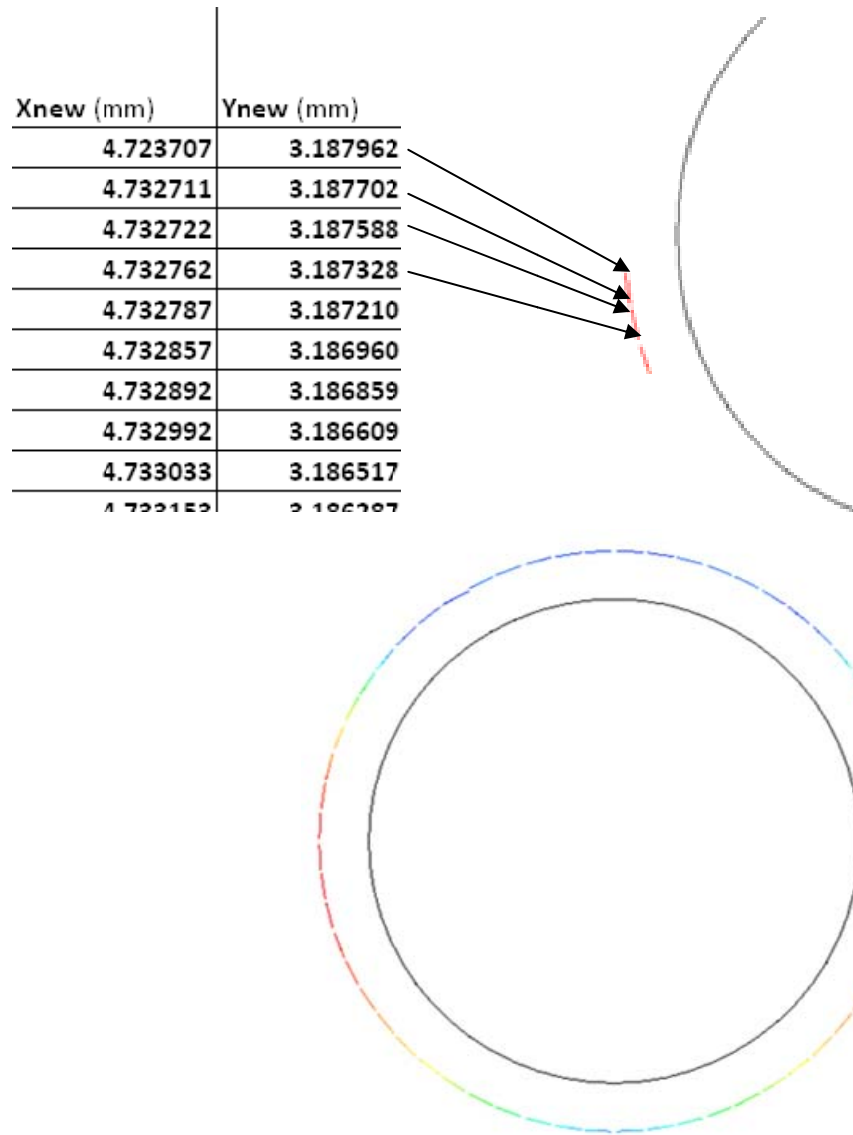
Figure B.11: Step 4 - Angle of face projection (“theta vector”) calculated from face angle (“theta face”) for a 1st quadrant face

Step 5: Conversion of projection angle back into radians and calculation of projected coordinates of each face based on 1 micron projection in terms of X and Y co-ordinates. These coordinates are later converted from metres in millimetres for ease of use in Fluent 6.3.26.

length face (m)	Theta face (degrees)	Theta vector (degrees)	Theta vector (rads)	Xnew (m)	Ynew (m)	Xnew (mm)	Ynew (mm)
2.60192E-07	-87.7974018	2.202598	0.038443	=G7-{0.00001*cos(N7)}		4.732701	3.187962
2.60192E-07			0.038443	0.004733	0.003188	4.732711	3.187702
2.63059E-07	-81.2538377	8.746162	0.152649	0.004733	0.003188	4.732722	3.187588
2.63059E-07			0.152649	0.004733	0.003187	4.732762	3.187328
2.59615E-07	-74.3577535	15.64225	0.273009	0.004733	0.003187	4.732787	3.187210
2.59615E-07			0.273009	0.004733	0.003187	4.732857	3.186960
2.69258E-07	-68.1985905	21.80141	0.380506	0.004733	0.003187	4.732892	3.186859
2.69258E-07			0.380506	0.004733	0.003187	4.732992	3.186609

Figure B.12: Step 5 – Projection of coordinates of face by 1 micron

Step 6: The coordinates in millimetres are imported manually into Fluent by the line creation under the surface toolbar.



Step B.13: Step 6 - Exporting of projected coordinates from MS-Excel to Fluent

Step 7: An XY-plot of velocity for each projected face is exported into MS-Excel and the velocity gradient is calculated. It is important to note that the velocity of the wall is zero. As results of force to be calculated are in SI units, the velocity gradient is divided by 10^6 as the projection of each face is by a distance of $1\text{ }\mu\text{m}$ (equals $1 \times 10^{-6}\text{ m}$).

Xnew (mm)	Ynew (mm)	Velocity(mic robo wall)	velocity at 1 mic translation	v_gradient (m/s/m)	dynam_visc	shear stress	A_face
4.723707	3.187962	0	90.3486	$= (T7-S7)/1000000$		1.612E-09	2.60192E-07
4.732711	3.187702	0		0		0	2.60192E-07
4.732722	3.187588	0	89.34715	8.93472E-05	0.00001784	1.594E-09	2.63059E-07
4.732762	3.187328	0		0		0	2.63059E-07
4.732787	3.187210	0	87.55595	8.7556E-05	0.00001784	1.562E-09	2.59615E-07
4.732857	3.186960	0		0		0	2.59615E-07
4.732892	3.186859	0	84.8977	8.48977E-05	0.00001784	1.515E-09	2.69258E-07
4.732992	3.186609	0		0		0	2.69258E-07

Figure B.14: Step 7 – Importing of velocity data and calculation of velocity gradient.

Step 8: Calculation of shear stress by multiplying the fluid viscosity by the velocity gradient.

Xnew (mm)	Ynew (mm)	Velocity(mic robo wall)	velocity at 1 mic translation	v_gradient (m/s/m)	dynam_visc	shear stress	A_face	F_shear_face
4.723707	3.187962	0	90.3486	9.03486E-05	0.00001784	$=U7*V7$	2.60192E-07	4.19383E-16
4.732711	3.187702	0		0		0	2.60192E-07	0
4.732722	3.187588	0	89.34715	8.93472E-05	0.00001784	1.594E-09	2.63059E-07	4.19304E-16
4.732762	3.187328	0		0		0	2.63059E-07	0
4.732787	3.187210	0	87.55595	8.7556E-05	0.00001784	1.562E-09	2.59615E-07	4.05518E-16
4.732857	3.186960	0		0		0	2.59615E-07	0
4.732892	3.186859	0	84.8977	8.48977E-05	0.00001784	1.515E-09	2.69258E-07	4.07812E-16
4.732992	3.186609	0		0		0	2.69258E-07	0
4.733033	3.186517	0	81.702975	8.1703E-05	0.00001784	1.458E-09	2.59422E-07	3.78129E-16
4.733153	3.186287	0		0		0	2.59422E-07	0
4.733196	3.186213	0	77.79515	7.77952E-05	0.00001784	1.388E-09	2.60768E-07	3.61911E-16
4.733336	3.185993	0		0		0	2.60768E-07	0
4.733399	3.185905	0	73.70766667	7.37077E-05	0.00001784	1.315E-09	2.56125E-07	3.36705E-16

Figure B.15: Step 8 – Shear stress calculation

Step 9: Calculation of shear force on each face by multiplying the shear stress by the contact surface area of each face (“A_Face”). The contact surface area of each face is calculated by multiplying the face length by 1.0 (due to a 2-d simulation being used, the depth of the model in the Z-direction is 1.0). Each force is placed in the corresponding categories as seen in figure 4.9 in section 4.3.2 (lead clockwise, lead anticlockwise, trailing clockwise and trailing anticlockwise). Shear forces belonging to each category is added up to use in analysis and optimisation as described in chapter 4 and chapter 5.

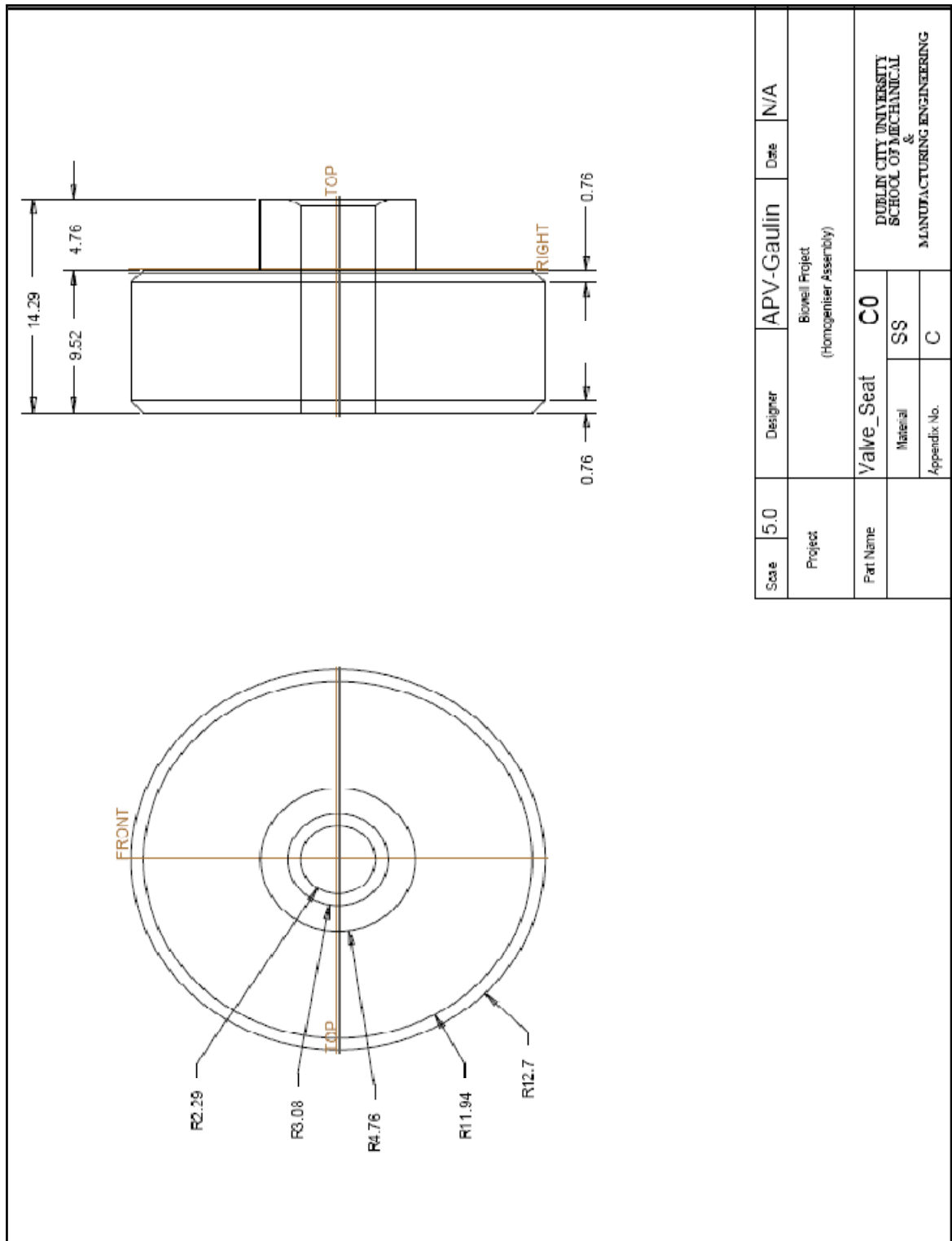
v_gradient (m/s/m)	dynam_visc	shear stress	A_face	F_shear_face	clockwise shear force	anti-clockwise shear force	
9.03486E-05	0.00001784	1.612E-09	2.60192E-07	=W7*X7	4.19383E-16		bottom shear clockwise
0		0	2.60192E-07	0	0		bottom shear clockwise
8.93472E-05	0.00001784	1.594E-09	2.63059E-07	4.19304E-16	4.19304E-16		bottom shear clockwise
0		0	2.63059E-07	0	0		bottom shear clockwise
8.7556E-05	0.00001784	1.562E-09	2.59615E-07	4.05518E-16	4.05518E-16		bottom shear clockwise
0		0	2.59615E-07	0	0		bottom shear clockwise
8.48977E-05	0.00001784	1.515E-09	2.69258E-07	4.07812E-16	4.07812E-16		bottom shear clockwise
0		0	2.69258E-07	0	0		bottom shear clockwise
8.1703E-05	0.00001784	1.458E-09	2.59422E-07	3.78129E-16	3.78129E-16		bottom shear clockwise
0		0	2.59422E-07	0	0		bottom shear clockwise
7.77952E-05	0.00001784	1.388E-09	2.60768E-07	3.61911E-16	3.61911E-16		bottom shear clockwise

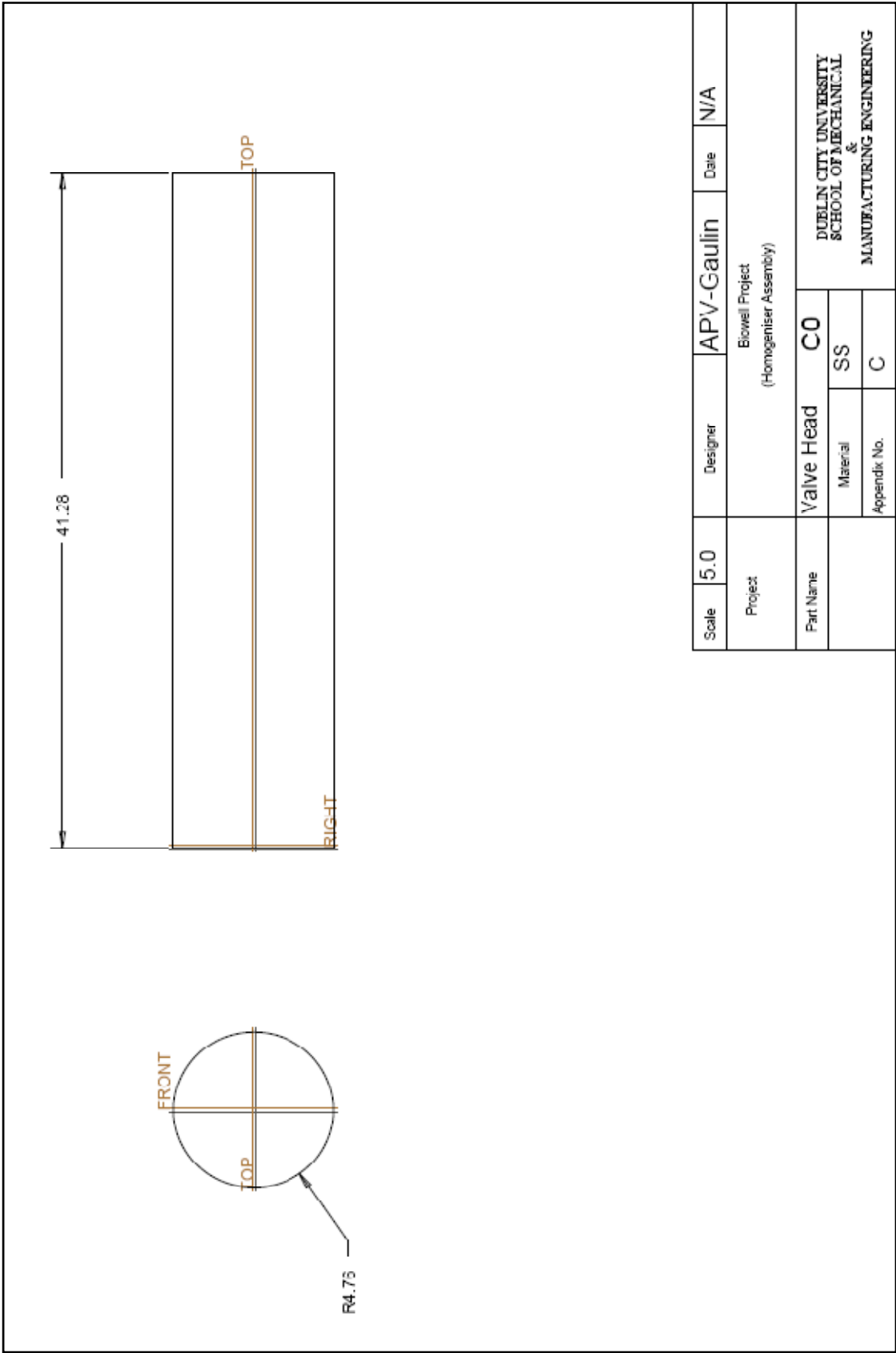
Figure B.16: Step 9 – Calculation of shear forces

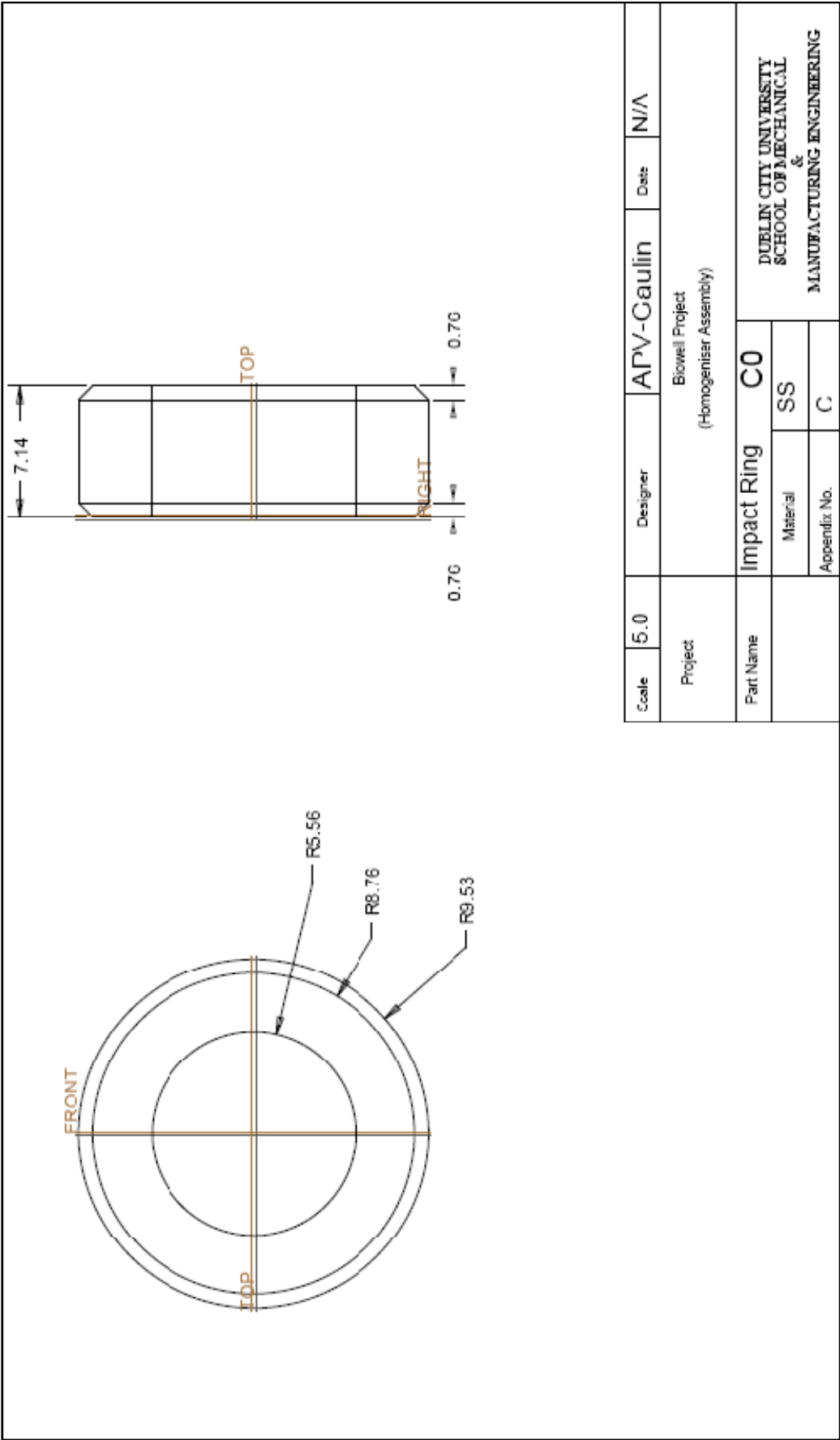
Appendix C - Drawings

C.1 M20 Model (Original Design)

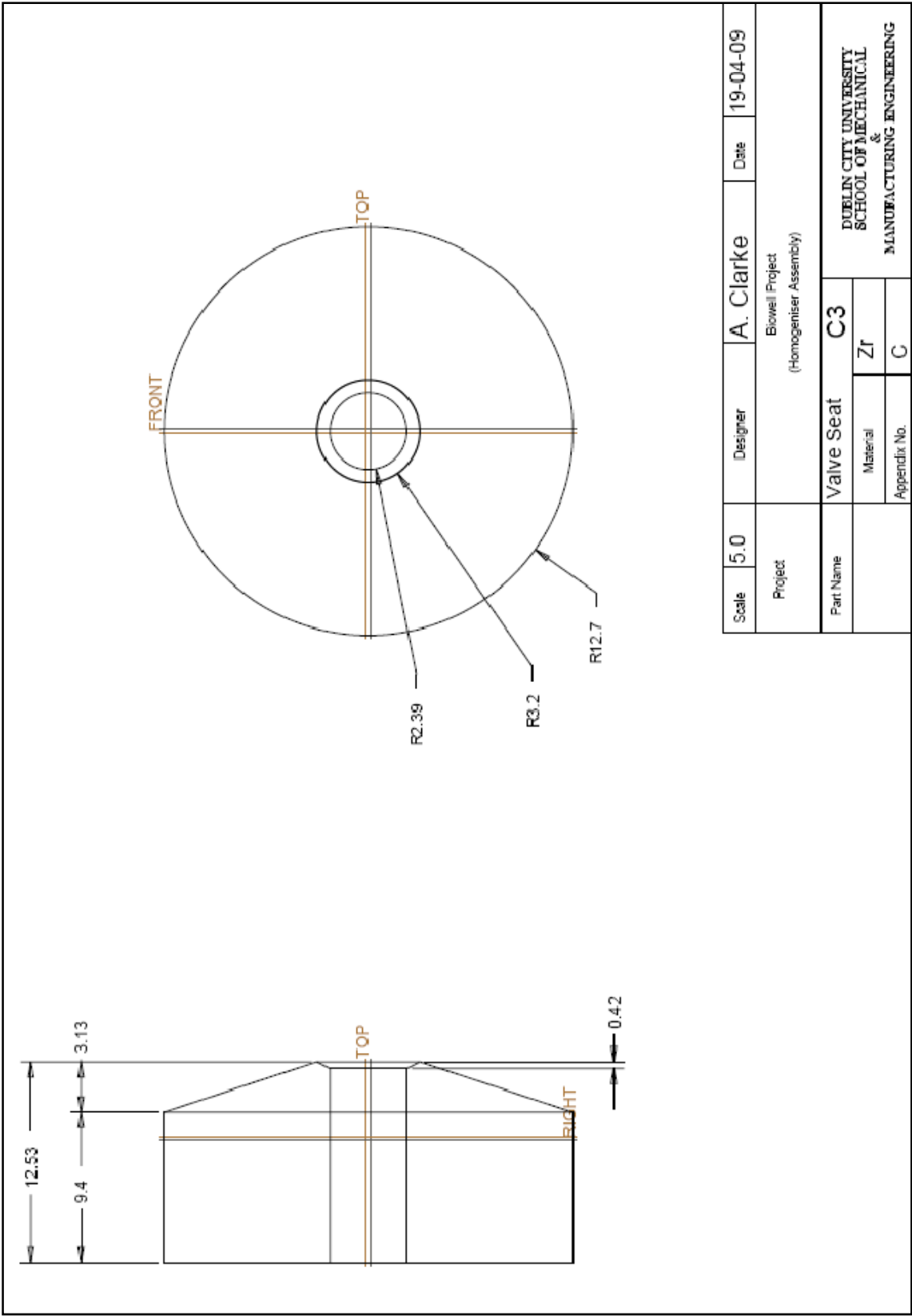
All drawings are in mm:

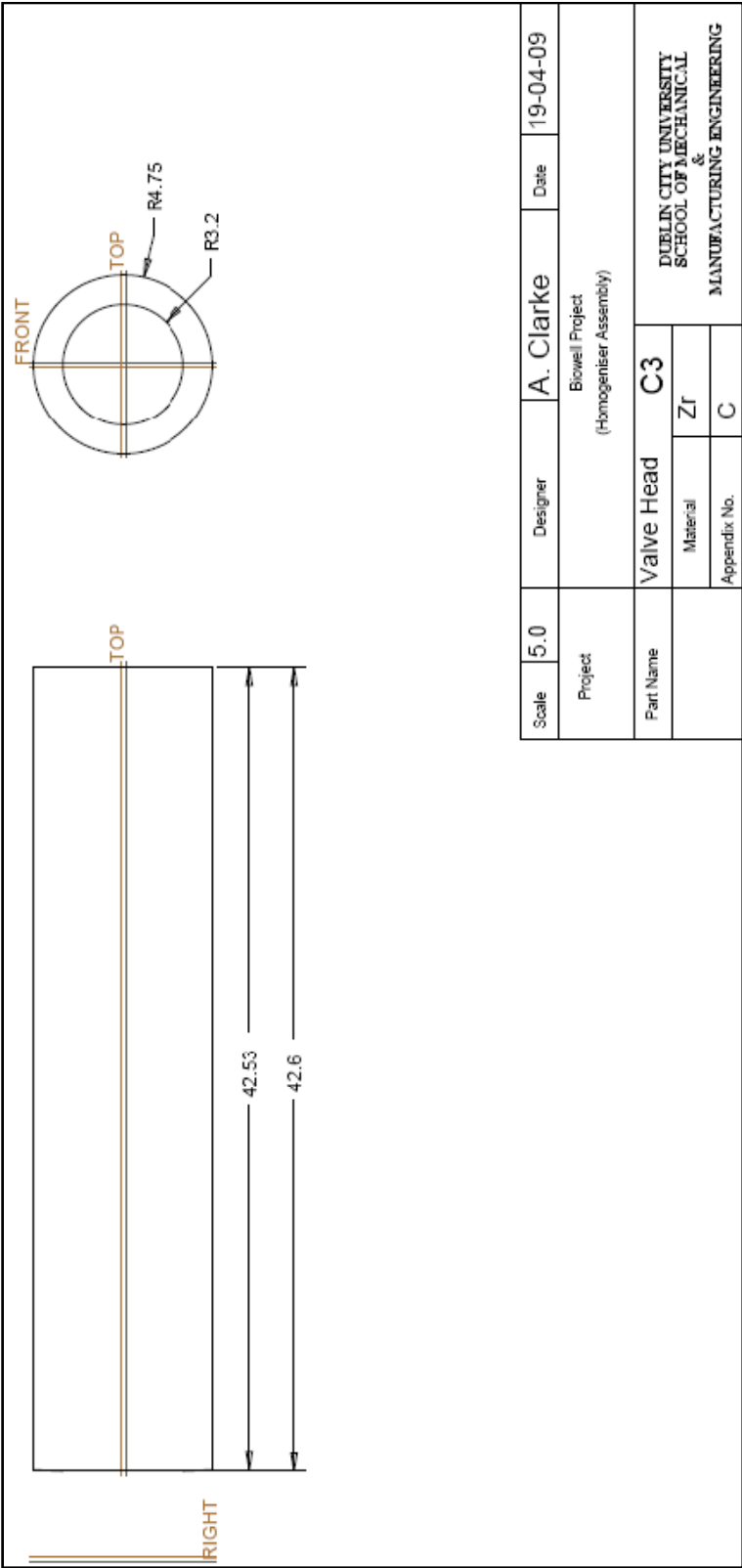






C.2 C3 Model (Optimised design)





Appendix D - Further work

D.1 Further Work on the Biowell Project

To determine the level of success of the design proposed in this work, the effectiveness of the old homogeniser valve will be compared to the new design. This will be achieved by passing the used and filtered microbes (after 2 weeks of anaerobic digestion with maize) through both valves and reintroducing into anaerobic digestion with maize (see figure D.1). The methane yields will be compared for both valves. An alternative approach would be to investigate the structure of yeast cells passed after homogenisation using the scanning electron microscope.

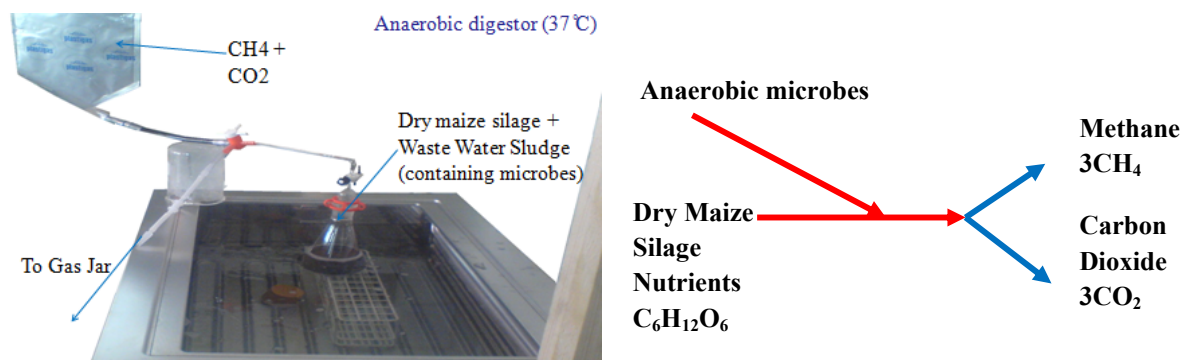


Figure D.1: Simple setup of anaerobic digestion

The Hollander beater is currently being optimised to break up maize in order to increase reactant area of the maize which would increase reaction rate and yield. Using the Hollander beater as well as the anaerobic digester has increased biogas yields by up to 21% in comparison to using just anaerobic digestion for the maize silage and waste water sludge with microbes.

The homogeniser is currently being setup and validated for experimental measurement of pressure drop vs. gap size using an LVDT (figure D.2). Work is also being carried out to successfully damp vibration of the homogeniser affecting the LVDT particularly with gaps smaller than 10 μm .

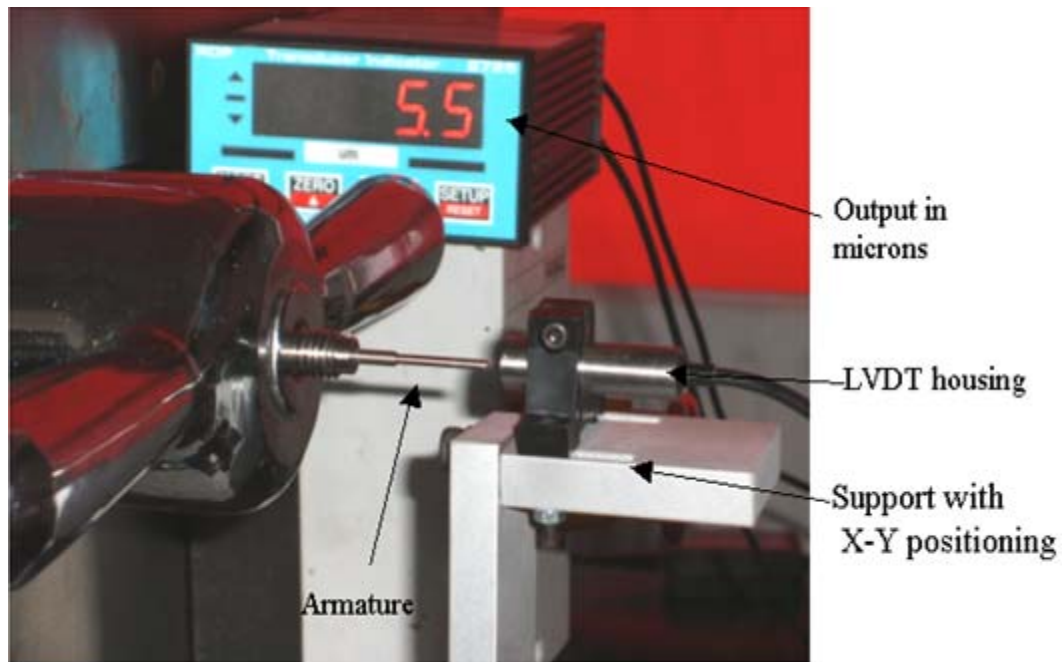


Figure D.2: LVDT being used to measure the gap size of the homogeniser

D.2 Cellrupt project

As results of cell breakage shear forces and optimisation are highly applicable to yeast cells due to the selection of a 5 μm diameter of the microbe passing, many applications could benefit from results obtained. A spin-off project has successfully obtained a proof of concept from results obtained from this research known as the Cellrupt project. This project will cover specific methodologies to improve cell rupture in the homogeniser as well as experimentally comparing cell rupture on a commercially available homogeniser valve against the optimised design from this thesis. Researchers working on the Biowell project have also joined the Cellrupt team as well as a lecturer and a newly appointed post doctorate researcher in the university specifically to continue work carried out so far.

References

- Agerkvist, I., Enfors, S.O. "Characterization of E. coli cell disintegrates from a bead mill and high-pressure homogenizers." *Biotechnology and Bioengineering* 36 (1990): 1083–1089.
- APV Gaulin. "Operation and Service Manual, Gaulin-Homogeniser." Wilmington, MA, USA, 1998.
- Asia Biogas. *Anaerobic digestion information*. 2008. [Online], <http://www.asiabiogas.com/about/process.html>, [Accessed: 20 May 2008].
- Ayazi Shamlou, P., Siddiqi, S.F., Titchner-Hooker, N.J., "A physical model of high-pressure disruption of Baker's yeast cells." *Chem. Eng. Sci.* 50, no. 9 (1995): 1383-1391.
- B. Balasundaram, S. T. L. Harrison. "Study of Physical and Biological Factors Involved in the Disruption of E. coli by Hydrodynamic Cavitation." *Biotechnology Progress* Vol. 22, no. 3 (2008): Pages 907 - 913.
- B. Balasundaram, S.T.L. Harrison, "Disruption of Brewers' Yeast by Hydrodynamic Cavitation: Process Variables and Their Influence on Selective Release", *Biotech. Bioeng.*, Vol. 94, Issue 2, 2006. *IN: Save, et al., "Use of hydrodynamic cavitation for large-scale microbial cell disruption", Trans Inst Chem Eng, Vol. 71C, Issue 75, 1997. Pages: 41-48, 2006.*
- Bosch, G., Rodi, W. "Simulation of vortex shedding past a square cylinder near a wall." *Int. J. Heat and Fluid Flow* 17 (1996): 267-275.
- Brennen, C.E., *Cavitation and bubble dynamics*. 1995.
<http://caltechbook.library.caltech.edu/1/5/BUBBOOK.pdf> (accessed 06 24, 2009).
- Brookman, J.S.G. "Further studies on the mechanism of cell disruption by extreme pressure extrusion." *Biotechnol Bioeng* 17 (1975): 465-479.
- Brookman, J.S.G. "Mechanism of cell disintegration in a high-pressure homogeniser." *Biotechnol Bioeng* 17 (1974): 371-383.
- Casoli, P., et al. "CFD analysis of a homogenizing valve in presence of cavitation." 2005. [Online], Available from:
www.automaatioseura.fi/confprog/downloadfile_public.php?conference=12&filename=12-12037.pdf [Accessed 14 July 2007].
- Charinpanitkul, T., Soottitantawat, A., Tanthapanichakoon, W. "A simple method for bakers' yeast cell disruption using a three-phase fluidized bed equipped with an agitator." *Bioresource Technology* 99, no. 18 (2008): 8935-8939.

- Debs-Louka, E., Louka, N., Abraham, G., Chabot, V., Allaf, K.,. ""Effect of Compressed Carbon Dioxide on Microbial Cell Viability"." *Appl Environ Microbiol.* 65(2): 626–631. (1999).
- Diels, A., et al. ""High pressure homogenisation as a non-thermal technique for the inactivation of micro-organisms"." *Critical reviews in microbiology* 32, No. 4, (2006): Pages 201-216,.
- Doulah, M.S., Hammond, T.H., and Brookman, J.S.G. "A hydrodynamic mechanism for the disintegration of *Saccharomyces cerevisiae* in an industrial homogeniser." *Biotechnol. Bioeng* 17 (1975): 845–858.
- Dyer, A., History today, P.958, September 1976. In *In: Slessor M & Lewis C, 'Biological energy resources', Spon Print, London, 1979.* 1976.
- Engler, C., Robinson, C. ""Disruption of *Candida utilis* cells in high pressure flow devices"." *Biotechnol Bioeng* 23 (1981): 765-780.
- Floury, J., et al. ""Analysis of a new type of high-pressure of homogeniser Part B. Study of droplet break-up and recoalescence phenomena"." *Chem Eng Sci* 59 (2004): 1285-1294, .
- Fluent Inc. *Fluent 6.3 Documentation.* 2007. [Online], http://www.fluentusers.com/fluent/doc/doc_f.htm, [Accessed 20 Dec 2008].
- Foster, D.,. ""Optimizing recombinant product recovery through improvements in cell-disruption technologies"." *Current Opinion in Biotechnology* 6 (1995): p 523-526.
- French patent no. 295.296, (1900), in A Diels et al., "Critical reviews in microbiology, "High pressure homogenisation as a non-thermal technique for the inactivation of micro-organisms"." 19 Pages.
- Gibson, A.H. ""On the Flow of Water through Pipes and Passages Having Converging or Diverging Boundaries"." *Proceedings of the Royal Society of London. Series A.* 1910. 366-378.
- Harrison, S.T.L., and Pandit, A.B., "The disruption of microbial cells by hydrodynamic cavitation", 9th International Biotechnology Symposium, Washington, DC, 1992., IN:. "Diels, A., et al., "High pressure homogenisation as a non-thermal technique for the inactivation of micro-organisms", Critical reviews in microbiology, Vol. 32, No. 4, Pages 201-216, 2006." 1992.
- Hetherington, P.J., Follows, M., Dunnill, P. and Lilly, M.D. ""Release of protein from Bakers yeast (*Saccharomyces cerevisiae*) by disruption in an industrial homogeniser"." *Trans. Instn chem. Engrs.* 49 (1971): 142–148.
- Jana, A.K., Das, G., Das, P.K.,. "The hydrodynamics of liquid-liquid upflow through a venturimeter." *International Journal of Multiphase Flow* 34, no. 12 (2008): 1119-1129.
- Kawaguchi, T. ""Entrance Loss for Turbulent Flow without Swirl between Parallel Discs"." *Bull JSME* 14, no. 70 (1971).
- Kelly, W., et al.,. ""Model-based control of a high pressure homogeniser"." *Proceedings of the American control conference anchorage, AK, USA , May 2002.*

- Kelly, W., Muske, K. "Optimal operation of high-pressure homogenisation for intracellular product recovery". *Bioprocess Biosys eng* 27 (2004): 25-37.
- Keshavarz-Moore, E., et al. "Disruption of baker's yeast in a high-pressure homogeniser: New evidence on mechanism". *Enzyme microb technol* 12 (1990): 764-770.
- Kleinig A.R., Middleberg A.P.J., "The Correlation of Cell Disruption With Homogeniser Valve Pressure Gradient Determined by Computational Fluid Dynamics". *Chem. Eng. Sci* 51, no. 23 (1996).
- Kondo, T., Kano, E. "INT. J. RADIAT. BIOL." 54, no. 3 (1988): 475-486.
- Kopp, J., Muller, J., Dichtl, N., Schwedes, J. "Anaerobic digestion and dewatering characteristics of mechanically disintegrated excess sludge". *Wat. Sci. Tech.* 36, no. 11 (1997): 129-136.
- Lapple, C.E., Shepherd, C.B., "Calculation of particle trajectories", *Ind. Eng. Chem.*, 1940: 605-617.
- Lei, C., Cheng, L., Kavanagh, K. "Re-examination of the effect of a plane boundary on force and vortex shedding of a circular cylinder". *Journal of wind engineering and industrial aerodynamics* 80 (1999): 263-286.
- Lenihan, S., *AMT Ireland Projects*. 2004.
<http://www.ucc.ie/en/DepartmentsCentresandUnits/AMTIreland/Projects/HighPressureProcessing/>
 (accessed 06 24, 2009).
- Miller, J., et al. "Using a CFD model to understand the fluid dynamics promoting E. Coli breakage in a high-pressure homogeniser". *Biotechnol Prog* 18 (2002): 1060-1067.
- Naglak, T.J., Hettwer, D.J., Wang, H.J. "Chemical permeabilization of cells for intracellular product release in separation processes in biotechnology". New York: Dekker Inc, 1990.
- Nakamura, K., Enomoto, A., Fukushima, H., Nagai, K., Hakoda, M. "Disruption of microbial cells by the flash discharge of high pressure carbon dioxide". *Biosci. Biotechnol. Biochem.* 58 (1994): 1297-1302.
- Nakayama, Y., "Action Of The Fluid In The Air Micrometer, 3rd Report, Characteristics Of Double Nozzle, No. 1, In The Case Of Compressibility Being Ignored". Edited by TRANSLATION 2597.800000. *Bulletin Of The Japan Society Of Mechanical Engineers* 7, no. 28 (1964).
- NASA. 2000. [Online],
http://earthobservatory.nasa.gov/Newsroom/NewImages/images.php3?img_id=3328, [Accessed: 10 Mar 2008].
- O'Reilly, E., *Masters Thesis*. Dublin City University, 2007.
- Perry, R.H., Green, D.W., *Perry's Chemical Engineers' Handbook (8th Edition)*. McGraw-Hill., 2008.
- Phipps, L.W., "The fragmentation of oil drops in emulsions by a high-pressure homogeniser". *J. Phys. D: Appl. Phys.*, 8 (1975).

Phipps, L.W., *J. Dairy Res.* 41 (1974a): 1-7.

Prescott, T.,. " "Research Internal Reports", Dublin City University, ." 2008.

Ramanan, R.N., Tey, B.T., Ling, T.C., Ariff, A.B. ""Classification of pressure range based on the characterization of Escherichia coli cell disruption on the high pressure homogeniser"." *American Journal of Biochemistry and Biotechnology* 5, no. 1 (2009): p. 21-29.

Shaw, John. "NRC wear materials expertise supports MicroSludge(TM) system commercialization". 4 Juin 2009. http://ifci-iipc.nrc-cnrc.gc.ca/media/success03-microsludge_e.html.

Shirgaonkar, I.Z.S., Lothe, R.R., and Pandit, A.B. "Comments on the mechanism of microbial cell disruption in high-pressure and high-speed devices." *Biotechnol. Prog.* 14 (1998): 657–660.

Siddiqi, S., Titchner-Hooker, N., Ayazi Shamlou, P. ""Simulation of particle size disruption changes occurring during high-pressure disruption of baker's yeast"." *Biotechnol Bioeng* 50 (1996): 145-150.

Slessor, M., Lewis, C. "*Biological energy resources*". London: Spon Print, 1979.

Sparrow, E.M., Abraham, J.P., Minkowycz, W.J.,. "Flow separation in a diverging conical duct: Effect of Reynolds number and divergence angle." *International Journal of Heat and Mass Transfer* 52, no. 13-14 (2009): 3079-3083.

Stevenson, M., Chen, X. ""Visualisation of the flow patterns in a high-pressure homogenising valve using a CFD package"." *J food eng* 33 (1997): pp. 151-165.

Stevenson, R.J., Laliberte, S., Hoy, P.M., Britch, D. *Full scale laboratory results from the trial of the MicroSludge at the joint water pollution control plant at Los Angeles County.* 2007.
<http://bvsde.per.paho.org/bvsaar/cdlodos/pdf/fullscale739.pdf> (accessed 12 June, 2009).

Taneda, S. ""Experimental investigation of the wake behind a sphere at low Reynolds numbers"." *J. Phys. Soc* 11 (1956): p. 1104.

Walstra, P., Smolders, P. ""Emulsion Formation" ." *In: Binks, B (Ed), Modern aspects of emulsion science* (Royal society of Cambridge, U.K), 1998: 56-98.

Email: andrew.clarke@dcu.ie

Website link: <http://andrew-clarke.webnode.com>

Nomenclature:

Δp	Pressure drop across valve (Pa)*
p	Nominal pressure (Pa)
ρ	Fluid density (kg/m ³)
u_i	Inlet velocity magnitude (m/s)
U	Max Velocity (m/s)
R_i	Radius of valve seat at gap entrance
R_e	Radius of valve seat at gap exit
ν	Kinematic viscosity
m	Constant calculated from $\frac{h}{2R_i}$
k_i	Loss coefficient across inlet (-)
k_g	Loss coefficient across gap (-)
k_e	Loss coefficient at valve exit (-)
Re	Reynolds number (-)
h	Gap size (m)**
Q	Volumetric flow rate
B	Half-thickness of gap size for momentum equation used to derive Kawaguichi calculation
μ	Dynamic viscosity
D_H	Horizontal distance (m)
ΔP_i	gap entrance pressure gradient (Pa/m)
R	number of cells disrupted as a fraction of the total number of cells
k	temperature (K)
P	Operating pressure (Pa)
N	Number of passes
a	Pressure component constant
b	Linear variable relating to cell concentration
ΔP_i	Inlet pressure loss (Pa)

P	Localised static pressure (Pa)
P_v	Vapour pressure (Pa)
P_r	Impact ring pressure (Pa)
C_v	Cavitation constant
ρ	Density (kg/m^3)
V_{th}	Localised velocity (m/s)
f_τ	fraction of total broken cells by channel shear stress to total cells
f_f	fraction of total broken cells by impact ring pressure to total cells
$\frac{\Delta V}{\Delta s}$	velocity gradient
τ_m	Fluid shear stress (Pa)
A_{Loc_N}	surface area covered by the local shear stress
τ	Surface tension (N)
R	radius of microbe/cell
G_w/D	Critical gap ratio
D_h	Hydraulic diameter

* Will be represented in calculations as Pa but as MPa when reporting results

** Will be represented in calculations as m but will adopt μm when reporting results